THE DEVELOPMENT OF ELECTROCHEMICAL ADVANCED OXIDATION PROCESSES FOR WASTEWATER TREATMENT: FROM TWO-DIMENSIONAL TO THREE-DIMENSIONAL

A Dissertation
Presented to
The Academic Faculty

by

Xiaoyang Meng

In Partial Fulfillment
of the Requirements for the Degree
Doctor of Philosophy in the
School of Civil and Environmental Engineering

Georgia Institute of Technology
December 2018

THE DEVELOPMENT OF ELECTROCHEMICAL ADVANCED OXIDATION PROCESSES FOR WASTEWATER TREATMENT: FROM TWO-DIMENSIONAL TO THREE-DIMENSIONAL

Approved by:

Dr. John Crittenden, Advisor
School of Civil and Environmental
Georgia Institute of Technology

Dr. Nian Liu
School of Chemical & Biomolecular Engineering
Georgia Institute of Technology

Dr. Yongsheng Chen
School of Civil and Environmental
Georgia Institute of Technology

Dr. Xing Xie
School of Civil and Environmental
Georgia Institute of Technology

Dr. Ching-Hua Huang
School of Civil and Environmental
Georgia Institute of Technology

Date Approved: November 8, 2018

To Meng Wei, Huang Jing, my parents who gave all their hearts to support me and hold faith in me all these years.

To Huang Gang, my uncle who supported me and guided me to become a better person.

To Maxiaoyun, my girlfriend Zhou who encouraged me to conquer all the difficulties along this path

I love you.

ACKNOWLEDGEMENTS

First, I would like to express my deepest gratitude to my thesis advisor, Dr. John Crittenden, who has supported my opportunity to study and conduct research in Georgia Tech. His guidance, teaching, mentoring and patience throughout my years of study have brought this thesis to fruition. My gratitude also goes to my committee members Dr. Ching-Hua Huang, Dr. Yongsheng Chen, Dr. Nian Liu, and Dr. Xing Xie for their time and precious comments on my research.

I would like to thank my friends and colleagues Dr. Bopeng Zhang, Yue Zhao, and Ming Liu for their inspiration and help with my research, study, and life. I thank every student in Dr. Crittenden's group, staff in Brook Byers Institute for Sustainable Systems, and colleagues in the department, Weiqiu Zhang, Dr. Jinming Luo, Su Liu, Osvaldo Broesicke, Junchen Yan, Zefang Chen, Dr. Xin Guo, Dr. Zhongming Lu, Yaye Wang, Thomas Igou, Michael Chang, Susan Ryan, Gay Burchfield and Kathryn Jonell for building such a wonderful culture and environment. I also thank my collaborators, visiting scholars Dr. Ruzhen Xie, Dr. Xiang Tu and Dr. Can Wang. I am also indebted to Dr. Guangxuan Zhu for his support on lab and instruments management.

My special thanks go to my friends Yijiong Rong, Chen Sun, Jinliang Li, Tongbo Chen, Xu Wang, Fan Xiang, and Dr. Jingyuan Zhang. Your friendships are invaluable to my life.

Last but foremost, my biggest thanks and love go to my girlfriend Zhou Maxiaoyun, my uncle Huang Gang and my parents Meng Wei and Huang Jing, without whose guidance and support I would not be here. Your love means everything to me.

TABLE OF CONTENTS

LIST OF TABLES

LIST OF FIGURES

LIST OF SYMBOLS AND ABBREVIATIONS

AC	Alternating current
AEM	Anion exchange membrane
AFM	Atomic force microscope
AOP	Advanced oxidation process
CEM	Cation exchange membrane
COD	Chemical oxygen demand
CV	Cyclic voltammetry
DC	Direct current
DI	Deionized
EAOP	Electrochemical advanced oxidation process
EE	Electron efficiency
EE/O	Electrical energy requirement for one order magnitude degradation
EG	Ethylene glycol
HPLC	High-performance liquid chromatography
IEC	Ion exchange capacity
LSV	Linear sweep voltammetry
NHE	Normal hydrogen electrode
PEM	Proton exchange membrane
PTFE	Polytetrafluoroethylene
ROS	Reactive oxygen species
SCE	Standard calomel electrode
SEM	Scanning electron microscope

SHE	Standard hydrogen electrode
SRP	Standard reduction potential
TOC	Total organic carbon

SUMMARY

Electrochemical oxidation has been used as a wastewater treatment method to remove organic contaminants for decades. During electrolysis, electron-rich organics are directly oxidized on anode surface and/or indirectly oxidized by oxidants that generated from the anode. Electrochemical oxidation is considered highly efficient for chemical oxygen demands (COD) reduction, especially for the destruction of emerging contaminants that are refractory to conventional methods. However, its large-scale applications are hampered by high electrode cost, high energy consumption, and low oxidation efficiency. Electrochemical advanced oxidation process (EAOP) is a new type of electrochemical oxidation. As an indirect electrochemical oxidation method, EAOP can generate hydroxyl radicals ($HO^{\cdot}$) from water on the anode. Hydroxyl radicals is a highly reactive oxidant that can react with nearly all organic contaminants and eventually mineralize them to CO_2 and H_2O non-selectively in ambient pressure and atmospheric temperature.

This study focuses on advancing the understanding of the electrochemical oxidation systems and developing EAOP a more commercially applicable technology. The efforts include: first, develop novel anode materials that can generate more hydroxyl radicals; second, investigate and improve in-reactor mass transfer process to increase the overall oxidation efficiency; and third, develop a novel electrochemical system that can significantly lower the energy consumption. To be specific, novel inactive semiconductor-based anode materials are fabricated. These anodes include TiO_2-based SnO_2-Sb/polytetrafluoroethylene resin (FR)-PbO_2, blue TiO_2-based SnO_2-Sb etc., are promising

to generate hydroxyl radicals with lower energy input and better stability. The mass transfer impact is quantitatively investigated regarding the hydrodynamic parameters. A mathematical model associated with electrochemical oxidation kinetics and mass transfer impact is established and validated with experimental data. A novel three-dimensional electrochemical system is developed with the integration of meshed electrodes and proton exchange membranes. In contrast with the conventional two-dimensional system, the oxidations in the three-dimensional system do not require additional electrolytes. Moreover, the three-dimensional configuration can significantly lower the overall energy consumption of using electrochemical method for wastewater treatment.

CHAPTER 1. INTRODUCTION

In the past decades, the development of industries brought tremendous wealth to the society and industries have become more complex than ever before. The problem brings to environmentalists is that most industries' factories produce wastewater and different wastewater streams contain various contaminants, especially organic contaminants. As well as the growing discharge of wastewater from the agriculture and human activities, how to treat these wastewaters become an urgent and grand challenge global issue and concern to be solved [1-3].

Biological treatment methods have been extensively developed for decades and they have been widely implemented as the technology to treat organic (as of COD and TOC) and ammonia in wastewater. However, it becomes ineffective when wastewater contains very high strength COD and lack of necessary nutrition for biomass. The operation of the bio-reactor requires extensive experience and, in many cases, post-treatment facilities are also required. On the other hand, many industries including paper mills, power plants, hospitals, dye industries, etc. produce complex organic products and they eventually end up in the wastewater [4-6]. Many of these organics pose refractory properties to biological treatment, such as antibiotics, fluorinated compounds, etc. Advanced treatment technologies are required for these industries to meet the discharge standards [7,8].

Over past decades, research efforts have been focused on developing more effective treatment technologies to totally remove persistent organics from wastewater. In this context, advanced oxidation processes (AOPs) received extensive attention [9,10]. AOPs produce highly reactive hydroxyl radicals ($HO\cdot$) in ambient temperature and atmospheric

pressure in aqueous phase [11-13]. Hydroxyl radical is a highly electrophilic specie and can react with almost all organics non-selectively. Hydroxyl radical is the second strongest oxidant ever known after fluorine, displaying a high standard reduction potential $E^0(H_2O/HO\cdot) = 2.78V/SHE$ and the rate constants for hydroxyl radicals with most organics are in an order of 10^6 to $10^{11}\ M^{-1}s^{-1}$ [14]. In addition, hydroxyl radicals has a very short half-life in nanoseconds which makes it self-eliminated in the system, is another advanced of using AOPs. Today, the most common AOPs are chemical-based and UV-based includes H_2O_2/O_3, nanobubble O_3, chemicals activated persulfate, UV/H_2O_2, UV/HOCl, UV/persulfate, UV/TiO_2, Fenton's reaction-based methods and electrochemical oxidation methods [11-16].

In the past decade, electrochemical oxidation (EO) and electrochemical advanced oxidation processes (EAOPs) have gained increasing attention as promising treatment technologies [17]. The former is also called anodic oxidation (AO) where organics can be directly oxidized on the anode surface by direct electron transfer reactions (direct oxidations) and/or indirect oxidation by other anodic generated reactive oxygen species (ROSs) weakly physisorbed on anode surface or diffused into the bulk solution. These ROSs includes active chlorine species, hydrogen peroxide, ozone, persulfates and hydroxyl radicals [18,19]. Primarily, current researches are focusing on the development of novel anode materials since the anode is the fundamental of oxidation reactions in the process [20]. However, although the production of radicals is important and the fundamental aspect in EAOPs, the utilization of these radicals for reactions is equally important and the mass transfer process is extremely important during the process of organic destruction. The half-

life of radicals are too short and in EAOPs they are mainly on the surface or near the surface of the anode, organics must be transported to the anode for more efficient reactions.

On the other hand, treatment energy (operational energy) is of great concern for all electrochemical-based technologies. Seldom researches have revealed applicable approaches to effectively reduce the energy requirement of all operational parameters, especially the most important one regarding electro-system: applied (cell) voltage. Therefore, due to the high capital and operation costs, the current implementation approach is to combine treatment strategies including biological processes, chemical coagulation, electrocoagulation, and other membrane processes to optimize the overall treatment facilities [21-23].

In this dissertation, a general approach of conventional EAOP which is classified as a two-dimensional electrochemical system is studied and the mass transfer impact is hence evaluated quantitatively. Moreover, a novel approach of using a three-dimensional electrochemical system is introduced to solve some shortcomings of the conventional systems. The application of EO/EAOPs in disinfection usage is also discussed in this dissertation. To be specific, the contains are introduced as follows.

In Chapter 2, the objectives and merits of this research are discussed and described.

In Chapter 3, the current research efforts on EO and EAOPs are summarized, especially the extensive research focus on anode materials.

In Chapter 4, a conventional two-dimensional system is developed and applied for an antibiotic treatment. A novel anode material is developed. The mass transfer impact is quantitatively evaluated of using an effectiveness factor approach.

In Chapter 5, a novel proton exchange membrane and meshed electrodes three-dimensional system is proposed. A mathematical model combined with mass transfer impact aspect is used to further understand the reaction kinetics in the system. A comprehensive comparison of EAOPs and AOPs regarding the EE/O.

Chapter 6 presents the application of EO in disinfection purpose. Algae contaminated wastewater is treated, and modeling rationality is provided to simulate the electrochemical oxidation processes during the degradation. Additionally, a new type of organics treatment: deuterated compounds destruction is attempted for using UV/H_2O_2 and a general approach of accessing their second-order rate constants by using the kinetic isotope effect is proposed.

Chapter 7 summarizes findings in the dissertation and recommends future research direction.

CHAPTER 2. RESEARCH OBJECTIVES

In this chapter, a high-level research objective is described, and the originality and merits of the research are also discussed.

2.1 Research Objectives

The overall research objective is to develop electrochemical advanced oxidation processes (EAOPs) as more commercially viable technologies. Throughout my research, I have applied integrated methodology by combining theoretical modeling and simulation with experiments. Data collected from experiments are used to validate mathematical models that provide more insights into underlying physical processes. Applying developed models renders predictive power and potential guidance to further experiments.

Specifically, a comprehensive literature review suggested that the fundamental of EAOPs development is the anode materials. Mass transfer process has a big impact on the overall oxidation efficiency. Following objectives are proposed.

1. Develop novel electrode materials that boost hydroxyl radical generation.

2. Investigate mass transfer impact to electrochemical oxidation quantitatively. Improve mass transfer using computational fluid dynamic simulations (class I and class II electrochemical systems).

3. Investigate the feasibility of using a three-dimensional electrode system for wastewater treatment, the configuration and its oxidation efficiency regarding different electrode materials and operational conditions (class III electrochemical system).

2.2 Merits of the Research

The findings of this dissertation are original and have deepened the understanding of EO and EAOPs. Specifically, the knowledge gained from this dissertation is dedicated to the development of better performing electrochemical systems and improving EAOPs through the following achievements:

1. Developed a novel TiO_2 nanotubes-based/SnO_2-Sb/PTFE resin-PbO_2 anode material that applicable for emerging contaminants treatment.
2. The mass transfer impact in the conventional two-dimensional system is quantitatively investigated and an effectiveness factor is derived and used to evaluate this impact. This rational approach can be used for all electrochemical system.
3. Developed a novel blue TiO_2 nanotubes-based/Aged SnO_2-Sb anode material that applicable for wastewater treatment.
4. Developed a novel three-dimensional electrochemical system that utilized meshed electrodes (gauze type) and proton exchange membrane configuration. Demonstrated the feasibility and rationality of using this system for wastewater treatment. Illustrated the possible reaction kinetics.
5. The feasibility of using EO for algae contaminated wastewater treatment is investigated and a rational modeling approach regarding active chlorines and hydrogen peroxide generation is developed.
6. The treatability of deuterated compounds of using UV/H_2O_2 is interpolated. A general approach of using kinetic isotope effect to access the second-order rate constants is proposed.

CHAPTER 3. RESEARCH BACKGROUND

3.1 General Review of Electrochemical Oxidation

The study of electrochemical oxidation for wastewater treatment is first original back to 19th century when the electrochemical decomposition of cyanide was investigated [24]. Before using EO for the treatment of organics, it was mainly used to recover heavy metal purposes [25]. Extensive investigation of technology sprinted after the 1970s. During the last decades, the researchers are mainly focusing on the efficiency in oxidizing various contaminants on different electrode materials, improvement of the electrocatalytic activity and electrochemical stability of electrode materials, investigation of factors affecting the process performance and exploration of the mechanisms and kinetics of contaminants degradation [26,27]. Bench-scale experiments are mainly focusing on the behaviors of the anode materials fabrication rather than the cathode's because the oxidation reactions which take place on the anode side is the focus of these systems.

In general, any EO and EAOP system requires an anode, a cathode, a closed circuit, a power supply, and a target treatment cell (can be a beaker, a reservoir or a tank in the bench, pilot and industrial scales, respectively) [26-28]. A general sketch shows in Figure 1.

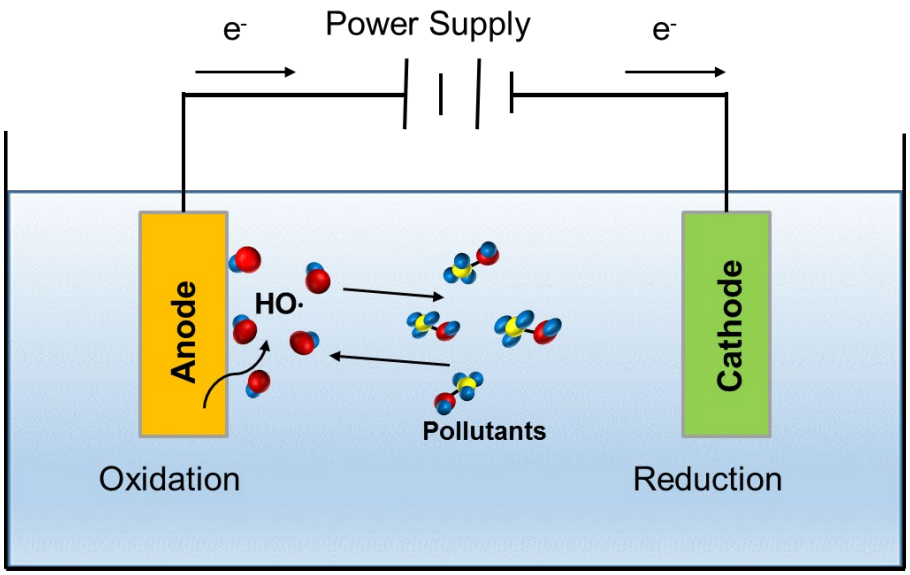

Figure 1 – A general sketch of a conventional two-dimensional electrochemical oxidation system in bench scale. The system contains an anode, a cathode, a circuit, and a power source. The pollutants can be rather oxidized on the anode surface or in the bulk solution.

The development of electrochemical oxidation is following the development of chemical oxidation since the generation of chemicals in-situ is more convenience for the treatment facilities. In principle, any success chemical oxidation should have its electrochemical counterpart. The converse should also be true providing the specific chemical oxidant. In practice, these two technologies are actually not parallel but almost entirely complimentary, a situation which assuredly changes as knowledge of the factors influencing chemical and electrochemical oxidation increases [29,30].

A large number of variables of the electrochemical procedure has been determined, the advantages of EO are generally numerous. The advantages include: convenience in work-up (there is no chemical oxidant or its products to remove which means that work up in many cases requires removal of only the solvent and electrolyte); relatively low cost (neglecting the capital cost of equipment, including items such as stable power supply,

potentiostat, voltmeter, ammeter, coulometer, reactor cell and electrodes; power is relatively inexpensive compared to chemical reagents); and yield (oxidation efficiency). In addition, owing to its complementary nature, unusual reaction products may be obtained from the electrochemical techniques such as the oxidation of electrolytes etc. [31,32]. For comparison, the reactions of several chemical oxidants will be discussed in the anodic oxidation section.

3.2 Anodic Oxidation

The anodic oxidation (AO) involves the pollutants oxidation by direct electron transfer to the anode surface M and heterogeneous reactive oxygen species (ROSs) produced as intermediates of oxidation of water to oxygen, including the powerful physisorbed hydroxyl radicals at the anode surface, denoted M(HO·) and weaker oxidants like hydrogen peroxide and ozone from water discharge at the anode surface.

$$M + H_2O \rightarrow M(HO\cdot) + H^+ + e^- \quad (1)$$

$$2M(HO\cdot) \rightarrow 2MO + H_2O_2 \quad (2)$$

$$M + H_2O \rightarrow M(HO\cdot) + H^+ + e^- \quad (3)$$

The efficiency of AO is highly dependent on the mass transfer of the contaminants from the bulk to the anode surface or its vicinity [33-35]. Moreover, studies performed during the last twenty years have shown the strong influence of the anode materials nature on both efficiency and selectivity. Two very distinct behaviors of organic pollutants degradation depending on the anode material have been reported: (1) partial organic

degradation along with the formation of byproducts and final products, and (2) large or total organic mineralization to carbon dioxide and water and other inorganic ions together with the production of refractory byproducts. The more accepted explanation of this kinetic was earlier proposed by Comninellis [36]. The model considered the interaction of M(HO·) with the anode surface as the responsible for the existence of two types of anode materials which is the active anode materials with low oxygen evolution overpotentials and inactive anode materials with high oxygen evolution overpotentials in which M(HO·) are so weakly absorbed at the anode surface and can react with organics on or near the surface of anode.

The AO process can be improved by the oxidation of electrolytes and general oxidants such as active chlorine species, persulfate, perphosphate, percarbonate, peroxides etc. [33,37]. While these ROSs are produced rather on anode or cathode side, salts can already compose the wastewater matrix or alternatively, they can be externally added into the system. In the presence of these indirect oxidation processes, the AO is generally called mediated oxidation. Active chlorines species are the main indirect oxidation agents that employed in wastewater treatment because all water streams contain chloride ions.

$$2Cl^- \rightarrow Cl_2 + e^- \tag{4}$$

$$Cl_2 + H_2O \rightarrow HClO + H^+ + Cl^- \tag{5}$$

In the solution, the HClO is in equilibrium with hypochlorite with a pKa of 7.5. Since HClO ($E^0 = 1.49V/SHE$) and Cl_2 ($E^0 = 1.36V/SHE$) exhibit higher redox potentials than ClO^- ($E^0 = 0.89/SHE$), the oxidation of organics should be faster in acidic than in alkaline media [38,39]. HClO content can be decreased due to their electrochemically

conversion to chlorate ion with the consequent attenuation of organics degradation since chlorate is not a good oxidant for organics at ambient temperature [24,40].

$$Cl^- + HO\cdot \rightarrow ClO^- + e^- \quad (6)$$

$$ClO^- + HO\cdot \rightarrow ClO_2^- + e^- \quad (7)$$

$$ClO_2^- + HO\cdot \rightarrow ClO_3^- + e^- \quad (8)$$

$$ClO_3^- + HO\cdot \rightarrow ClO_4^- + e^- \quad (9)$$

The strong persulfate, perphosphate, and percarbonate can also be produced via indirect oxidations on inactive anodes.

$$2SO_4^{2-} \rightarrow S_2O_8^{2-} + 2e^- \quad (10)$$

$$2PO_4^{3-} \rightarrow P_2O_8^{4-} + 2e^- \quad (11)$$

$$2CO_3^- \rightarrow C_2O_6^{2-} + 2e^- \quad (12)$$

The production of hydrogen peroxide and its stability depend on factors such as cell configuration, electrode properties, and operational conditions. Parasitic reactions such as hydrogen peroxide electrochemical reduction at the cathode surface in much lesser extent, hydrogen peroxide disproportion in the bulk solution can occur using both undivided and divided electrochemical cells, diminishing the hydrogen peroxide accumulation the system [33,34,41].

$$H_2O_2 + 2H^+ + 2e^- \rightarrow 2H_2O \quad (13)$$

$$2H_2O_2 \rightarrow O_2 + 2H_2O \quad (14)$$

3.3 Anode Materials

As a general rule, the higher potential for oxygen evolution potential of the anode materials, the weaker is the interaction of M(HO·) with the anode surface and the higher is the chemical reactivity towards organics oxidation [42]. Ruthenium dioxide (RuO_2), Iridium dioxide (IrO_2), Platinum (Pt), graphite and other sp2 carbon-based electrodes are typical examples of active anodes and usually have overpotentials lower than 1.8V/SHE as can be seen in Table 1. Carbon-based materials cannot be robust enough against incineration, sometimes even when the low current density conditions [43]. On the other hand, lead dioxide (PbO_2), tin dioxide, (SnO_2), boron-doped diamond (BDD) and sub-stoichiometric TiO_2 electrodes can be considered as inactive electrodes presenting the oxygen evolution overpotential from 1.8 to 2.6 V/SHE. The BDD anode is the most potent inactive and commercially viable anode so far, thereby being considered the most suitable anode for AO [33,40,44]. However, the fabrication of this anode is very high which hampers it large scale applications [45]. The characteristics of BDD electrodes including the substrate nature, e.g. silicon (Si), titanium (Ti), niobium (Nb), the boron content, the sp3/sp2 rationed the BDD layer thickness can strongly influence the organics oxidation [46]. Recently, the substoichiometric TiO_2 has been reported as a promising anode material. There are several sub-oxides of TiO_2, collectively known as Magneli phases (Ti_nO_{2n-1}, $4 \leq n \leq 10$), where the most conductive compounds of the series are Ti_4O_7 and

Ti_5O_9. Ceramic Magneli phase electrodes mainly consisting of Ti_4O_7 are commercially available and is known as the tradename Ebonex® [47,48].

For graphite electrodes, the maximum current efficiency (CE) obtained was as high as 70% at very low current densities ranging from 0.03 to 0.32 A/m^2 [49]. When current densities increased to 10 to 100 A/m^2, the CE values are only 6-17%. Despite the satisfactory results obtained in oxidizing simple inorganic contaminants at low current densities, Pt electrodes show poor efficiencies in anodic oxidation of organic contaminants [50]. The carbon black addition was found to enhance the performance of Ti/Pt anodic oxidation of aqueous phenol significantly. As mentioned before, IrO_2 has been widely investigated as an electrocatalyst for O_2 evolution. The low current efficiency is expected.

PbO_2 is the most widely investigated anode material for EO. Usually, PbO_2 electrodes are prepared either by anodically polarizing metal lead in H_2SO_4 solutions or by electrochemically coating PbO_2 films on Ti substrate. To increase the activity PbO_2 is sometimes doped by Bi, Fe, Ag or other active metals [51]. For oxidation of organics, PbO_2 is very efficient with a reasonable value of current efficiency. The operational current density is also of reasonable value, 80-160 A/m^2. PbO_2 electrodes are relatively cheap and effective in oxidizing contaminants. The only concern for this material is the formation of a lead ion from the electrochemical corrosion and may pose toxicity when it ends up in the downstream [52,53].

Pure SnO_2 is an n-type semiconductor with a band gap of about 3.5 eV. The valence band arises due to the overlap of filled oxygen 2p levels. The tin 5s states are at the bottom of the conduction band [54]. This kind of oxide exhibits very high resistivity at room

temperature and thus cannot be used as an electrode material directly. However, its conductivity can be improved significantly by doping Ar, B, Bi, F, P or Sb [27]. In electrochemical application, Sb is the most common dopant of SnO_2. Doped SnO_2 films are usually used as transparent electrodes in high-efficiency solar cells, far IR detectors, and transparent heating elements [55]. The conductive SnO_2 films can be prepared by vapor deposition, sputtering, spray pyrolysis, sol-gel, and brush-dry-bake techniques [56]. The onset potential for oxygen evolution overpotentials on Sb-doped SnO_2 is about 1.9 V/SHE, similar to PbO_2. Kotz et al first proposed Sb-doped SbO_2 coated Ti electrode [57]. The CE obtained was about 5 times higher than that on Pt since Pt is too active. Many researchers reported the CE for this electrode could as high as 58% - 71% regarding the degradation of phenol and benzoic acid. Nevertheless, it has been reported there was no substantial difference in activity between SnO_2-Sb_2O_5 and PbO_2 in treating the landfill leachate. This might be associated with the presence of high concentrations of chlorides in this type of waste. Despite the high efficiency for contaminants oxidation, SnO_2-Sb electrodes lack sufficient electrochemical stability just like PbO_2. Lipp and Pletcher conducted a long-term test of SnO_2-Sb in 0.1 M H_2SO_4 solution at a constant voltage 2.44 V/SHE and found the current dropped from initial 0.2 to about 0.1 A within a few hours and to 0.06 A after 700 hours [58]. It was also reported that the service life of Ti-based SnO_2-Sb was only 12 h under an accelerated life test performed at a current density of 1000 A/m^2 in a 1 M H_2SO_4 solution. At 10,000 A/m^2, this electrode can only last a few minutes. Although the addition of IrO_2 into the SnO_2-Sb mixture increased the service life significantly, the resulting electrodes have only a 1.5 V oxygen evolution overpotential [59].

Pure TiO_2 has a band gap of 3.05 eV and thus shows poor conductivity at room temperature. TiO_2 is usually used as a photocatalyst in wastewater treatment. By doping with Nb and/or Ta, TiO_2 conductivity can be dramatically increased to be used as an electrocatalyst for contaminants oxidation. This type of electrodes is usually followed by annealing the films at 650 – 800 degrees in the presence of H_2 and a small amount of water vapor to reduce the Nb(V) to Nb(IV). The preferred molar concentration of (Nb+Ta) in the oxide coating is 2-6%. TiO_2 electrodes are stable at low current densities but their lifetime is significantly shortened when operated at high current densities [60,61]. Another conductive titanium oxide is Ebonex that is also able to serve as anode material. Ebonex is a non-stoichiometric titanium oxide Ti_4O_7 and Ti_5O_9, and made by heating TiO_2, and surface passivation under extreme conditions may be an issue [62].

Table 1 – Potential of oxygen evolution for various anode materials, V/SHE

Anode materials	Values (V)	Conditions	Reference
Pt	1.3	0.5 M H_2SO_4	[63]
Pt	1.6	0.5 M H_2SO_4	[63]
IrO_2	1.6	0.5 M H_2SO_4	[65]
Graphite	1.7	0.5 M H_2SO_4	[64]
PbO_2	1.9	1 M $HClO_4$	[66]
SnO_2	1.9	0.5 M H_2SO_4	[67]
Pb-Sn (93:7)	2.5	0.5 M H_2SO_4	[63]
Ebonex (titanium oxide)	2.2	1 M H_2SO_4	[68]
Si/BDD	2.3	0.5 M H_2SO_4	[69]
Ti/BDD	2.7	0.5 M H_2SO_4	[70]
DiaChem	2.8	0.5 M H_2SO_4	[63]

3.4 Three-Dimensional System Development

Reactors based on a porous three-dimensional electrode are contributing substantially to the electrochemical approach. Such electrodes can have a very high surface area as well as leading to more turbulent mass transport conditions adjacent to the electrode surface. This combination of properties leads to a much-enhanced rate of electrolysis as many are seen quantitatively by comparing the expressions for the mass transport controlled current [71,72]. At two-dimensional electrode,

$$I_L = nFAk_fC \tag{15}$$

At three-dimensional electrode,

$$I_L = nFA_eV_ek_fC \tag{16}$$

Where n is the number of electrons transferred in the electrode reaction, F is the Faraday constant, A is an area of a plate electrode, k_f is the mass transfer coefficient, c is the concentration of reactant in solution, A_e is the specific electrode surface area per volume (m^2/m^3). And V_e is the volume of reactor. The three-dimensional electrode area available in many forms. Many are available in both carbon and a range of metals and the materials available may be extended further by plating and other coating methods (e.g. metal coated glass microspheres and plated polymetric foams have been used extensively. The examples of such configuration of three-dimensional systems are rather porous type electrode materials. Moreover, cells have been constructed with both planar and cylindrical geometry. They have been operated in both the flow through (parallel electrolyte and

current flow) and the flow by (electrolyte flow perpendicular to the current flow) modes. In the case of the particulate beds, they may be operated (1) as packed beds when the particles are in continuous, intimated contact or (2) as moving beds including slurries, tumbled particles, vibrated or fluidized beds. The latter leads to better mass transport but the intermittent contact between particles can lead to problems of conductivity in the electrodes have appeared [73-75].

3.5 Summary

Electrochemical oxidation has been extensively studied for wastewater treatment applications and proved a promising technology for organic removal. However, the large-scale applications are hampered by poor anode materials, short service life, high fabrication cost, and low oxidation efficiency. Researchers in the past were mainly focused on investigated the treatability of certain compounds on certain electrode materials. However, the break-through study on the improvement of oxygen evolution overpotentials does not emerge. SnO_2-Sb as a promising electrode material can be coated on the surface of various metals substrate and the coating methods are promising to sustain the activity and stability of the coating layer. Ti exhibit a good base substrate and hypothetically, TiO_2 and another reductive form of Ti can provide high current efficiency and stability. On the other hand, most of the studies rather mentioned the impact of the mass transfer of the mass transfer controlled current. Seldom studies revealed interconnection between mass transfer and overall oxidation efficiency, and furthermore, quantify this impact. For the three-dimensional electrochemical system, previous studies are primarily focused on the porous anode configuration (active anode materials) and investigated flow-by and flow-through modes. Few studies focused on integrated system configuration to answer several

fundamental questions which the obstacles of the large-scale application of EO are: high energy requirement mainly caused by high cell voltage requirement, poor hydroxyl radicals generation regarding novel anode materials and problematic mass transfer configurations.

CHAPTER 4. TWO-DIMENSIONAL ELECTROCHEMICAL OXIDATION DEVELOPMENT: REACTION KINETICS AND MASS TRANSFER IMPACT

4.1 Abstract

Electrochemical oxidation has been proposed for the destruction of organic contaminants; however, this process is hampered by low oxidation efficiency and high energy costs. Moreover, the hydrodynamic performance of an electrochemical system may impact the oxidation rate by influencing the mass transfer process. This work introduces a TiO_2-based SnO_2-Sb/polytetrafluoroethylene resin (FR)-PbO_2 electrode that can destroy the antibiotic ofloxacin in a continuous-flow reactor. The electrode has a large overpotential for oxygen evolution (1.5 V vs. normal hydrogen electrode, NHE), which minimizes O_2 production and favors hydroxyl radical (HO·) generation. Our results indicate that the major pathway of ofloxacin destruction occurs through an addition of a hydroxyl radical to the ring structure and show that the overall oxidation efficiency reaches values as high as 88.45%. Growing TiO_2 nanotubes on Ti material increases the conductivity of the electrode, whereas the electrical efficiency per order (EE/O, kWh/m^3) for oxidation is decreased by 20.2%. The effects of current density, initial concentration, pH value, and electrolyte concentration are investigated. The reaction kinetics of ofloxacin follow the pseudo-first-order kinetic model. A differential column batch reactor (DCBR) that can simulate various alternative flow conditions is used for all bench experiments. The effects of fluid velocity and electrode spacing on the oxidation rate are determined to investigate the impact of mass transfer by measuring the mass transfer coefficient k_f, and a

dimensionless effectiveness factor Ω (between 0-1) is then derived to quantify this impact. Our experiments and calculations indicate that the mass transfer reduces the oxidation rate by more than 55% (Ω <0.55) for an electrode spacing of 1 cm at a fluid velocity of 0.033 m/s. The method of using Ω to quantify the mass transfer impact incorporates the scaling laws for mass transfer and is independent of the system scale, which makes it feasible for using different electrode types in forced-flow electrochemical systems from bench to pilot scales.

4.2 Introduction

Pharmaceuticals and personal care products (PPCPs) have been recognized as detrimental pollutants because of their potentially hazardous impacts on humans and the environment [76-80]. Many studies have reported the presence of PPCPs in aquatic environments worldwide [76-78]. Antibiotics are among the commonly detected pharmaceuticals in wastewater and other bodies of water subject to pollution from drug manufacturers. These chemicals are considered contaminants because they can lead to antibiotic-resistant pathogen communities [79,80], which can spread their genes to indigenous microbes and increase their antibiotic resistance ability [81-85]. Accordingly, the removal of antibiotics in aquatic environments is important. Ofloxacin ($C_{18}H_{20}FN_3O_4$) is one of the most commonly used second-generation topical fluoroquinolones [86]. This antibiotic is a pyridine carboxylic acid derivative of nalidixic acid and has a tricyclic structure with a methyl group at the C-3 position in the oxazine ring. Similar to many other antibiotics, ofloxacin possesses broad-spectrum antibacterial activity that prevents it from

being removed effectively by biological treatment plants [87]. Advanced treatment technologies are required to remove/destroy ofloxacin in wastewater.

Advanced oxidation processes (AOPs) are promising technologies for the destruction of organic contaminants in aqueous systems [84, 88, 89]. AOPs produce hydroxyl radicals (HO·) at ambient temperature and atmospheric pressure. Electrophilic hydroxyl radicals will react non-selectively with electron-rich organic compounds via hydroxylation and dehydrogenation until the electron-rich organic compounds are completely mineralized to H_2O and CO_2 [90-92]. Consequently, hydroxyl radicals can attack a variety of sites on ofloxacin molecules (e.g., moieties, such as the quinolone moiety) and eventually mineralize them.

Electrochemical oxidation processes have shown an outstanding ability to oxidize and destroy a variety of toxic and refractory organic contaminants [93-96]. These contaminants can be oxidized by the chemisorbed "active oxygen" or "higher oxide" formed on the surface of anodes known as active anodes (e.g., Ti/IrO_2, Ti/RuO_2, and Pt) [97, 98]. The contaminants can also interact directly with the reactive oxygen species (ROS) physisorbed on the surface of anodes known as inactive anodes (e.g., Boron-doped diamond (BDD), Ti/SnO_2, and Ti/PbO_2) [97, 99-101]. Both of these anodes could form organic films and cause anode-fouling during organic contaminant degradation. In addition to this aspect, inactive anodes have many other advantages over active anodes, such as lifetime and oxidation efficiency [101-103]. In recent years, extensive studies have been conducted on inactive anodes with the objective of improving ROS generation [97, 99-102].

Quantum theories have been used to explain the creation of ROS at the anode. During electrolysis, electrons flow from the anode and produce valence band holes (h^+) if the conduction band has a larger energy level than the valence band (such as with a semiconductor). The band gap determines the power of the excitons, i.e., the conduction band electrons e^-_{cb} and valence band holes h^+. The valence band holes, in turn, react with water and create ROS [104, 105]. Anodic oxidation can generate ROS, including oxygen (O_2), hydrogen peroxide (H_2O_2), ozone (O_3) and hydroxyl radicals ($HO\cdot$), from water [106, 107]. However, dissolved O_2, among other ROS, is a poor oxidant unless it becomes involved in radical chain reactions that produce other powerful ROS. H_2O_2 and O_3 can create hydroxyl radicals via a variety of reactions; however, our main objective is to create h^+ with a high enough reduction power that it can directly react with water to create hydroxyl radicals. Thus far, BDD has been considered the best inactive anode. It has been shown that the BDD anode, which has a large band gap ($\Delta E = 5.45$ eV), can generate a lot of hydroxyl radicals and lead to a high oxidation efficiency in a variety of different organic contaminant treatments [108]. However, the fabrication of a BDD anode is costly and technically difficult. A titanium-based electrode constructed by coating the second layer with materials such as SnO_2-Sb exhibits relatively high oxidation activity [109, 110]. Pure SnO_2 is an n-type semiconductor with a band gap of 3.5 eV, and its conductivity increases significantly by doping the Sb material [111]. Applying a third outer layer of PbO_2 increases the electrochemical stability of the SnO_2-Sb electrode; moreover, it provides more surface sites for reactions [111, 112]. Ideally, every electron that flows out of the anode should create one hydroxyl radical. However, most h^+ and e^-_{cb} recombine before they can undergo chemical reactions on an electrode surface, and the energy supplied is simply

wasted. TiO_2 nanotubes (NT) representative of a novel material has been reported as an efficient catalyst in photolysis [113]. Reports have shown that NT exhibits good electron transportation properties and a much slower recombination speed for h^+ and e^-_{cb} [114]. Thus, it would be reasonable to suppose that NT is a candidate anode material for hydroxyl radical generation.

Although the degradation efficiency can be improved by fabricating a novel and active electrode to enhance electrochemical oxidation, the degradation rate of the observed contaminants is typically lower than that of theoretical calculations. A possible reason for this discrepancy is that theoretical batch experiments are usually conducted in a completely mixed system, such as a beaker with stirring. Compared with completely mixed systems, a forced flow electrochemical system, such as a plug flow reactor (PFR), is more realistic with respect to the high energy consumption required for mixing in a pilot scale system. However, in forced flow reactors, the mass transfer process will significantly influence the overall reaction rate because electrolysis usually occurs on the surface of the electrode and reactants are transported from the bulk solution to the surface [115]. Compared with the rate of mass transfer, surface reactions are typically much faster. A number of studies have reported that the hydrodynamic design of an electrochemical system will influence its oxidation/reduction efficiency, power requirements and total costs because of the mass transfer limitation [116-119]. However, few of these studies have quantified this mass transfer impact by investigating individual hydrodynamic parameters that characterize the reactor, such as electrode spacing and pumping fluid velocity, which is more important among other factors [119, 120]. Without understanding the relationship between oxidation efficiency and mass transfer, the total cost of different electrode types, reactor designs,

power requirements, etc. cannot be predicted. Therefore, it is important to investigate the impact of the mass transfer on the electrochemical oxidation rate and build a quantitative correlation between theoretical reaction rates and observed reactions rates.

In this study, we fabricate a TiO_2-based SnO_2-Sb/polytetrafluoroethylene resin (FR)-PbO_2 anode that has an overpotential for oxygen evolution higher than the oxygen-forming reduction potential (E^0 = +1.23 V), which means that our anode does not generate O_2. By increasing the applied potential, anodic reactions generate more powerful ROS, such as H_2O_2 (E^0 = +1.77 V), O_3 (E^0 = +2.07 V) and hydroxyl radicals (E^0 = +2.74 V) [121, 122]. Our novel approach to improving the electrochemical performance of anodes involves (1) growing TiO_2 NT on Ti foil, (2) implanting a SnO_2-Sb layer on top of the NT layer, and (3) electrodepositing PbO_2 with polytetrafluoroethylene resin (FR). The electrochemical oxidation efficiency is investigated for various current densities, pH values, and electrolyte concentrations. The reaction kinetics are described using a pseudo-first-order kinetics model and a critical parameter for electrochemical systems: the electrical efficiency per order (EE/O), which is calculated to evaluate the impact of various effect factors. The impact of mass transfer is investigated by examining different electrode spacings and fluid velocities using a differential column batch reactor (DCBR), which simulates the flow condition of a PFR at the bench scale. In the present study, the laminar flow condition (Reynolds number, Re<1000) occurs, which is a real condition for most electrochemical systems [116]. The mass transfer coefficient k_f is calculated using a correlation proposed by Sonin and Probstein for the laminar flow condition [116]. A dimensionless effectiveness factor Ω is derived to quantitatively determine the impact of mass transfer, and it reflects the ratio of the observed reaction rate to the theoretical reaction rate.

4.3 Materials and Methods

All chemicals used in the experiments were analytical reagent grade or higher. Ofloxacin, ethylene glycol (EG), ammonium fluoride (NH_4F), potassium fluoride (KF), lead nitrate ($Pb(NO_3)_2$), tin (IV) chloride, and antimony (III) chloride were purchased from Sigma-Aldrich (St. Louis, MO, USA). The titanium foils (thickness: 0.25 mm, 99.5% purity) were purchased from Alfa Aesar, Haverhill, MA, USA. All solutions were prepared in deionized water (Milli-Q system, 18.2 MΩ – cm).

4.3.1 Electrode Fabrication

The electrode was fabricated in three steps.

Step 1. Grow the TiO_2 NT layer on the titanium foil. This step follows the procedure described by Chen et al. [113]. The titanium foil was polished using 2000 grit abrasive paper to obtain a flat surface. The foil was then chemically degreased and etched by immersion in methanol and then 6 M nitric acid solution for 5 and 10 min, respectively. The foil was then rinsed using ultrapure water and dried in air at room temperature. The NT array was prepared in a cylindrical electrochemical reactor (250 mL) that was continuously stirred using a magnetic stirrer. The titanium foil (20×50×0.25 mm) was used as an anode, and a platinum gauze electrode (40×40×0.5 mm) was used as a cathode for the electrode. The electrodes had a spacing of 20 mm, and the anodization temperature was 60 °C. Ethylene glycol antimony solution containing 0.5 w% NH_4F and 2 v% reagent grade deionized water was used to grow the TiO_2 nanotubes. The anodization was

galvanostatically performed using a potentiostat (PowerLab 2/20, AD Instruments) with a 10 mA/cm^2 current density for 60 min. The samples were then rinsed in ultrapure water and dried in a nitrogen gas stream. The anatase crystals were formed by calcining the NT in an oxygen atmosphere for 2 h at 500 °C, and then the NT was cooled at a rate of 1 °C/min and hereafter is referred to as the TiO_2-NTs foil.

Step 2. Fabricate Sb-doped SnO_2 intermediate layer over NT. The intermediate layer was created using the sol-gel method according to Lin et al. [102]. The molar ratio of $SnCl_4 \cdot 4H_2O$ to $SbCl_3$ in sol-gel was 10:1. The NT foil was dipped in the sol-gel for 10 min, dried under vacuum at 140 °C and calcined at 500 °C. This process was repeated 15 times before the anode was lastly annealed for 2 h at 500 °C.

Step 3. Electrodeposition of PbO_2 onto the NT-based SnO_2-Sb electrode. Electrodeposition for the final layer was conducted using an electrolyte containing 0.5 M $Pb(NO_3)_2$, 0.1 M HNO_3, 0.05 M KF and 0.4 mL/L polytetrafluoroethylene resin (FR). Anodization of the current density was 30 mA/cm^2 for 30 min at 60 °C.

4.3.2 Electrode Characterization

The surface morphology and composition were analyzed using a field emission scanning electron microscope with an energy dispersive spectrometer (FE-SEM, Zeiss Ultra 60 microscope). X-Ray diffraction patterns were measured using a Philips X' pert diffractometer, which was equipped with an Xcelerator module and Cu Kα radiation. X-ray photoelectron spectroscopy (XPS) spectra were measured using a Thermo K-Alpha

XPS system and a monochromatic Al Kα source to analyze the electrode surface at a depth of less than 5 nm near the surface. Linear sweep voltammetric (LSV) measurements were conducted at room temperature (25 ± 1 °C) in conventional three-electrode electrochemical cells driven by PARSTAT (Pine Wave Now) at a scan rate of 10 mV/s in 0.5 M H_2SO_4. Our anode served as the working electrode (1 cm × 1 cm), and platinum gauze and Hg/Hg_2Cl_2 (KCl) served as the counter electrode and the reference electrode, respectively. Hereafter, the anode created by following these steps will be referred to as the TiO_2-based SbO_2-Sb/FR-PbO_2 electrode.

4.3.3 Electrochemical oxidation experiments

Our electrochemical flow reactor was a differential column batch reactor (DCBR). A reservoir contained the test solution, which was pumped through the electrochemical cell and then returned to the reservoir. In principle, the DCBR acts as a differential slice of a plug flow reactor (PFR), in which the influent concentration is equal to the effluent concentration. The solution in the reservoir was recirculated using a peristaltic pump, and its flow rate was adjusted using a stroke rate controller. We sampled the influent, effluent and reservoir simultaneously, and their concentrations were similar for the different flow rates used in this study. Therefore, all our samples were collected from the reservoir. The TiO_2-based SnO_2-Sb/FR-PbO_2 electrode (2 cm × 5 cm) was used as the anode and a stainless steel foil (corrosion resistant 316) with the same shape and size served as the cathode. The electrode spacing varied between 0.5 and 3 cm. For each run, an aqueous ofloxacin solution (10-50 mg/L; the volume of solution in the reservoir was 300 mL) containing 0.005-0.5 M Na_2SO_4 electrolyte solution was used. The reservoir was

completely mixed (500 revolutions per minute), and the current density was controlled between 5-50 mA/cm^2 using Extech 382200. The DC power supply and the voltage varied between 4.5 and 8.6 V. The fluid velocity through the electrochemical cell was varied between 0.003 and 0.048 m/s and required a pumping rate between 30 and 576 mL/min, which corresponded to a reactor detention time of 10.3 min to 0.54 min. Samples were collected from the reservoir at various times during the electrochemical oxidation experiments. The concentrations of ofloxacin were determined using an HPLC-DAD system (Agilent Technologies, series 1200) equipped with a C18 column (Extend, 3.5 μm, 4.63 × 150 mm) operated at a flow rate of 1 mL/min. The mobile phase was composed of 15% HPLC-grade acetonitrile and 85% ultrapure water acidified with 5 mM H_3PO_4. A UV detector set at λ = 287 nm was used to detect the ofloxacin. The sample injection volume was 10 μL.

4.4 Results and Discussions

4.4.1 Morphology of the TiO_2-based SnO_2-Sb/FR-PbO_2 Electrode

Figure 2 displays the SEM images of the top view of the a) TiO_2-nanotube layer, b) SnO_2-Sb intermediate layer, and c) polytetrafluoroethylene resin (FR)-PbO_2 surface layer. Figure 2a shows that the nanotubes are uniformly arranged and have a high density. The top of the nanotube is open and presents circular and oval shapes. The diameters of the nanotubes are between 18 and 22 nm. This thin and uniformed nanotube layer provides tunnels for electrons to reach the inner titanium substrate. Only high-energy electrons that have sufficient power can pass through these tunnels, which theoretically increases the

band gap of the anode material. The image in Figure 2b shows the tube after dip coating 15 times using the sol-gel method and calcination of the Sb-doped SbO_2 intermediate layer covering the TiO_2 nanotube layer. The use of an intermediate layer can reduce the interface resistance between the inner substrate and outer PbO_2 and improve the electrochemical performance [123]. The morphology of the deposited FR-PbO_2 is shown in Figure 2c. The surface of the doped F^--PbO_2 is a compact and homogeneous film that covers the intermediate layer. Compact F^--PbO_2 has been shown to provide sufficient surface area and electrochemical oxidation performance [124]. During the electrodeposition of PbO_2, the substitution of active oxygen sites with F^- anion inhibited large crystal formation, which resulted in more surface area with more surface sites for reactions. Our deposited PbO_2 was uniformly arranged on the anode surface and had small crystalline shapes. The thickness of the PbO_2 layer was 71 μm, which was calculated based on the Faraday equation [125].

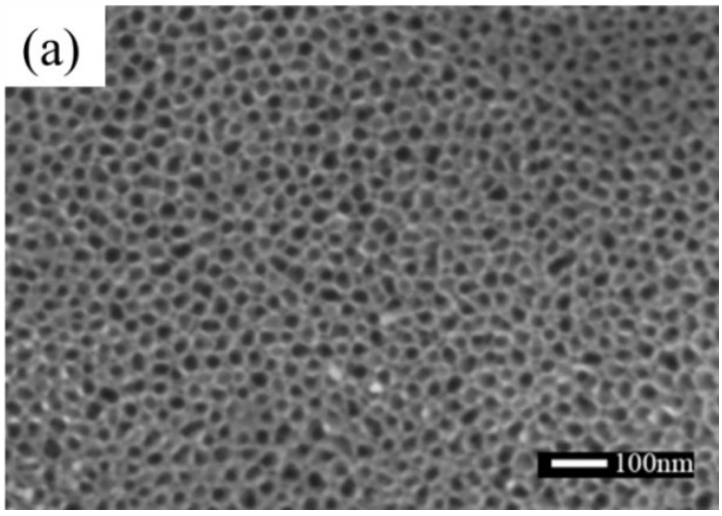

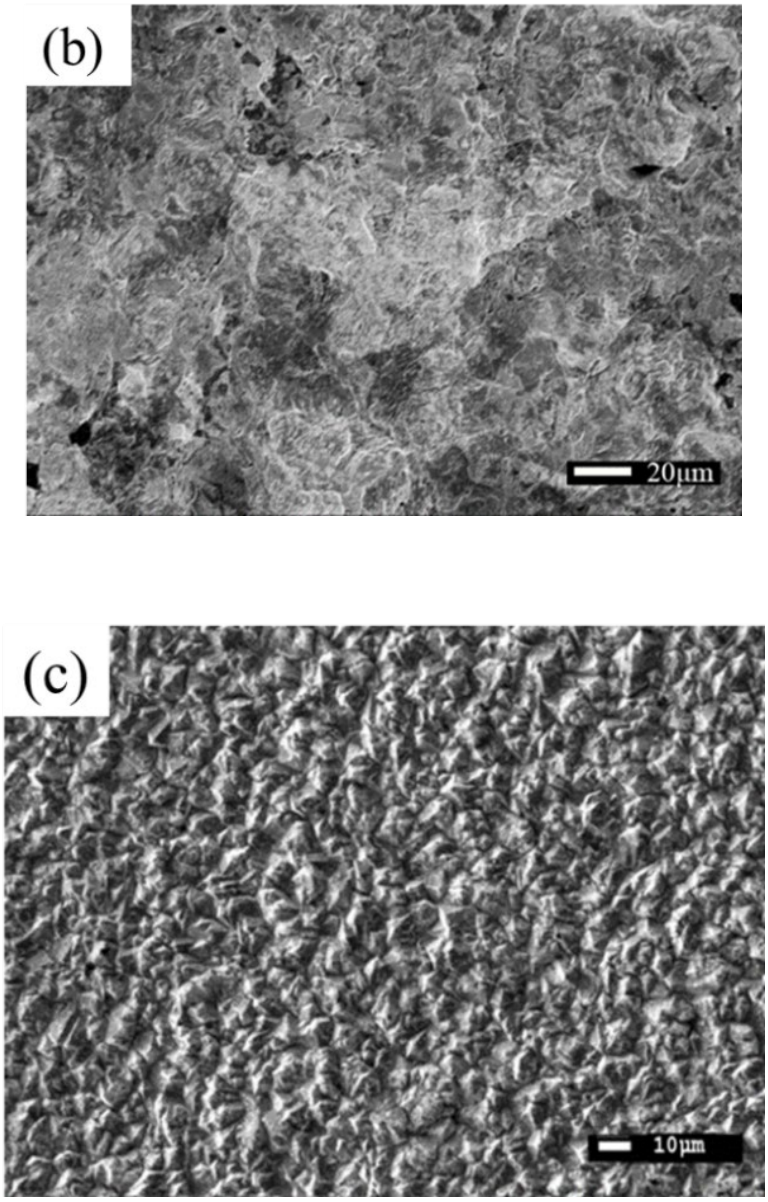

Figure 2 - SEM of the different layers of the electrode: (a) TiO_2 nanotube layer; (b) SnO_2-Sb intermediate layer; and (c) TiO_2-based SbO_2-Sb/FR-PbO_2 electrode surface.

4.4.2 Electrode characterizations

X-ray diffraction (XRD) was used to estimate the crystal size, and the results are shown in the Appendix. The XRD showed that the F^--PbO_2 on the surface had a β-PbO_2

crystallographic structure. The average crystal size of our electrode was calculated as 34.88 nm according to the Scherrer formula, whereas the average pure PbO_2 crystal size is 60.97 nm [126]. Accordingly, our electrode has smaller crystals and thus more active sites.

Linear sweep voltammetry (LSV) experiments were conducted to evaluate the electrochemical properties of our electrode. Figure 3 shows the current flow as a function of the applied potential on an electrode with/without a TiO_2 NT layer for the purpose of examining the impact of NT regarding ROS generation. The results of both electrodes indicated that a significant current flow did not occur until the voltage increased to 1.5 V. This 1.5 V overpotential for oxygen evolution is higher than the O_2 standard reduction potential (E^0 = +1.23 V), which demonstrates that our electrodes do not generate O_2. The LSV results match our bench experiment observations, which did not show significant oxygen/bubble creation during electrolysis. Moreover, the 1.5 V overpotential for the oxygen evolution of our electrode favors ROS generation, and it represents the lowest potential for a current flow that eliminates O_2 while also allowing for the generation of other ROS, i.e., H_2O_2 (E^0 = +1.77 V), O_3 (E^0 = +2.07 V) and (HO·) (E^0 = +2.74 V).

Figure 3 shows that using the TiO_2 nanotube layer on an electrode does not improve the performance of our electrode from an electrochemical characterization perspective because the SnO_2-Sb material (ΔE = 3.5 eV) in the intermediate layer actually has a larger band gap than the TiO_2/TiO_2 NT (ΔE = 3.05 eV) material. Growing the NT layer between the Ti substrate and SnO_2-Sb material does not further enlarge the band gap. However, by comparing the actual electrochemical performance of these electrodes, we find that using

the electrode with the NT layer will significantly increase the conductivity of the electrode and decrease the energy usage, i.e., electrical efficiency per order (EE/O).

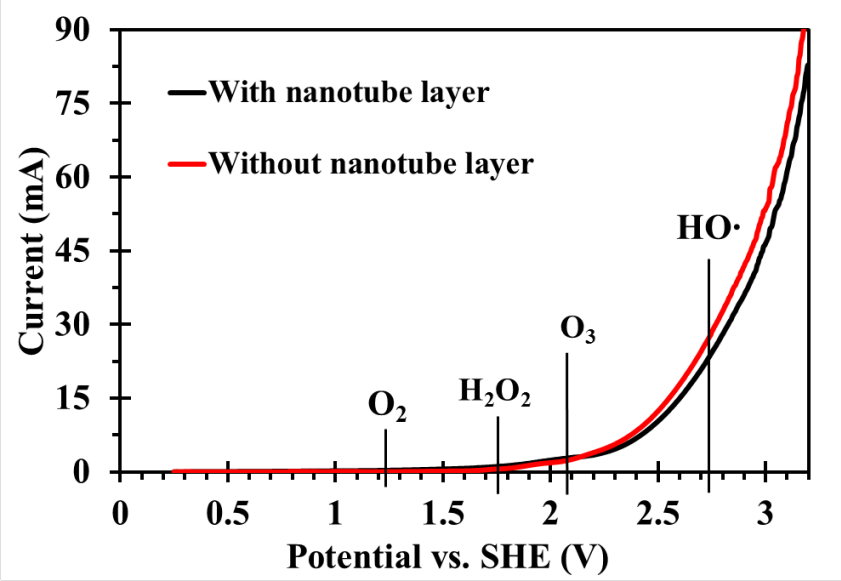

Figure 3 - Linear sweep voltammetry (LSV) of the electrodes with/without the TiO_2 nanotube layer for a 0.5 mol/L H_2SO_4 solution at a scan rate of 10 mV/s; O_2, H_2O_2, O_3 and HO· standard reduction potentials (pH = 0) are 1.23 V, 1.77 V, 2.07 V, and 2.74 V, respectively.

4.4.3 EE/O and oxidation efficiency

Energy efficiency is a critical factor for electrochemical treatment technologies, which usually produce a huge energy cost when applied at the pilot scale [127-129]. Evaluating the performance of an electrode based on its electrochemical efficiency and energy efficiency simultaneously is more sufficient from a practical point of view. The EE/O calculation is used in this study to characterize the energy efficiency of the electrodes and various operational conditions. EE/O is calculated according to the following equation:

$$EE/O = \frac{U \cdot J \cdot A \cdot t}{V \cdot \log(\frac{C_0}{C_t})} \quad (17)$$

where EE/O is the electrical energy required to reduce the concentration of the contaminant by one order of magnitude (kWh/m^3), U is the voltage (V), J is the current density (mA/cm^2), A is the electrode surface area (cm^2), t is the reaction time (h), V is the total volume of the reactor (cm^3), and C_0 and C_t are the concentrations of ofloxacin at the beginning and at time t, respectively (mg/L). We examined the electrochemical performance of the electrode with/without the TiO_2 NT layer and found that both can destroy 99% of 20 mg/L ofloxacin in 90 min in the DCBR under the following operational conditions: anode surface area 10 cm^2, electrode spacing 1 cm, fluid velocity 0.033 m/s, current density 30 mA/cm^2, 0.05 M Na_2SO_4 as electrolyte, pH 6.25, and temperature 25 °C. However, we found that the average applied potential on the electrode without TiO_2 NT is 6.8 V, which is obviously higher than the average of 6.0 V for the electrode with TiO_2 NT. By calculating the EE/O for both electrodes, we found that the electrode with TiO_2 NT has an average EE/O of 5.26 kWh/m^3, which is 20.2% lower than the average EE/O of 6.32 kWh/m^3 for the electrode without TiO_2 NT. With regard to energy efficiency, we conducted all of our remaining bench experiments with the electrode with the TiO_2 NT layer, which is the TiO_2-based SnO_2-Sb/FR-PbO_2 electrode.

To access the degradation efficiency of our electrode, the oxidation efficiency η_c was calculated based on Pacheco's method [123]. Oxidation efficiency represents the efficiency of electrons that are used by the electrode to destroy contaminants during electrolysis. η_c

is the ratio of the rate of total organic carbon (TOC) destruction to the rate of chemical oxygen demand (COD) reduction, which is calculated based on the following equation:

$$\eta_c = \frac{32}{12} \cdot (\frac{n}{4x}) \cdot \frac{d(TOC)}{d(COD)} \tag{18}$$

where TOC is expressed in mg (C)/L, COD is expressed in mg (O_2)/L, and n is the number of electrons transferred from the anode for a complete oxidation reaction. x is the number of carbon atoms of the organic compound.

In the present study with ofloxacin as the parent contaminant, the lumped overall destruction reaction is as follows:

$$C_{18}H_{20}FN_3O_4 + 41H_2O \rightarrow 18CO_2 + F^- + 3NO_3^- + 102H^+ + 98e^- \tag{19}$$

The ratio $\frac{d(TOC)}{d(COD)}$ for our TiO_2-based SbO_2-Sb/FR-PbO_2 electrode is shown in the Appendix. The TOC and COD were examined for an operating current density of 30 mA/cm^2 and reactor volume of 310 mL (the DCBR contains a reactor (10 mL) and reservoir (300 mL)), with a flow rate of 400 mL/min, pH of 6.25 and electrolyte concentration of 0.05 M Na_2SO_4. Employing eq. (18) and (19), the oxidation efficiency for the destruction of 20 mg/L of ofloxacin is 88.45%. This result demonstrates that during oxidation, 88.45%

electrons are effectively used for ofloxacin destruction (i.e., not wasted in O_2 generation) and its byproducts are mineralized effectively.

4.4.4 Oxidation by-products analysis

The byproducts of the electrochemical oxidation of ofloxacin were investigated at a current density of 50 mA/cm^2 and analyzed via liquid chromatography-mass spectrometry (LC-MS). The identification of byproducts is plotted in Figure 4. Five different major by-products were found, and their evolutionary pathways are shown. The m/z value of 362 represents the precursor, i.e., ofloxacin. During the initial attack of hydroxyl radicals, a quinolone transformation occurred and yielded P1. A similar reaction occurred in the solar Fenton treatment of ofloxacin [130]. The pathway for P2 with a m/z of 336 was attributed to the net loss of $–C_2H_2$. P3 was formed because of the demethylation of the piperazinyl ring, a mechanism that was also reported for the ofloxacin breakdown caused by a photocatalytic treatment [82]. The inset of Figure 4 demonstrates that the compound with a m/z of 378 is the major byproduct from ofloxacin destruction and represented by P4 in Figure 4. The formation of P4 is the product of a hydroxyl radical addition to the ofloxacin piperazinyl ring and results in an aldehyde derivative. The results identify the formation of hydroxyl radicals from anodic reactions, and hydroxyl radicals are the major oxidizers among other ROSs in the electrochemical oxidation process.

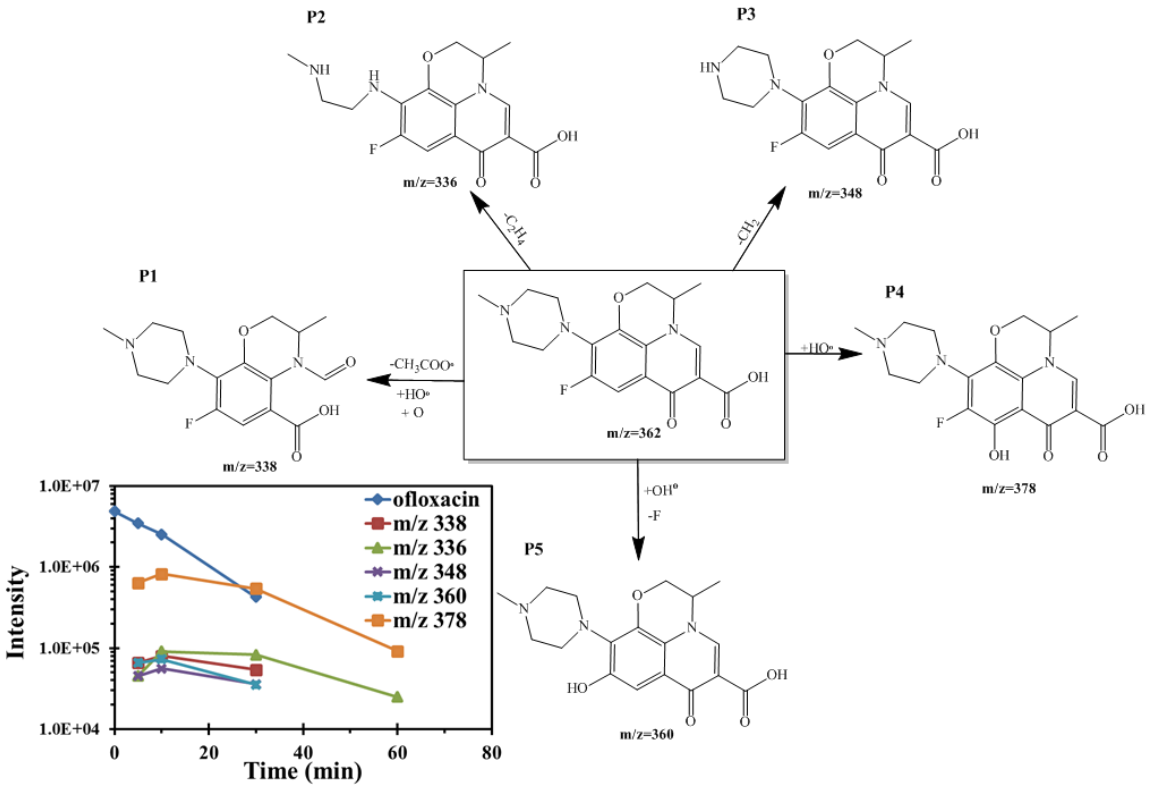

Figure 4 - Proposed reaction pathways for the destruction of ofloxacin in electrochemical oxidation. The m/z is the mass/charge ratio. Ofloxacin is 362. Inset graph shows the identification of byproducts.

4.4.5 Effect of the operational parameters current density, initial concentration, pH value and electrolyte concentration

Operational conditions influence the performance of electrochemical processes [102]. In the present study, the effects of four major factors, the current density, initial ofloxacin concentration, pH and electrolyte concentration, were investigated by fitting the experimental data with a pseudo-first-order kinetic model. The experiment results for each factor are plotted in Figure 5a-d. The fitted kinetic rate constants (i.e., pseudo-first-order rate constant in this paper) and calculated EE/O results are summarized in Table 2. All

kinetic experiments were conducted at 25 °C; thus, the impact of temperature on the kinetic rate constants is neglected.

Current density is a primary impact factor in an electrochemical system because it determines the energy, energy efficiency with respect to the size of a reactor, resistance of the material, etc. In this work, the impacts of current densities ranging from 5 mA/cm^2 to 50 mA/cm^2 were investigated, and the results are shown in Figure 5a. As the current density increases, the oxidation rate increases dramatically. The rate constant increases from 0.006 min^{-1} at 5 mA/cm^2 to 0.074 min^{-1} at 50 mA/cm^2. The results for the rate constants were plotted vs. current density, and a linear relationship was observed ($R^2 = 0.9918$). Moreover, by considering the byproducts analysis, which demonstrates that ofloxacin is mainly destroyed through the addition of a hydroxyl radical to an aromatic ring, it appears that as the current density increases, the production of hydroxyl radicals increases linearly as well. High current densities favor ofloxacin destruction. However, the EE/O results listed in Table 2 indicate that the electrical energy input almost doubled from 3.78 kWh/m^3 at 5 mA/cm^2 to 6.74 kWh/m^3 at 50 mA/cm^2. A high oxidation rate requires a much higher energy input. From an engineering perspective, the most practical design of a reactor should consider the capital and energy costs simultaneously. As the current density increases, the capital costs should decrease because a smaller treatment device would be used and the energy costs should increase. Consequently, the total cost of the operation (capital costs plus operational costs) should be at a minimum.

Five different initial ofloxacin concentrations were examined for a current density of 30 mA/cm^2. Figure 5b shows the ofloxacin destruction over time for 10, 20, 30, 40 and 50

mg/L, respectively. The results demonstrated that the reaction rate decreases as the initial concentration increases from 10 to 50 mg/L. The EE/O has the same trend as the concentration and increases from 3.66 kWh/m^3 to 15.01 kWh/m^3. However, we found that when the concentration increases from 20 mg/L to 50 mg/L, the rate constants do not increase significantly because as ofloxacin is destroyed by hydroxyl radicals, the hydroxyl radicals can further react with the byproducts. The production of hydroxyl radicals is limited by the input current density. Therefore, a smaller reaction rate is expected as the initial concentration increases.

pH has a considerable impact on the AOP reaction because many radical chain reactions involve the participation of protons [131]. The effect of pH on the electrochemical oxidation of ofloxacin was investigated in a range from pH 4 to pH 11. The results plotted in Figure 5c show that the ofloxacin destruction rate increases from 0.029 min^{-1} to 0.054 min^{-1} as the pH increases from 4 to 11, and the EE/O also decreases from 6.10 kWh/m^3 to 3.98 kWh/m^3. The reason for this enhancement is because of the decreased hydroxyl radical reduction potential, which decreases from 2.74 V at pH 0 to 2.5 V at pH 4. As the applied potential and current density are maintained, more hydroxyl radicals will be generated because the energy barrier for this reaction decreases and more energetic valence band holes on the anode surface become available for the reaction. In addition, the reduction potential further decreases as the pH increases from 4 to 11.

Figure 5d shows the effect of different electrolyte concentrations on ofloxacin oxidation. Na_2SO_4 was selected as the electrolyte for ofloxacin oxidation to avoid the generation of chlorinated species. When the electrolyte concentration increases from 0.005

M to 0.1 M, the oxidation rate slightly increases. However, when the electrolyte concentration further increases to 0.5 M, the reaction rate decreases significantly. The rate constants were calculated, and a peak was observed at 0.1 M. When the electrolyte concentration increases to 0.5 M, it significantly inhibits oxidation compared with a smaller electrolyte dosage. One possible explanation for this finding is that in an electrochemical system, sulfate ions under high applied potential will produce persulfate, which can significantly scavenge hydroxyl radicals [132, 133]. When the sulfate concentration increases, this inhibition effect becomes significant. The proposed scavenging mechanism reactions are as follows [133]

$$S_2O_8^{2-} + 2e^- \rightarrow 2SO_4^{2-} \qquad E^0 = +2.01\ V \tag{20}$$

$$S_2O_8^{2-} + HO\cdot \rightarrow HSO_4^- + SO_4^-\cdot + 0.5O_2 \quad k = 1.2\times10^7\ L\cdot mol^{-1}\cdot s^{-1} \tag{21}$$

$$SO_4^-\cdot + HO\cdot \rightarrow HSO_5^- \qquad k = 1.0\times10^{10}\ L\cdot mol^{-1}\cdot s^{-1} \tag{22}$$

Based on the discussion regarding the effect of the current density, initial concentration, pH and electrolyte concentration, a set of proper operating conditions were identified that can promote the oxidation performance, rate constants and EE/O for the oxidation of ofloxacin using the electrochemical method: current density = 30 mA/cm^2,

initial concentration = 20 mg/L, pH = 6.25 and electrolyte concentration = 0.05 M. These mild conditions were also used for the investigation of the mass transfer impact.

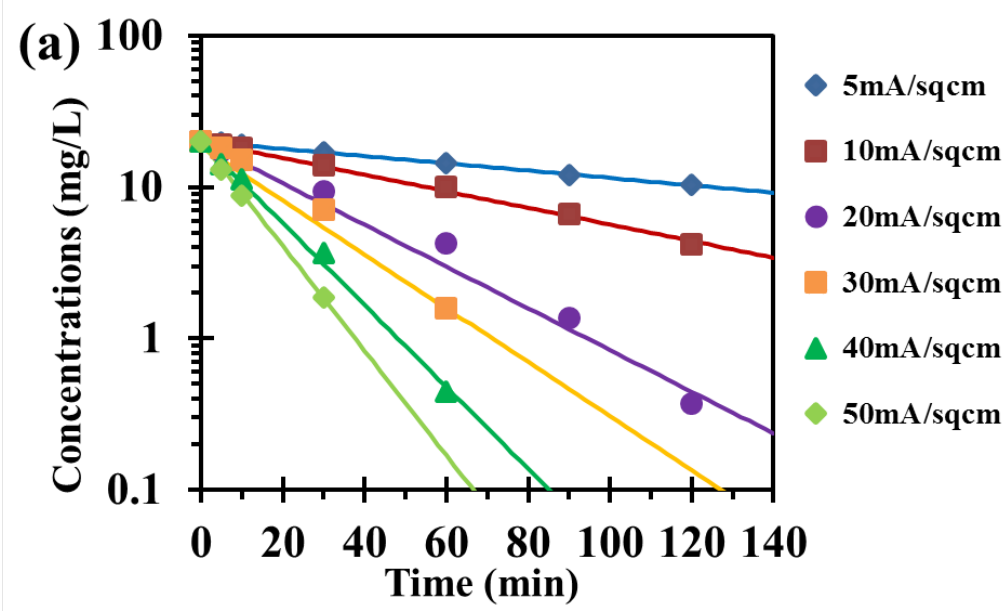

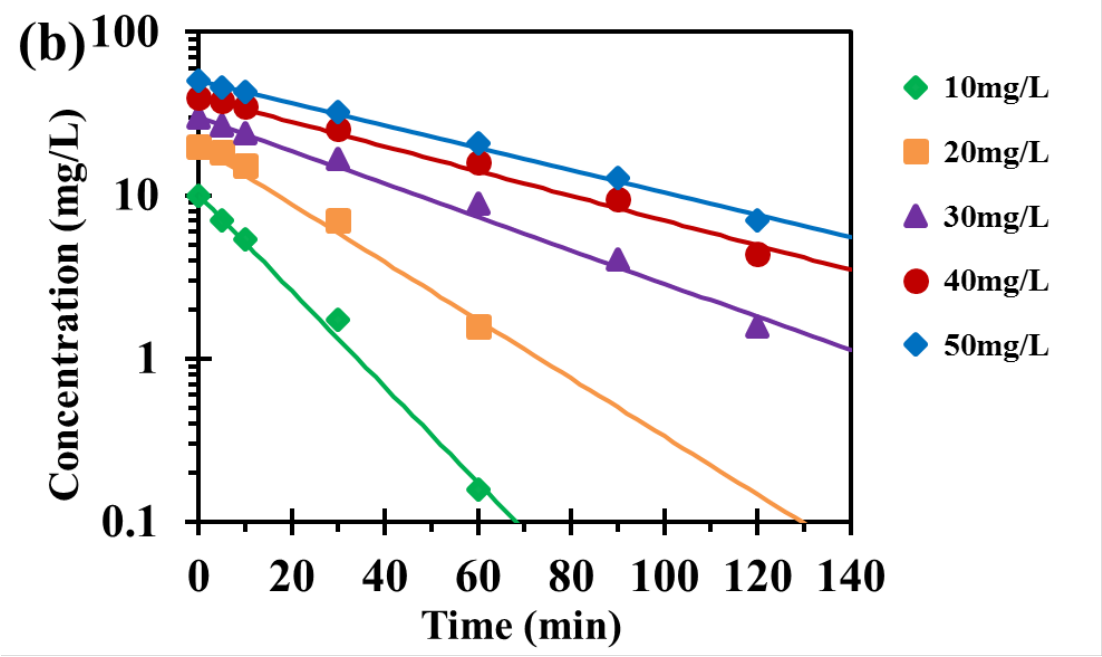

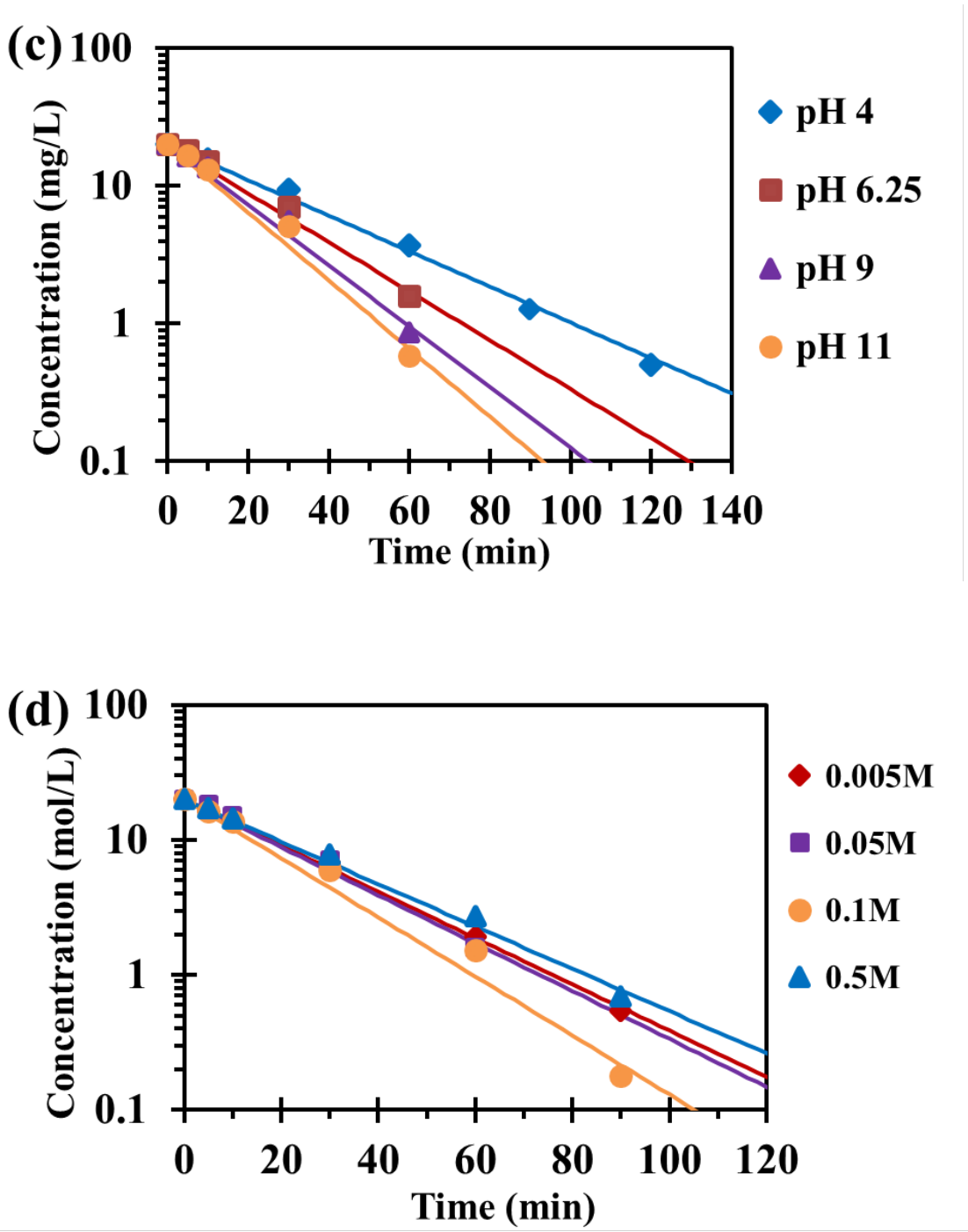

Figure 5 - Effect of the following operational parameters: (a) current density, (b) initial ofloxacin concentration, (c) pH, (d) Na_2SO_4 concentration. The temperature

for all kinetic experiments is 25 °C. The dots are experimental data fitted by pseudo-first-order kinetic model lines.

Table 2 - Summary of pseudo first-order rate constants, EE/O at different current densities, initial ofloxacin concentrations, pH values and electrolyte Na_2SO_4 concentrations. Operational conditions are 30 mA/cm^2 current density, 20 mg/L initial ofloxacin concentration, 6.25 pH, 0.05 M Na_2SO_4 concentration and 25 °C temperature.

	Current density (mA/cm^2)						pH			
	5	10	20	30	40	50	4	6.25	9	11
Pseudo first-order rate constants (min^{-1})	0.006	0.013	0.032	0.039	0.059	0.074	0.029	0.039	0.048	0.054
Electric efficiency per order (EE/O) (kWh/m^3)	3.78	3.91	4.25	5.26	5.64	6.74	6.10	5.44	4.48	3.98

	Initial concentration (mg/L)					Na_2SO_4 concentration (M)			
	10	20	30	40	50	0.005	0.05	0.1	0.5
Pseudo first-order rate constants (min^{-1})	0.063	0.039	0.023	0.017	0.016	0.038	0.039	0.048	0.035

Electric efficiency per order (EE/O) (kWh/m^3)	3.66	5.26	9.69	12.88	15.01	23.41	5.44	5.26	2.98

4.4.6 Discussion of the mass transfer impact

A number of studies have reported a mass transfer limitation in electrochemical systems [116, 119, 120]. In this study, we quantitatively investigated this impact using a differential column batch reactor (DCBR). A DCBR allows us to conveniently investigate two hydrodynamic factors for the electrochemical reactors: electrode spacing and fluid velocity. These two factors are important because increasing velocities can increase the mass transfer rate and decreasing electrode spacing will increase the surface area per volume of the reactor that is available for mass transfer. For both factors, increasing velocity and decreasing electrode spacing can reduce the impact of the mass transfer on the electrochemical oxidation rate. Our investigation of these variables is presented in this section.

We used the convective mass transfer coefficient to quantitatively compare the impact of mass transfer. The convective mass transfer coefficient is a diffusion rate constant that is the driving force of the mass transfer rate, mass transfer area, and concentration changes. In this study, this coefficient is calculated based on the correlation proposed by Sonin et al. [134] and experimentally confirmed by Grossman et al. [135]. This correlation is

essentially equivalent to Leveque's law for heat transfer [116, 134]. Note that this correlation is valid for a reactor geometry length to spacing ratio of less than 126 and Sherwood number (Sh) >>1, which is suitable in the present study.

$$Sh = \frac{k_f \cdot d}{D_l} = 3.3 \cdot (\frac{d}{l} \cdot \mathrm{Re} \cdot Sc)^{\frac{1}{3}} \tag{23}$$

$$\mathrm{Re} = \frac{\rho \cdot u \cdot d}{\mu} \tag{24}$$

$$Sc = \frac{\mu}{\rho \cdot D_l} \tag{25}$$

where k_f is the mass transfer coefficient (m/s); d is the electrode spacing (hydrodynamic characteristic length of the reactor, m); D_l is the ofloxacin diffusivity, (3.3×10^{-6} cm^2/s), which is calculated using the Hayduk-Laudie correlation [131]; l is the length the fluid travels in the reactor (m); Re is the Reynolds number; Sc is the Schmidt number; u is the fluid velocity (m/s); and ρ and μ are the fluid density (kg/m^3) and fluid dynamic viscosity ($kg \cdot m^{-1} \cdot s^{-1}$), respectively.

Figure 6a shows the ofloxacin concentrations as a function of time for different electrode spacings. The pseudo-first-order rate constants, EE/O and mass transfer coefficients are plotted in Figure 6b and c. We examined the electrode spacings of 0.5 cm,

1 cm, 2 cm, and 3 cm. The fluid velocity was 0.033 m/s, which corresponds to a DCBR detention time of 1.6 s and a reservoir detention time of 45 s through the reactor. Obviously, the reaction rate increased as the electrode spacing decreased. The pseudo-first-order rate constant increased from 0.035 min^{-1} to 0.054 min^{-1} when the electrode spacing decreased from 3 cm to 0.5 cm. We calculated the mass transfer coefficient for different electrode spacings, which explains certain increases in reaction rates. This surface area per reactor volume times the mass transfer coefficient is equal to the first-order destruction rate for a zero concentration of ofloxacin on the surface of the electrode. The mass transfer coefficient increased from 4.35×10^{-6} m/s to 7.92×10^{-6} m/s when the electrode spacing decreased from 3 cm to 0.5 cm. The surface area per volume times the mass transfer coefficient decreased from 1.58×10^{-3} s^{-1} to 1.45×10^{-4} s^{-1} when the electrode spacing increased from 0.5 to 3 cm.

The EE/O also improved with smaller electrode spacing. The EE/O decreased from 16.34 kWh/m^3 to 3.50 kWh/m^3 as the electrode spacing decreased from 3 cm to 0.5 cm. The EE/O decreased significantly because of the decreased applied potential, which decreased from 9.2 V to 5 V as the electrode spacing decreased to 0.5 cm.

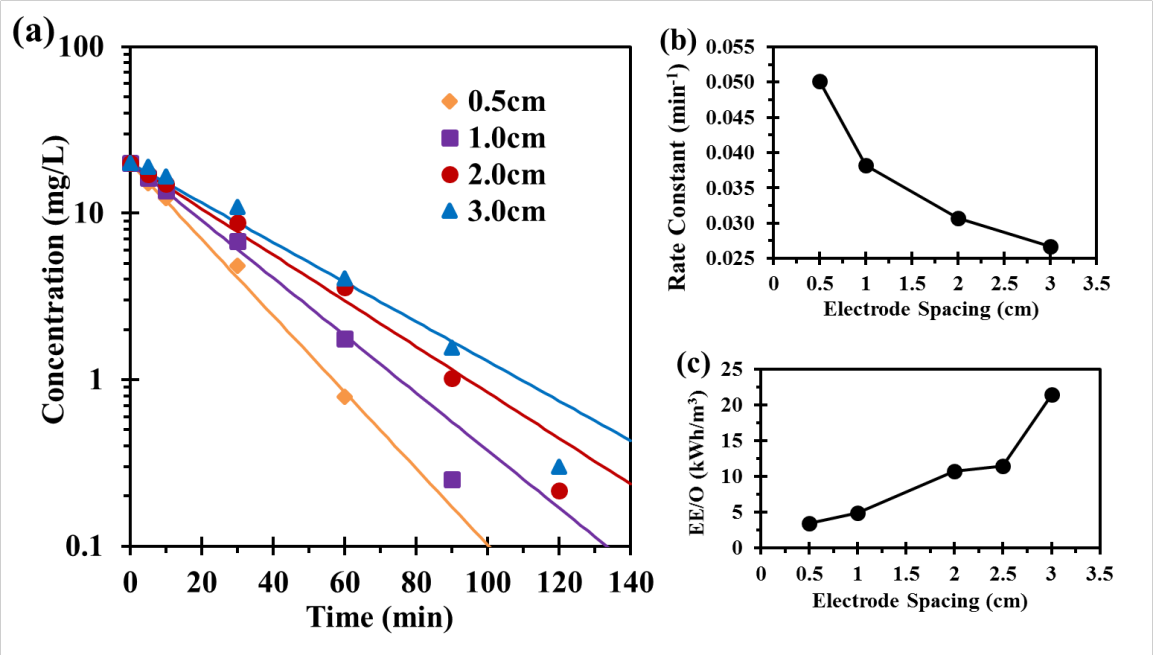

Figure 6 - Effect of electrode spacing: (a) ofloxacin destruction in different electrode spacings, (b) pseudo first-order rate constants, and (c) EE/O. Anode surface area = 10 cm^2, fluid velocity = 0.033 m/s, current density = 30 mA/cm^2, initial ofloxacin concentration = 20 mg/L, voltage = 5-9.2 V, electrolyte = 0.05 M Na_2SO_4 solution, pH = 6.25, temperature = 25 °C. The dots are experimental data and fitted by pseudo first-order kinetic model lines.

Figure 7a shows the ofloxacin concentration as a function of time for various fluid velocities. The pseudo-first-order rate constant and EE/O is plotted in Figure 7b and c, respectively. We tested five different fluid velocities: 0.003 m/s, 0.008 m/s, 0.017 m/s, 0.033 m/s and 0.048 m/s. Figure 7 shows that the reaction rate increases when the fluid velocity increases. The rate constant increases from 0.025 min^{-1} to 0.048 min^{-1} as the fluid velocity increases from 0.0025 m/s to 0.048 m/s. Theoretically, the fluid velocity is proportional to the Reynolds number for a given electrode spacing. Increases in the Reynolds number also increase the Sherwood number and mass transfer coefficient. Our calculations illustrate that the mass transfer coefficient increases dramatically from 2.65×10^{-6} m/s to 7.10×10^{-6} m/s as the velocity increases. Our EE/O calculation excludes

the energy use of the stirring reservoir and pumping because our investigation focuses on the energy cost difference that is directly proportional to the mass transfer. The EE/O decreases from 9.50 kWh/m^3 to 4.96 kWh/m^3 as the fluid velocity increases from 0.003 m/s to 0.048 m/s. The results indicate that the increased velocity favors mass transfer processes and enhances the energy efficiency.

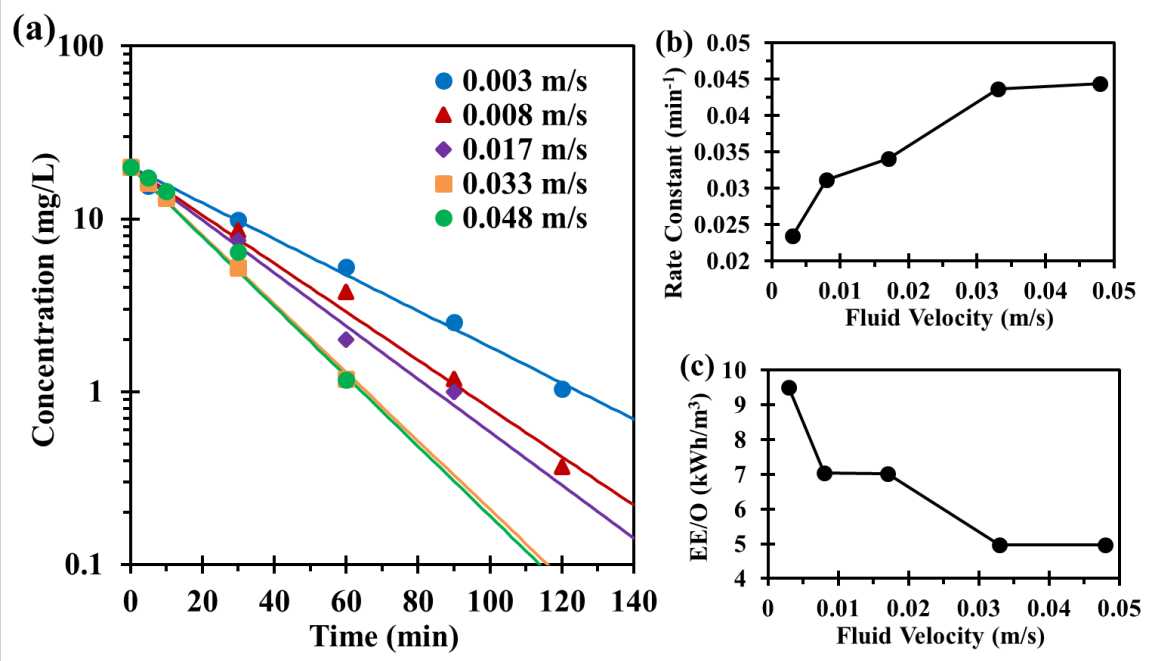

Figure 7 - Effect of fluid velocity: (a) ofloxacin destruction for different fluid velocities, (b) pseudo-first-order rate constants, and (c) EE/O. Anode surface area = 10 cm^2, electrode spacing = 1 cm, electrolyte = 0.05 M Na_2SO_4 solution, current density = 30 mA/cm^2, initial ofloxacin concentration = 20 mg/L, voltage = 6.3-6.4 V, pH = 6.25, temperature 25 °C. The dots represent experimental data fitted by pseudo-first-order kinetic model lines.

We use the effectiveness factor to determine the impact of the mass transfer on the electrochemical oxidation rate. The effectiveness factor is defined by the ratio of the observed reaction rate r_{Obs} to the maximum reaction rate r_{Max} (no mass transfer resistance).

$$\Omega = \frac{r_{Obs}}{r_{Max}} \tag{26}$$

In this study, we used the boundary layer diffusion model to simulate the process of ofloxacin diffusion from the bulk solution to the anode surface [136]. We assume that the ofloxacin concentration C_B does not present a gradient in the bulk solution and that the concentration in the diffusion layer is C_S. The ofloxacin concentration in the diffusion layer C_S is smaller than C_B because of the diffusion restriction, i.e., the mass transfer resistance. The destruction of ofloxacin reactions occurs only within the diffusion layer. Therefore, we present the expression of the observed reaction rate r_{Obs} and maximum reaction rate r_{Max} as follows:

$$r_{Obs} = k_s \cdot C_S = k \cdot C_B \tag{27}$$

$$r_{Max} = k_s \cdot C_B \tag{28}$$

where k_s is the surface reaction rate constant (min^{-1}) and k is the observed pseudo-first-order rate constant (min^{-1}). Theoretically, the mass transfer rate M_A ($mg \cdot L^{-1} \cdot s^{-1}$) caused by the surface reaction ($M_A = k_s \cdot C_S$) is equal to the M_A related to the mass transfer ($M_A = k_f \cdot a_v \cdot (C_B - C_S)$), where k_f is the mass transfer coefficient (m/s) and a_v is the

surface area per volume of the reactor (m^2/m^3). Therefore, the concentration in the diffusion layer C_S can be expressed as follows:

$$C_S = \frac{k_f \cdot a_v \cdot c_B}{k_f \cdot a_v + k_s} \tag{29}$$

Figure 2c shows that our anode has a rough surface (larger surface area than a flat plate). Hence, we use a dimensionless surface roughness factor θ to represent the roughness of the anode surface, and the surface area per volume a_v is $\frac{\theta}{d}$ (m^{-1}) in this study. Using Eqs. (27), (28), and (29), the surface reaction rate k_s and roughness factor θ can be determined by fitting the experimental observed pseudo-first-order rate constants. Using the fitted k_s and observed rate constants, the effectiveness factor Ω for different electrode spacings and fluid velocities can be calculated as follows:

$$k = k_s \cdot \frac{k_f \cdot \theta}{k_f \cdot \theta + k_s \cdot d} \tag{30}$$

$$\Omega = \frac{k}{k_s} \tag{31}$$

Figure 8 shows the effectiveness factor as a function of the fluid velocity. The mass transfer coefficients for various velocities, k_f, were calculated using the correlation in Eq.

(7). These calculations were performed under the conditions of an applied current density of 30 mA/cm^2, initial ofloxacin concentration of 20 mg/L, pH 6.25, electrolyte Na_2SO_4 concentration of 0.05 M and electrode spacing of 1 cm. The surface reaction rate k_s and the roughness factor θ were fitted by minimizing the Objective Function (OF) of the pseudo-first-order rate constants in the model and from the data. The parameters k_s and θ in Figure 8are 0.0017 s^{-1} (0.1 min^{-1}) and 1.86 in this study, respectively. To confirm the surface roughness factor, we examined the electrode surface using atomic force microscopy (AFM) and estimated the electrode surface area. The surface roughness factor increases as the electrode surface area increases. A larger surface area indicates that more reaction sites (in nm scale) are available. The AFM results are shown in the Appendix. By assuming that the rough surface obstacles all have the half sphere geometry (smallest geometry), the surface area of the electrode is 1.79 times as large as the scanning base area, which is similar to our fitting results.

The effectiveness factors reflect the mass transfer resistance, which has a value between 0 and 1. If the value of the effectiveness factor is equal to 1, then the mass transfer resistance is negligible. Figure 8 shows that the effectiveness factor increases when the fluid velocity increases. The highest examined effectiveness factor (as shown here) was 0.444 at a fluid velocity of 0.048 m/s. These results indicate that the overall electrochemical rate was 44.4% without mass transfer resistance. The effectiveness factors calculated for other operational conditions (e.g., electrode spacing) present similar results as shown in the Appendix. It was found that the mass transfer reduces the oxidation rate by more than 55% ($\Omega < 0.55$) for an electrode spacing of 1 cm at a fluid velocity of 0.033 m/s. Consequently, the mass transfer process has a considerable impact on the overall electrochemical

oxidation rate. The rational method presented here that uses the effectiveness factor to evaluate the mass transfer resistance can be applied to other electrochemical systems.

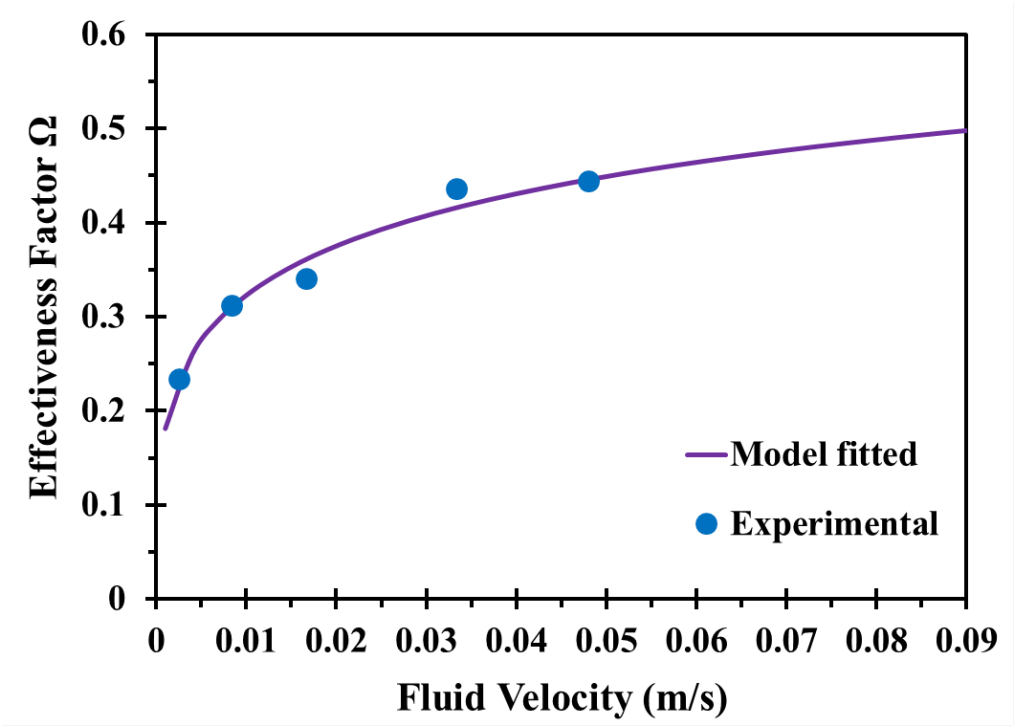

Figure 8 - Effectiveness factor for different fluid velocities and the best fit model. Anode surface area = 10 cm^2, electrode spacing = 1 cm, electrolyte = 0.05 M Na_2SO_4 solution, current density = 30 mA/cm^2, initial ofloxacin concentration = 20 mg/L, voltage = 6.3-6.4 V, pH = 6.25, temperature = 25 °C.

4.5 Conclusions

This study reported the fabrication of a TiO_2-based SnO_2-Sb/polytetrafluoroethylene resin (FR)-PbO_2 electrode catalyst and its application for the destruction of the antibiotic ofloxacin. To obtain a relatively large band gap and good conductivity, a layer of TiO_2 nanotubes with diameters between 18 and 22 nm was grown on Ti foil and a polytetrafluoroethylene resin material was used to improve the adherence of the outer PbO_2

layer. The obtained electrode catalyst exhibited a high surface area, more oxidation active sites, good electrical conductivity, and high oxidation efficiency. In addition, the overpotential for oxygen evolution was greater than 1.5 V, which is characterized by linear sweep voltammetry. The results showed that over 99% of 20 mg/L ofloxacin (11.95 mg TOC) can be destroyed after 1 hour at an oxidation efficiency as high as 88.45%, which indicates that most of the energy (electrons) was used to effectively decrease TOC. A practical operational current density of 30 mA/cm^2 was selected for the batch experiments after simultaneously considering the oxidation rate and energy consumption. The destruction of ofloxacin favors high pH conditions, and its pseudo-first-order rate constants increased by 86% while its EE/O decreased by 35% as the pH increases from 4 to 11. This electrochemical oxidation can be run under a relatively low electrolyte condition, e.g., 0.05 M Na_2SO_4. Moreover, the hydrodynamic design of a forced-flow electrochemical system has a significant impact on the mass transfer process. Narrowing the electrode spacing and increasing the fluid velocity will enhance the mass transfer process and then increase the overall oxidation rate. The impact of mass transfer was quantified by calculating the mass transfer coefficient and deriving an effectiveness factor. This effectiveness factor represents the correlation between the observed reaction rate and the theoretical reaction on the electrode surface. The experiments and calculations both indicate that the mass transfer reduced the oxidation rate by more than 55% for an electrode spacing of 1 cm at a fluid velocity of 0.033 m/s. Therefore, this study demonstrated the feasibility of using a TiO_2-based SnO_2-Sb/polytetrafluoroethylene resin (FR)-PbO_2 electrode catalyst to destroy ofloxacin in the aqueous phase. Our derived effectiveness factor can be used in all types of forced-flow electrochemical systems with different electrode types.

CHAPTER 5. THREE-DIMENSIONAL ELECTROCHEMICAL OXIDATION DEVELOPMENT: REACTION KINETICS AND SYSTEM INTEGRATION

5.1 Abstract

Reducing the energy requirement and minimizing byproduct formation are crucial to developing commercially viable electrochemical oxidation technologies for wastewater treatment. We developed a three-dimensional electrochemical system that can significantly reduce applied voltage and effectively degrade organic contaminants in wastewaters that have low ionic strength. The design also minimized the byproducts from the oxidation of electrolyte. We used a woven titanium mesh as a substrate and grew blue TiO_2 nanotubes on it. Then we coated the nanotubes with SnO_2-Sb using a sol-gel process and aged the composite. This nanotube mesh was the anode and the cathode was a stainless wire mesh with no modification. The three-dimensional electrode system consisted of these components: (1) composite anode, (2) proton exchange membrane (PEM) and (3) stainless-steel cathode. They were compressed firmly together to create the three dimensional (3-D). The PEM was commercially available Nafion and served as the electrolyte in this configuration. For the 3-D system, we had placed the anode of a 3-D electrode toward the wastewater and the wastewater flowed past the anode. For the two-dimensional (2-D) electrode system, the composite nanotube was the anode and the cathode was stainless-steel mesh. The wastewater flowed between the anode and cathode. We compared the performance of the 3-D electrochemical system to the performance of the 2-D system. We

used various ionic strength wastewaters (0.1 M, 0.05 M, 0.01 M, 0.005 M, 0.001 M Na_2SO_4 and a surface water) and the target compound was benzoic acid (BA). We found that the 3-D system could reduce the applied voltage up to 79% (60.4 V versus 12.7 V) for 0.001 M Na_2SO_4 that maintains a 30 mA/cm^2 current density when degrading 28 mg/L (~0.23 mM) BA. The electrical energy per order (EE/O) was reduced 63% for 3-D electrode versus a 2-D electrode (61.47 kWh/m^3 versus 22.64 kWh/m^3). For Na_2SO_4 concentrations greater than 0.05 M, the 2-D electrode had a lower EE/O. We also compared the performance of the 2-D and 3-D electrodes to the other AOPS (UV/H_2O_2, UV/ Persulfate, O_3/H_2O_2, UV/ TiO_2 and UV/ Chlorine). We found that for low BA concentrations (20 mg/L) the EE/O for the 2-D and 3-D electrodes were much higher than the other AOPs. However, higher BA concentrations (2000 mg/L) the EE/O for the 2-D and 3-D electrodes were much lower than the other AOPs. This suggests that electrochemical oxidation may be cheaper for higher concentrations.

5.2 Introduction

Electrochemical oxidation has been proposed as a wastewater treatment technology for decades. It has many advantages for the destruction of organic contaminants because no oxidants need to be added to the wastewater and an electron is a clean reactant. Electrochemical oxidation devices can operate under room temperature and pressure and have distinct advantages including high efficiency, amenability to automation, easy upgrade for remote controlled operation and versatility because they can oxidize most organics [135,136] However, some of the drawbacks significantly hamper large-scale applications of electrochemical oxidation. The key concern is high electrical energy

consumption for low ionic strength (low conductance) wastewaters and toxic byproducts can be formed from the oxidation of some of the electrolytes [137-139].

Recent research on electrochemical oxidation technologies has focused on developing anode materials that more powerful and efficient. They have focused on developing inactive anodes that generate strong oxidants from the oxidation of water or ions on the anode surface, such as hydroxyl radicals ($HO^{\cdot}$). As opposed to direct oxidation reactions on the anode surface (Eq. 32) (i.e., active electrodes oxidize organics on the surface of the anode by direct electron withdrawal from the organic compound, which can lead to electrode fouling).

$$H_2O \rightarrow HO^{\cdot} + H^+ + e^- \tag{32}$$

These processes are called electrochemical advanced oxidation processes (EAOPs) [140,141]. Hydroxyl radicals initiate radical chain reactions and eventually mineralize organics to H_2O and CO_2 [142,143].

Hydroxyl radical is a very strong oxidant ($E^0 = +2.74$ V vs. NHE) and its generation from water on anode surface also creates a free electron that can flow to the cathode and a proton [144]. On the cathode surface, the reduction reactions can generate hydrogen gas ($E^0 = 0$ V) and/or hydrogen peroxide ($E^0 = 0.62$ V) under aerobic conditions [145-147].

$$H^+ + e^- \rightarrow \frac{1}{2}H_2 \tag{33}$$

$$H^+ + e^- + \frac{1}{2}O_2 \rightarrow \frac{1}{2}H_2O_2 \tag{34}$$

The main goal for researchers is to generate more hydroxyl radicals with less energy input. Adding electrolytes to the solution is an easy way to increase the transport of protons and electrons with less energy. Basically, increasing the ionic strength reduces the required applied voltage to conduct a same number of electrons (maintain current flow) because it increases the flow of anions and cations to the anode and cathode, respectively. However, many researchers have reported that electrolysis of chlorides containing wastewaters produces chlorination byproducts, such as hypochlorous acid, chlorate or even perchlorate. These chlorinated oxidants undergo complex reactions and produce what are commonly called disinfection byproducts (DBPs) that may result in significant toxicity concerns for electrochemical treated wastewater effluent [148]. Decreasing electrode spacing is another practical approach to lower the energy and many papers published highly efficient micrometer even millimeter scale micro-reactors. Yet in large-scale wastewater treatment, decreasing the electrode spacing will dramatically increase the capital cost of the devices and prevent their applications [149-151].

Proton exchange membranes (PEMs) and proton exchange ceramics (PECs) can effectively conduct protons to the cathode and support redox reactions. They have been well studied and applied in fuel cell field [152]. They can serve as a substitute to electrolytes in the solution while at the same time avoid generating additional byproducts. We could not use PECs because protons that are generated at the anode cannot penetrate the PEC (semiconductors are not proton conductible) [153,154]. Therefore, we used a Nafion N-117 membrane (a commercially available and highly efficient PEM) as the electrolyte media. We used a titanium woven wire mesh anode that was further modified to form a nanocomposite anode and a stainless-steel wire mesh cathode. PEM was placed between

the nanotube composite anode and the stainless wire mesh cathode. We call this a 3-D electrode. This configuration allows oxidation of water on the anode surface to form hydroxyl radical. The PEM increases: (1) the production of hydroxyl radicals that react with organics, (2) the electron flow for a given electrical potential, and (3) proton flow through PEM to the cathode for hydrogen production.

The anode material is the key component that determines the hydroxyl radical production efficiency in EAOPs [155]. According to quantum theories, during electrolysis, electrons flow from semiconductor anode creates excitons: valence band holes h^+ and conduction band electrons e_{CB}^-. The band gap size is the potential difference between the hole and conduction band electron and the band gap determine how energetic the excitons are. It is the hole that reacts with water to generate hydroxyl radicals. The Boron-doped diamond electrode (BDD) has been considered the best anode material because it has a large band gap ($\Delta E = 5.45$ eV), high efficiency and remarkable longevity. However, its fabrication is complex and costly, which prevent its use in large-scale applications [156-157]. Growing TiO_2 nanotubes from a Ti substrate has become a mature technique and TiO_2 nanotubes anode favor hydroxyl radical production because it has relatively large band gap ($\Delta E = 3.2$ eV) [158]. Recently, Blue-black TiO_2 nanotubes have been fabricated and they have a slightly larger band gap ($\Delta E = 3.3$ eV) and enhanced stability [159]. Also, the nanotube structure can lower the excition recombination rate, and this increases reaction rate of valence band holes with water. Pure SnO_2 is an n-type semiconductor and has a band gap of 3.5 eV. Its conductivity can be significantly increased by doping it with Sb [160,161]. In addition, a recent study showed that using aged sol-gel can improve the crystallinity (smaller crystal size and more surface sites) of the SnO_2-Sb material and enhance its

longevity under high current flow conditions [162,163]. Consequently, we used blue TiO_2 nanotubes as the base material and coated with an aged SnO_2-Sb layer.

Herein, we compare a three-dimensional (3-D) electrochemical oxidation system to a two-dimensional (2-D) electrochemical oxidaton system. The 2-D system is comprised of a woven mesh blue TiO_2 nanotubes/SnO_2-Sb (BTNA/TA) as the anode (describe above) and a stainless steel wire mesh as the cathode. We used benzoic acid as a probe molecule (it has a relatively high rate constant with $HO^{\cdot} = 5.9 \times 10^9\ M^{-1}s^{-1}$) and we varied the ionic strength using Na_2SO_4. A mathematic model was used to gain insight of the electrolyte impact for both systems and investigate the possible mechanisms of the 3-D system. Furthermore, we used models to compare 2-D & 3-D electrochemical oxidation systems to five conventional AOPs (UV/H_2O_2, H_2O_2/O_3, UV/persulfate, UV/HOCl, and UV/TiO_2).

5.3 Materials and Methods

5.3.1 Experimental Section

Experimental section. All chemicals that were used in the experiments were analytical reagent grade or higher from Sigma-Aldrich (St. Louis, MO, USA). Nafion^{TM} N-117 membrane (0.18 mm thick, $\geq 0.9\ meq/g$ exchange capacity), Titanium gauze (40 mesh woven from 0.127 mm diameter wire, 64% open, calculated surface area ~7.182 cm^2/10 cm^2), and stainless-steel gauze (100 mesh woven from 0.025 mm diameter, type 304) were purchased from Alfa Aesar, Haverhill, MA, USA. All solutions were prepared in deionized water (Milli-Q system, 18.2 MΩ-cm). Surface water was taken from Lanier Lake, Buford, GA (~112.5 µs/cm). Benzoic acid concentration was measured with an HPLC-DAD system (Agilent Tech, 1200 Series) equipped with a C18 column (Extend, 3.5 µm,

4.63 × 150 mm) operated at a flow rate of 1 mL/min. The mobile phase was composed for 40 v% acetonitrile and 60 v% ammonium acetate solution. pH was adjusted to 4.2 with H_3PO_4. The UV detector was set at $\lambda = 228$ nm. The injection volume was 5 µL.

The meshed anode, the cathode is compressed firmly with PEM in a pack and the configurations of the pack and the bench scale flow cell are illustrated in Figure 9.

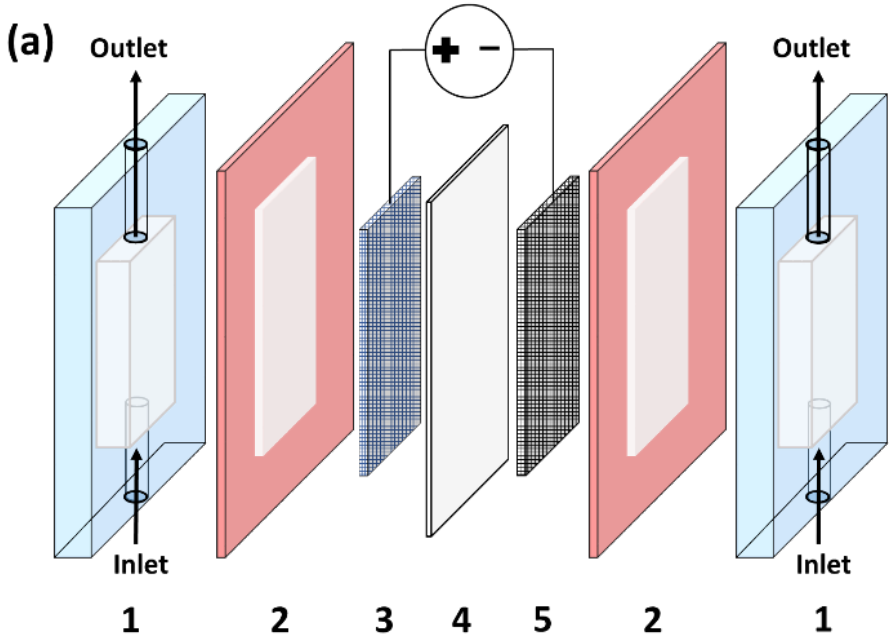

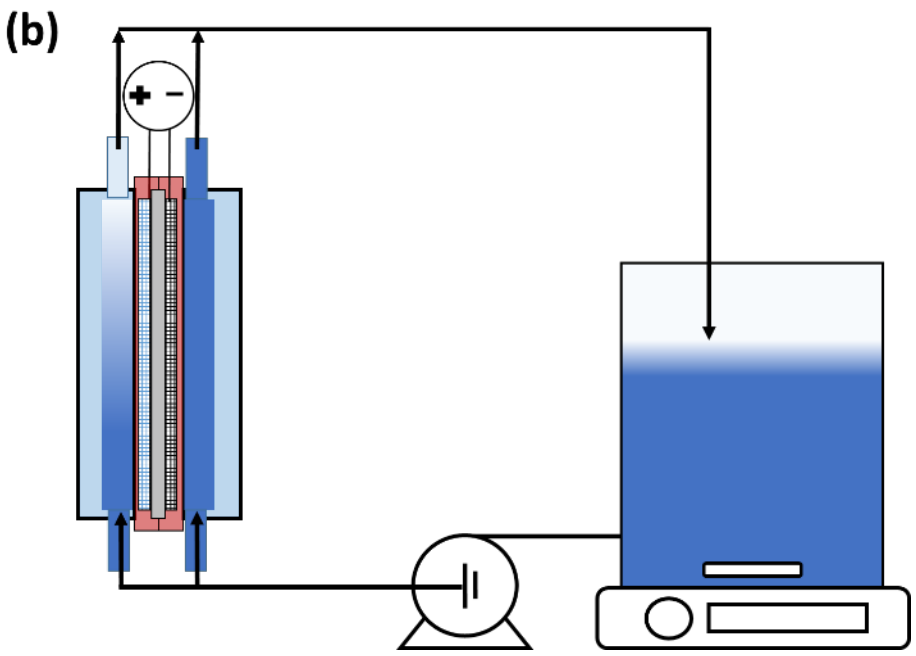

Figure 9 - Bench-scale 3-D electrochemical oxidation system configuration. (a) Schematic of the (Anode|PEM|Cathode) stack; 1. Frame, 2. Rubber septa, 3. Woven mesh anode, 4. Proton exchange membrane, and 5. Woven mesh cathode. (b) Schematic of the differential column batch reactor (DCBR) operation. The cell is separated by the 3-D electrode and cathode and anode chamber are independent from each other. Effluent of the anode and cathode chambers are mixed in the reservoir and flow is returned to chambers. Oxidation only occur in the anode chamber. The electrode spacing in the 3-D and 2-D systems are 0.3 cm and 1 cm, respectively.

5.3.2 Anode Fabrication

The Radio Cooperation of America (RCA) clean method was modified to clean the titanium gauze and we followed these steps [164-166]. (1) First, we boiled the titanium gauze the in a $H_2O/NH_4OH/H_2O_2$ solution (volume ratio 5:1:1, 0.71, 0.13 and 0.16 g/cm^3, respectively) in 75 – 80 C° for 10 min. (2) Second, we immersed the titanium gauze

in an HF/H_2O_2 solution (volume ratio 1:100, 0.001 and 1.1 g/cm^3, respectively) for 15 s. (3) Third, we washed the titanium gauze in a $H_2O/HCl/H_2O_2$ (volume ratio 6:1:1, 0.75, 0.24 and 0.14 g/cm^3, respectively) solution for 3 min. (4) Fourth, we rinsed and dried the titanium gauze in the air for 10 min.

TiO_2 nanotubes were grown on titanium gauze ($2\ cm \times 5\ cm$). Similar fabrication methods have been reported by several researchers [167-168]. The nanotubes were synthesized using anodic oxidation at a constant voltage of 42 V in an ethylene glycol solution containing a with 0.25 wt% NH_4F and 2 wt% H_2O solution for 6 hours at 60 ºC (this produces ~16 μm length nanotubes). The cathode was a platinum gauze ($5\ cm \times 5\ cm$) and was place 1 cm from the anode. A second anodization step was carried out to improve the nanotubes structure [169]. Second anodization was carried out in an ethylene glycol solution that contained 5 wt% H_3PO_4 using at 42 V for 1 h. Blue TiO_2 nanotubes were prepared using cathodization in a 1 M $NaClO_4$ solution at 10 mA/cm^2 current density for 15 min. The blue nanotubes were then ultrasonically cleaned with ethanol for 10 min. Then they were dried in vacuum for 1 h. Finally, they were rinsed using DI water and baked in 450 ºC furnace for 1 h.

The nanotubes where coated with SnO_2/Sb using a sol-gel method. First citric acid was dissolved in an ethylene glycol solution at 60 ºC which was stirred for 30 min to form citrate esters. Then the temperature was increased to 90 ºC and then $SnCl_4$ and $SbCl_3$ were added. At that point, the temperature was increased to the boiling point and stirred for 1 h after all salts dissolved completely. After a complete cooldown, a clear light-yellow sol-gel solution will form. The molar ratio of the chemicals were: ethylene glycol/citric acid/

$SnCl_4/SbCl_3 = 140:30:9:1$, 0.866, 0.278, 0.111 and 0.017 g/cm^3, respectively. The sol-gel was aged for 30 days and was continuously stirred. We used the following steps for our dip-coating method to form the gel layer: (1) We immersed the nanotubes structure in the sol-gel for 5 min and pulled it out at a speed of 5 cm/min. (2) We then dried the coated nanotube structure at 140 ºC for 10 min. (3) We then baked the coated nanotube structure at 500 ºC for 10 min and then allowed it to cool down to room temperature. (4) We then washed it with DI water and air dried it. This dip-coating procedure was repeated 15 times to increase the coverage of the coating layer. (5) The last step was baking the coated nanotube array in the furnace for 2 h at 500 ºC.

5.3.3 Modelling

Numerous mathematical electrochemical oxidation modeling approaches have been reported [170-172]. However, to the best of our knowledge, there is no comprehensive electrochemical oxidation kinetic model established that works for all systems, because the complexity of reactions (i.e., oxidation reactions on anode surface (direct) and oxidation reactions in solution with anode generated hydroxyl radicals, oxygen, hydrogen peroxide, ozone (indirect oxidation) that occur all at the same time in EAOPs).

Therefore, a simplified model was used to mainly compare 2-D & 3-D systems focusing on indirect oxidation regime because our anode has a very large band gap. The limiting current density j_{lim} (mA/cm^2) of a system depends on the mass transfer coefficient k_f (m/s), and the organic compound concentration, C_e (mol/L). When the current density is smaller than direct limiting current density ($j \leq j_{lim,d}$), the oxidation is mainly controlled by direct electron transfer.

$$\text{Organic} \rightarrow \text{Products} + ne^- \quad (35)$$

$$j_{lim,d} = n \cdot F \cdot k_f \cdot C_e \quad (36)$$

Where n is the number of the electron that transferred in direct oxidation and F is the Faraday constant.

When applied current density is larger than direct limiting current density but smaller than indirect limiting current density ($j_{lim,d} \leq j \leq j_{lim,id}$), the oxidation is controlled by direct electron transfer and indirect oxidation together.

$$\text{Organic} + H_2O \rightarrow \text{Products} + mH^+ + me^- \quad (37)$$

$$j_{lim,id} = m \cdot F \cdot k_f \cdot C_e \quad (38)$$

Where m is the number of electrons that transferred in indirect oxidation. For a high flow rate, the concentration of target compound in the inlet C_{in} is approximately equal to the concentration at outlet, C_{out} for the differential column batch reactor (DCBR). In this case, the DCBR act as a completely mixed batch reactor (CMBR) and its observed first-order rate constant k_{obs} can be estimated as follows:

$$k_{obs} = \frac{V_R+V}{V \cdot t} \cdot \ln \frac{C_0}{C_t} \quad (39)$$

Where V_R is the volume of reservoir (cm^3); V is the volume of differential reactor (cm^3); t is oxidation time (min); C_o and C_t are initial organic concentration in the reservoir and concentration at time t ($mol \cdot L^{-1}$), respectively; When current density is larger than indirect limiting current density, the oxidation is controlled mainly by mass transfer [173-

175]. In addition, the oxidation of sulfate electrolyte also plays a crucial role in electrochemical oxidation. The sulfate electrolytes can be oxidized and generate active oxidants that also oxidize target organics [176-177]. This part of oxidation is called salt effect. A general modeling approach considers mass transfer and salt effect shows as follows:

$$r = -k_f \cdot (C_B - C_S) \cdot A - k_{SE} \cdot C_B \tag{40}$$

$$(V + V_R)\frac{dC}{dt} = -V(A \cdot k_f + k_{SE}) \cdot C_B \tag{41}$$

$$C_t = C_0 \cdot e^{-\frac{V(A \cdot k_f + k_{SE}) \cdot t}{V + V_R}} \tag{42}$$

Where r is the overall oxidation rate ($mol \cdot L^{-1} \cdot s^{-1}$); C_B and C_S are organic concentrations in the bulk solution and on the anode surface ($mol \cdot L^{-1}$), C_S is essentially zero for relatively high current densities and low initial organic concentrations; k_{SE} is the salt effect rate constant (s^{-1}); A is the surface area per volume of the differential reactor (cm^2/cm^3).

The mass transfer coefficient can be calculated from Sherwood number, Sh, of the system and Sh can from this correlation [178,179].

$$Sh = \frac{k_f \cdot d}{D_l} = 3.3 \cdot \left(\frac{d}{l} \cdot Re \cdot Sc\right)^{\frac{1}{3}} \tag{43}$$

$$\mathrm{Re} = \frac{\rho \cdot u \cdot d}{\mu} \tag{44}$$

$$\mathrm{Sc} = \frac{\mu}{\rho \cdot D_l} \tag{45}$$

Where d is characteristic length (electrode spacing here, cm); l is the length of the reactor (cm), D_l is the diffusivity (cm^2/s); Re is the Reynold number; Sc is the Schmidt number; ρ is the solution density (g/cm^3) and μ is the fluid dynamic viscosity ($kg \cdot m^{-1} \cdot s^{-1}$).

This correlation is valid for flow in a channel, a reactor length to electrode spacing ratio of less than 126 and Sherwood number $\gg 1$, which is suitable for this study.

5.4 Results and Discussions

5.4.1 Anode Characterization

Figure 10 displays the SEM characterization of the fabricated anode. Figure 10a shows that after 10 dip coating, the SnO_2/Sb layer is still not uniform and blue TiO_2 nanotubes (estimated to be 18-22 nm in diameter, Appendix) are exposed. It has been suggested that indirect oxidation will not take place on the top of the nanotube array, because the number of surface reaction sites are very limited [180-183]. SnO_2/Sb has a higher bandgap (3.5 eV) and the SnO_2/Sb coating layer enhances the anode conductivity. We confirmed that dip coating the nanotube array 15 times can produce a fully coated, uniform surface with less cracking on outer surface (Figure 10b). Figure 10c shows the non-aged sol-gel resulting an average 2-3 μm SnO_2-Sb crystal size on the surface. Figure 2d shows the 30-days aged sol-

gel resulting a smaller (~0.5 μm), uniform and more compact surface which provides more surface area and surface sites for oxidation.

Linear sweep voltammetry (LSV) experiments were conducted to evaluate the electrochemical properties of the anode. Figure 11 compares the electrochemical performance of a reference BDD electrode and our fabricated BTNA/TA electrode. The results show our fabricated electrode has an over potential of 2.78 V and is higher than the BDD anode which had an over potential of 2.42 V. The LSV results match our experimental observations, i.e., we observed only small amount of bubbles at the anode which is mainly oxygen, a very poor oxidant. The results indicate our anode has similar/stronger electrochemical oxidation performance to the BDD. The standard reduction potentials of primary reactive oxygen species (ROSs) that could be generated on the anode are shown. Accordingly, electrons that flow out from the anode create a very energetic valence band hole h^+ as compared to these reduction potentials. These holes react with water and will tend to create strong oxidants (i.e., $HO\cdot$) rather than weak oxidants (e.g., O_2 or H_2O_2), which just wastes energy.

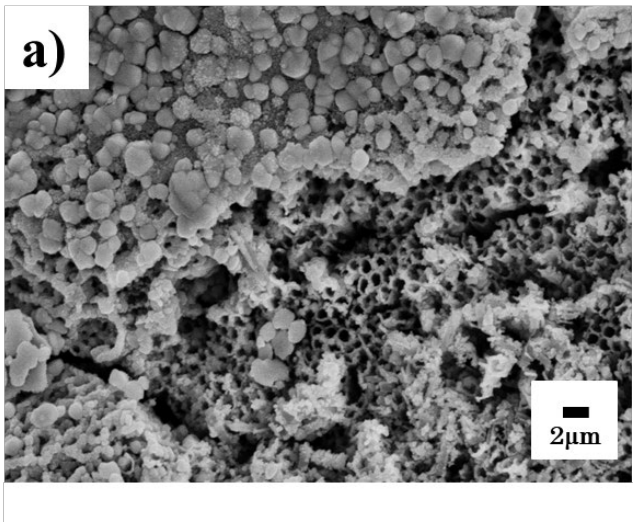

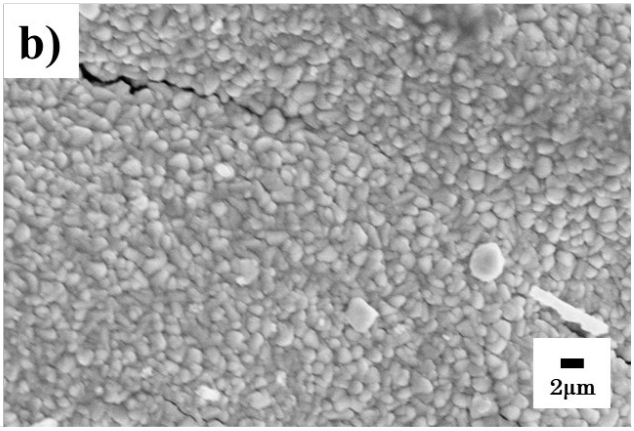
b)
2µm

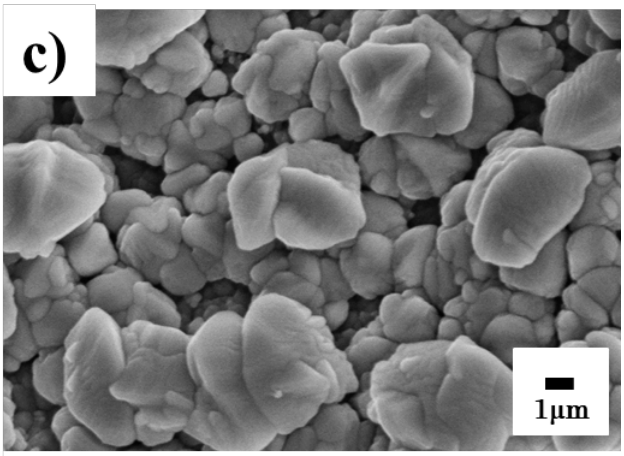
c)
1µm

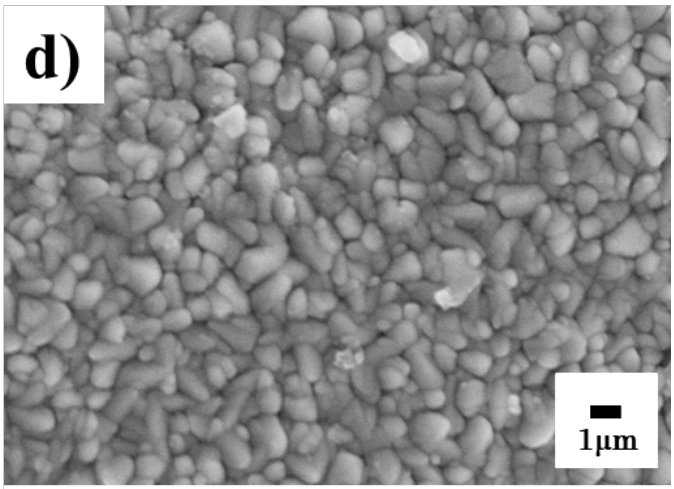

Figure 10 - Anode SEM characterizations. (a) blue TiO_2 nanotubes array half coated with SnO_2/Sb (coated 10 times), (b) fully coated SnO_2/Sb surface (coated 15 times), (c)

non-aged sol-gel coated SnO_2/Sb surface (coated 15 times), and (d) aged (30 days) sol-gel coated SnO_2/Sb surface (coated 15 times).

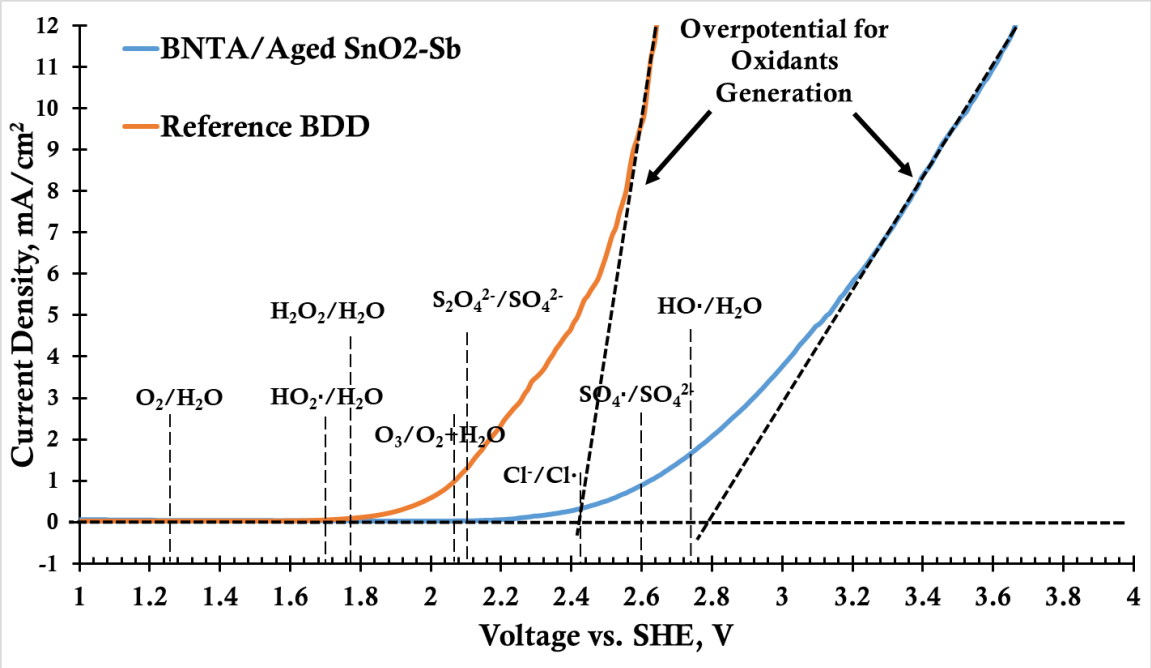

Figure 11 - Linear sweep voltammetry of our BTNA/TA and Boron-Doped Diamond electrode for a 0.5 M H_2SO_4 solution at a scan rate of 10 mV/s; A platinum mesh and a saturated calomel electrode (SCE) served as the auxiliary electrodes and the reference electrode, respectively; O_2, $HO_2\cdot$, H_2O_2, O_3, $S_2O_4^{2-}$, $Cl\cdot$, $SO_4^{-}\cdot$ and $HO\cdot$ have standard reduction potentials (pH = 0) +1.23 V, +1.7 V, +1.77 V, +2.07 V, +2.1 V, +2.43 V, +2.6 V and +2.74 V, respectively; the fabricated woven mesh electrode has surface area ~7.182 cm^2 and BDD has 12 cm^2.

5.4.2 Electron Efficiency

Electron efficiency, η, is a useful figure of merit to evaluate the energy efficiency of electrochemical oxidation treatment system. The electron efficiency was calculated based

on Pacheco's method [186]. Electron efficiency compares how many electrons leave the anode to the number of electrons that resulted from oxidation. We compared electron efficiency for both 2-D and 3-D systems for the same operational conditions. η, is the ratio of total organic carbon (TOC) destruction as compared to the chemical oxygen demand (COD) destruction. It determines how much oxidation occurs for electrons that leave anode.

$$\eta = \frac{32}{12} \cdot \frac{n}{4x} \cdot \frac{d(TOC)}{d(COD)} \tag{46}$$

Where TOC is expressed in mg (C)/L, COD is expressed in mg (O_2)/L, and n is the number of electrons transferred from the anode for complete oxidation. x is the number of carbon atoms in the organic compounds. The stoichiometric equation for benzoic acid is:

$$C_7H_6O + 12H_2O \rightarrow 7CO_2 + 30H^+ + 30e^- \tag{47}$$

The ratio of $\frac{d(TOC)}{d(COD)}$ for our anode is shown in Appendix. The TOC and COD were measured for a constant current density 30 mA/cm^2, a flow rate of 400 mL/min (fluid velocity was 0.03 m/s in 2-D system and 0.11 m/s in 3-D system), initial pH is 5.17, the water was a surface water (should have negligible salt impact). Employing Eq. (15) and (16), we found that the electron efficiency for the destruction of 1 mM benzoic acid (~122 mg/L) is 86.6% (±10%) and 106.65% (±15%) for the two and 3-D systems after 4 h oxidation. This result demonstrates that during oxidation, nearly 87% and almost all electrons are effectively used for benzoic acid destruction (i.e. not wasted in producing O_2 and other ROS which do not oxidize benzoic acid) and the byproducts are mineralized effectively. It is interesting to note that the electron efficiency may larger than 100%. A possible explanation is that

some dissolved oxygen is utilized and undergoes radicals chain reactions. Also, for this case we did not add any additional electrolytes and no salt effect was encountered.

5.4.3 Comparison of the two-dimensional and three-dimensional system

In the conventional 2-D system, electrolyte concentration is crucial because the applied cell voltage is large in low ionic strength water streams, unless we add extra electrolyte or reduces the electrode spacing. However, reducing electrode spacing will dramatically increase the capital cost of an electrochemical device because more electrodes units are required [187]. In the 3-D system, proton exchange membrane (PEM) serves as the electrolyte for proton conduction and theoretically, it does not require extra electrolyte if the proton exchange capacity is high. In our bench experiments, we compared two systems in various ion strength conditions by adding a different amount of Na_2SO_4 as the electrolyte. Table 1 shows the applied voltage. In general, voltage elevates when ion strength decreases in both systems. The 3-D system has a significant voltage reduction effect in all conditions, especially in low conductivity situations. The 2-D system reaches a maximum voltage of the power source (60 V±1V) at 0.001 M Na_2SO_4 solution (measured conductivity 260 μS/cm) and real surface water (112.5 μS/cm). Current flow in DI water for the 2-D system is negligible at the highest voltage we could supply. On the other hand, the 3-D system does have current flow even in DI water (as low as 4 μS/cm). The voltage for the 3-D electrode is 79.06% lower than that the 2-D electrode for a 0.001 M Na_2SO_4 condition. The result shows the use of PEM can effectively establish a current flow in the 3-D system for low electrolyte concentration. The use of meshed (gauze type) electrode materials provides distinct advantages for electron conduction, proton mitigation from surface reaction sites to PEM and hydroxyl radicals production. During the electrolysis, we

also observed that the current slowly decrease and dramatically increase. This phenomenon repeated several times in almost all experiments. A possible explanation is that the meshed electrode hinders bubbles from being released from the surface and the bubbles cover the reaction sites and slow down the current flow and oxidation reactions.

Table 3 - Comparison of applied voltages for two & three-dimensional systems under various electrolyte concentrations. The operational current density is 30 mA/cm^2 (surface water 10 mA/cm^2 due to the 2D system reached maximum voltage). The electrode spacing of the 2D system is 1 cm. The current flow of the 2D system in DI water is negligible.

	Electrolyte Na_2SO_4	M	DI water	Surface water	0.001	0.005	0.01	0.05	0.1
	Conductivity	µS/cm	4	112.5	260	1074	1964	8740	16210
2D	Voltage	V	ND	60.4	60.3	28	17.7	8.3	7.3
3D	Voltage	V	28.5	16.9	12.7	10.6	7.9	7.5	5.8
	3D Voltage Reduction	%	ND	71.97%	79.06%	62.14%	55.37%	9.64%	20.55%

Many researchers reported that the oxidation of electrolytes plays important roles in electrochemical oxidation. Here the oxidation of sulfate electrolyte can generate radicals and these radicals can react with organics. Although the primary objective is to generate most powerful hydroxyl radicals, it is impossible to avoid the generation of other radicals because most of them have smaller reduction potentials than hydroxyl radicals (E^0 = 2.74

V). For instance, the standard reduction potentials for commonly seen electrolytes generated chloride radicals ($Cl^{2-}\cdot$), chlorine radicals ($Cl\cdot$) and sulfate radicals ($SO_4^{2-}\cdot$) are +0.67 V, +2.43V and +2.60 V respectively [188]. Theoretically, the 3-D system does not require electrolyte for conduction, however, the oxidation of electrolytes still occurs when electrolytes are present. By employing Eq. 42, we quantified the effect of sulfate electrolyte oxidation generated radicals oxidizing organics (name as the salt effect). Figure 12 plot the experimental data of 2-D & 3-D electrochemical oxidation systems for benzoic acid degradation in various electrolyte (Na_2SO_4) concentrations and the model fittings that considered salt effects. The mass transfer coefficient k_f and other hydrodynamic parameters were determined by Eqs. 40-42.

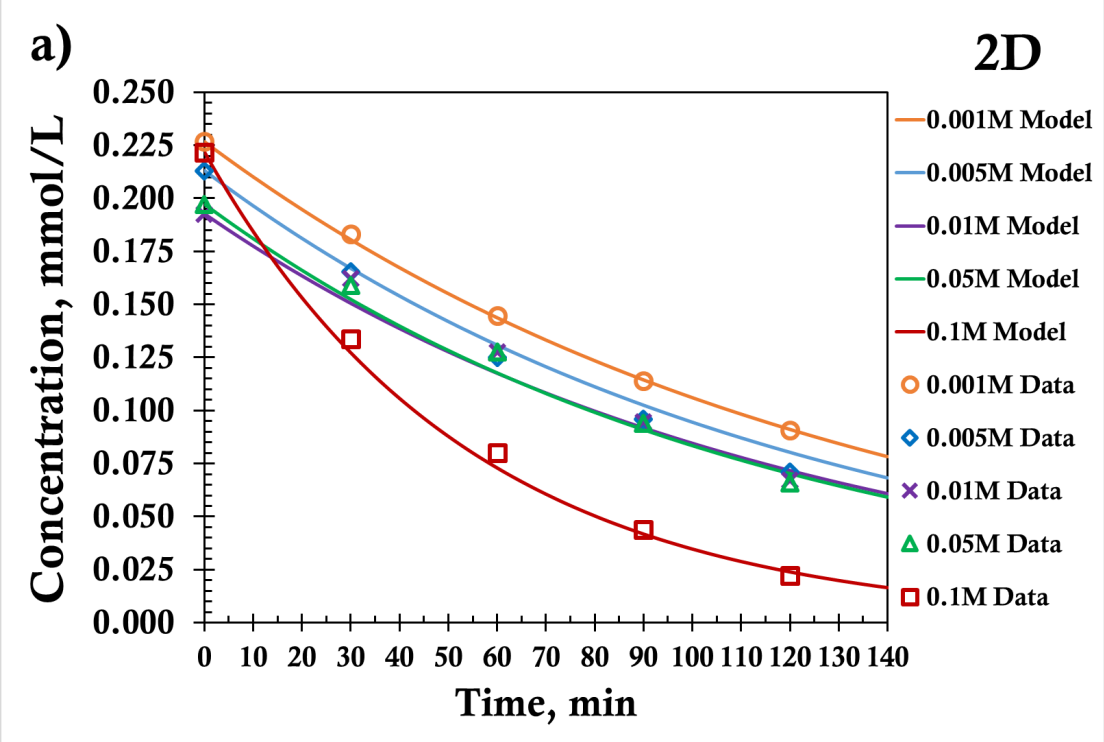

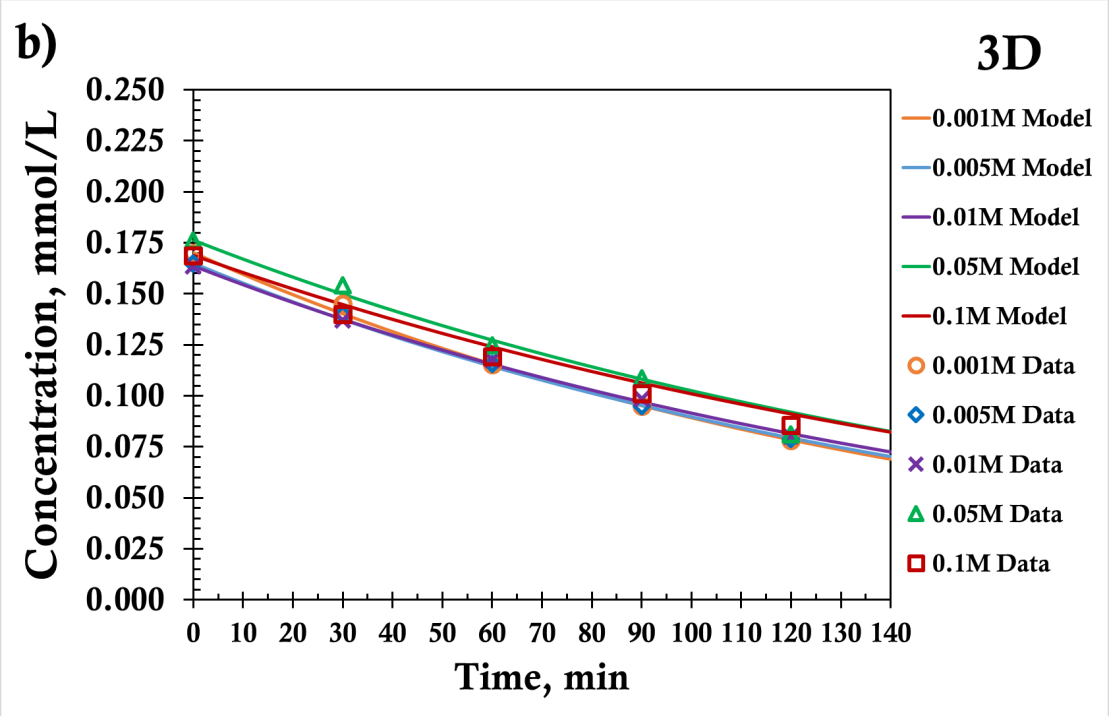

Figure 12 - 2-D & 3-D electrochemical systems in 0.001M, 0.005M, 0.01M, 0.05M and 0.1M Na_2SO_4 electrolyzed solution for benzoic acid degradation. The dots are experimental data and the lines are fitted model. The reactor is a differential column batch reactor and the oxidation reactions only take place in the anode chamber. The initial concentrations are 0.2 mmol/L (~24.4 mg/L), pH is 4-4.5, the operating current density is 30 mA/cm^2, electrode spacing in the 2-D system is 1 cm, the hydrodynamic characteristic length in the 3-D system is 0.3 cm, the pumping flow rates for both systems are 400 mL/min (Re=370).

From the results we observe, the reaction rates in the 3-D system are identical because the current density is operated all at 30 mA/cm^2. The reaction rate is not increased by adding more sulfate electrolyte and mainly controlled by current density. In the 2-D system, the overall oxidation rates are similar except for 0.1 M Na_2SO_4 solution. The reaction rate is

significantly higher than other conditions and this is because of the salt effect ($k_{SE} = 3.09 \times 10^{-4}\ s^{-1}$). The salt effect rate constants that fitted from model lists in Table 4. All fittings are excellent because the objective functions are small (OF < 0.07).

Table 4 - The rate constants of benzoic acid degradation that attributed to oxidized sulfate electrolyte (salt effect) for various concentrations. The operational current density is 30 mA/cm^2 (surface water 10 mA/cm^2 due to the 2-D system reached maximum voltage). The electrode spacing of the 2-D system is 1 cm, the hydrodynamic characteristic length in the 3-D system is 0.3 cm.

	Electrolyte Concentration (Na_2SO_4)	**M**	**0.001**	**0.005**	**0.01**	**0.05**	**0.1**
2D	k_{SE} Salt Effect Rate constant	s^{-1}	1.26×10^{-4}	1.35×10^{-4}	1.37×10^{-4}	1.43×10^{-4}	3.09×10^{-4}
3D	k_{SE} Salt Effect Rate constant	s^{-1}	1.07×10^{-4}	1.01×10^{-4}	9.63×10^{-5}	9.02×10^{-5}	8.52×10^{-5}
	3D Salt Effect Reduction	%	15.23%	25.20%	29.69%	37.05%	72.42%

The salt effect for the 2-D system increases as the sulfate electrolyte concentration increases and reaches its peak at the highest concentration (0.1M). This is because as the sulfate concentration increases, the concentration of sulfate radicals increases, and they are causing the oxidizing of benzoic acid. On the contrary, the salt effect in the 3-D system

decreases as the increasing sulfate electrolyte concentration and the salt effect in Table 4 is only 1.76% - 2.2% of the BA destruction in 3-D system with various ionic strength. In the 3-D system, the proton exchange membrane (PEM) prohibits anions from migrating from cathode chamber to anode chamber and oxidation rate of sulfate would be lower. It appears that increasing sulfate electrolyte concentration improve the production of hydroxyl radicals for the 3-D system. The applied voltage plays a crucial role in electrochemical oxidation and a higher voltage favors the production of powerful radicals. To quantify the correlations between salt effects, voltage and sulfate electrolyte concentration in two systems, we calculated the statistic correlation coefficient. The correlation coefficients are 0.913 and 0.973 for salt effect in 2-D system vs. sulfate electrolyte concentrations and salt effect in a 3-D system vs. applied voltage. The results demonstrate strong correlations (close to 1) salt effect is mainly determined by sulfate electrolyte concentration in 2-D system. The salt effect in 3-D system is mainly determined by the applied voltage.

Electric energy consumption per order of destruction (EE/O) is an important figure of merit. In the electrochemical oxidation system, the EE/O (kWh/m^3) can be calculated as eq (16).

$$\mathrm{EEO} = \frac{\mathrm{U} \cdot \mathrm{J} \cdot \mathrm{S} \cdot \mathrm{t}}{\mathrm{V} \cdot \log\left(\frac{\mathrm{C_0}}{\mathrm{C_t}}\right)} \tag{48}$$

Where U is the voltage (V), J is the current density (mA/cm^2), S is the surface area (cm^2), t is the electrolysis time (min), V_R is the volume of reservoir (cm^3), V is the volume of differential reactor (cm^3), and C_0 and C_t are the initial concentration and concentration in

time t, respectively. Figure 13 - EE/O of 2-D and 3-D electrochemical electrode system. The reactor is a differential column batch reactor and the oxidation reactions only take place in the anode chamber. The initial concentrations are ~0.2 mmol/L benzoic acid (~24.4 mg/L), pH is 4-4.5, the operating current density is 30 $\mathrm{mA/cm^2}$, electrode spacing in the 2-D system is 1 cm, the hydrodynamic characteristic length in the 3-D system is 0.3 cm, the pumping flow rates for both systems are 400 mL/min (Re=370).shows the calculated EE/O results for two and 3-D systems. EE/O in both systems decrease when sulfate electrolyte concentration increases. The 2-D system has a lower EE/O for 0.1 M Na_2SO_4 concentration (4.46 kWh/m^3) than the 3-D system (12.25 kWh/m^3) and slightly higher EE/O (13.19 kWh/m^3vs. 11.81 kWh/m^3) for a 0.05 M Na_2SO_4 electrolyte concentration. For lower sulfate concentrations, the 3-D system has lower EE/O. For 0.001 M concentration, the three-dimension system reduced the energy consumption by 63.17%. Moreover, the 2-D system cannot operate in DI water condition where 3-D can and its EE/O is 34.03 kWh/m^3.

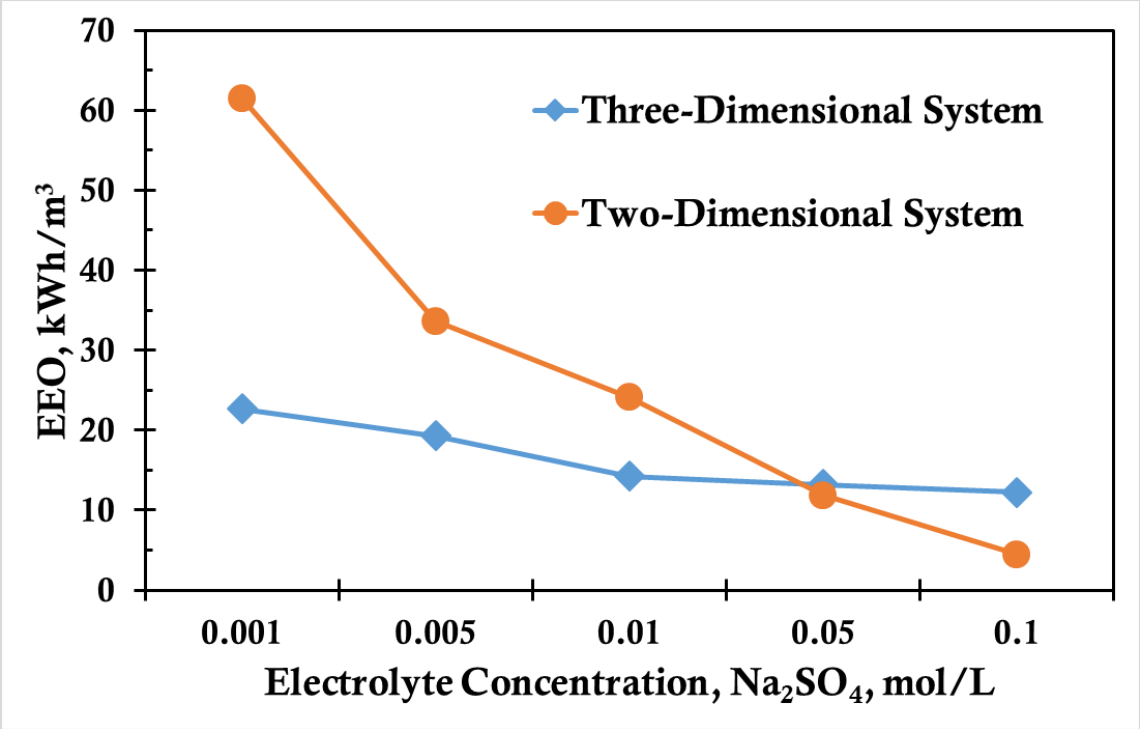

Figure 13 - EE/O of 2-D and 3-D electrochemical electrode system. The reactor is a differential column batch reactor and the oxidation reactions only take place in the anode chamber. The initial concentrations are ~0.2 mmol/L benzoic acid (~24.4 mg/L), pH is 4-4.5, the operating current density is 30 mA/cm^2, electrode spacing in the 2-D system is 1 cm, the hydrodynamic characteristic length in the 3-D system is 0.3 cm, the pumping flow rates for both systems are 400 mL/min (Re=370).

From these results, we found that the 3-D system has smaller applied voltages and salt effect rate constants than the 2-D system for all conditions. It is these two parameters impact the overall EE/O. To further drive the analysis, we investigated the contribution of applied voltages and salt effect rate constants on the EE/O. To estimate the voltage impact and salt impact we used the following equations:

$$Voltage\ Impact\ = \frac{UR_{3D}}{UR_{3D}+SI_{2D}} \tag{49}$$

$$Salt\ Impact\ = \frac{SI_{2D}}{UR_{3D}+SI_{2D}} \tag{50}$$

$$UR_{3D} = \frac{U_{2D}-U_{3D}}{U_{2D}} \tag{51}$$

$$SI_{2D} = \frac{k_{SE,2D}-k_{SE,3D}}{k_{SE,3D}} \tag{52}$$

Where UR_{3D} is the voltage reduced that 3-D system comparing to 2-D system; SI_{2D} is the salt effect increased that 2-D system comparing to 3-D system; U is the applied voltage (V); k_{SE} is the salt effect rate constant (s^{-1}). Figure 6 shows the 3-D system can reduce the overall EE/O by more than 63%, 42% and 41% for the three low sulfate concentrations, but it increases the EE/O by more than 11% and 174% for two higher sulfate concentrations. For lower sulfate concentrations, the applied voltage has the greatest impact on the EE/O and the 3-D system has a significantly voltage. For higher sulfate concentrations, the salt effect has a very high contribution to BA destruction and 2-D system has a lower EE/O than the 3-D system.

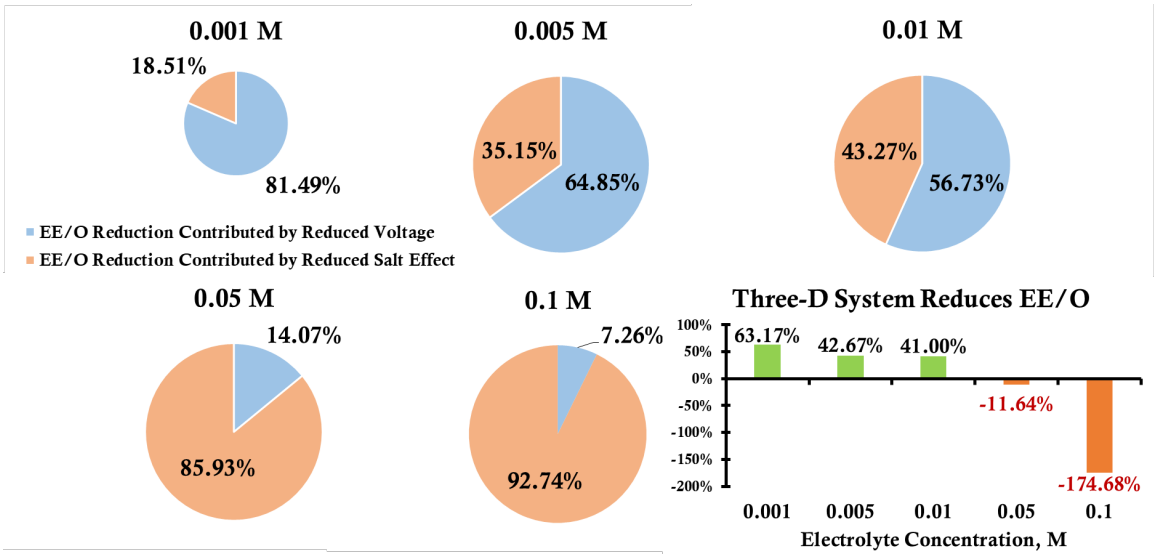

Figure 14 - The distribution of voltage and salt effect contribution regarding the EE/O reduction by the 3-D system. The distributions are calculated by the difference of applied voltage between 2-D & 3-D system as compared to the 3-D voltage and the difference of salt effect between 2-D & 3-D system as compared to the 2-D system. The EE/O reduction percentage is performed by using the difference between 2-D & 3-D results compared to the 2-D value.

5.5 Environmental Implications

Full-scale electrochemical oxidation devices have been installed for many applicable industrial wastewater treatment plants such as the paper mill, dye industry, refinery etc. The shortcomings are high energy consumption and potential byproducts that would be formed from the oxidation of electrolytes and other sources. However, we find electrochemical oxidation technologies have distinct energy efficiency (EE/O) advantages for high strength wastewater treatment. Substituting Eq (10) into Eq (16), a governing equation shows as follow:

$$EE/O = \frac{U \cdot J \cdot S}{0.434 \cdot V \cdot (A \cdot k_f + k_{SE})} \quad (53)$$

EE/O is independent of the concentration of target organic contaminants when applied current density is higher than the limiting current of the solution and the overall oxidation rate is mainly controlled by the mass transfer process. Experimental data for 0.2 mM (24 mg/L) and 1 mM (122 mg/L) benzoic acid degradation with electrochemical oxidation had nearly EE/O values (Appendix). In addition, we compared the smallest EE/O of 2-D & 3-D electrochemical oxidation systems with several conventional advanced oxidation processes (AOPs) including H_2O_2/O_3, UV/H_2O_2, UV/persulfate, UV/HOCl and UV/TiO_2 using models that predict the removal of the parent compound. The modeling parameters are summarized in SI (Appendix) and the model predicted EE/O values are listed in Table 5.

Table 5 - Summary of model simulation results for H_2O_2/O_3, UV/H_2O_2, UV/persulfate, UV/HOCl, UV/TiO_2, two- & three-dimensional electrochemical oxidation systems. The initial benzoic acid concentrations for AOPs are 20 mg/L, 200 mg/L, and 2000 mg/L and the Reynolds numbers (Re) for EAOPs are 19 ($Q = 20$ mL/min), 463 (500 mL/min) and 2037 (2000 mL/min).

AOPs	Minimal EE/O (kWh/m^3)		Minimal EE/O (kWh/m^3)		Minimal EE/O (kWh/m^3)	
Benzoic Acid Initial Conc.	$20\ mg/L$ (~16 mg/L TOC)		$200\ mg/L$ (~140 mg/L TOC)		$2000\ mg/L$ (~1379 mg/L TOC)	

H_2O_2/O_3	0.015		6.79		176.48	
UV/H_2O_2	0.9		27.18		1768	
UV/persulfate	1.28		40.22		8208	
UV/HOCl	3.67		24.42		833.5	
UV/TiO2	10.38		90.72		882.71	
Electrolyte (Na_2SO_4)	**2D EE/O (kWh/ m^3)**	**3D EE/O (kWh/m^3)**	**2D EE/O (kWh/ m^3)**	**3D EE/O (kWh/m^3)**	**2D EE/O (kWh/ m^3)**	**3D EE/O (kWh/m^3)**
	Re = 19		Re = 463		Re = 2037	
0.001 M	64.66	24.05	60.15	22.6	56.34	21.36
0.01 M	26.76	15.52	25.04	14.48	23.57	13.6
0.1 M	4.69	12.94	4.55	12.07	4.43	11.32

The results from Table 5 demonstrate that the electrochemical oxidation systems have much higher EE/O as compared to conventional AOPs for low concentrations (20 mg/L). EAOPs require 1 or 2 order of magnitude more energy to oxidize 90% of the parent compound, even for high Reynolds numbers (high mass transfer) conditions. When the initial concentrations increase to 200 mg/L, EAOPs exhibit a comparable EE/O level with conventional AOPs. EAOPs have much higher energy efficiency for treating 2000 mg/L benzoic acid, (~1379 mg/L TOC) and 3-D system have lower EE/O than 2-D in 0.001 M and 0.01 M conditions. Consequently, conventional AOPs such as H_2O_2/O_3 and UV based

technologies are good candidates for micropollutant oxidation because the operational energy inputs are much smaller than electrochemical oxidations. However, EAOPs have lower energy requirement for high strength wastewater treatment (using high current density and Re numbers). The chemical dosage for conventional AOPs for high strength wastewaters are very large and this will dramatically increase operational costs. The 3-D system can save more energy than the 2-D system in low ionic strength conditions because they have significantly lowered the required voltage. Furthermore, the 3-D system has smaller salt effect rate constants (up to 72.42%) which indicates the 3-D system does not depend on electrolytes for oxidation and has less tendency to generate DBPs from the oxidizing of electrolytes. The 3-D electrochemical oxidation system is a more energy efficient technology for low ion strength industrial wastewater treatment and a safer technology has the potential for reclaim or portable water treatment.

CHAPTER 6. ELECTROCHEMICAL OXIDATION APPLICATIONS AND EMERGING CONTAMINANTS TREATMENT

6.1 Abstract

Electrochemical oxidation was proposed as a promising technology for algal control in drinking water treatment. To be effective, the electro-generated oxidants should have long half-lives and could continually inhibit the growth of algae. In this study, we used the electrochemical system equipped with a Ti/RuO_2 anode which focus on generating long half-lives chlorines and H_2O_2. Compared with other more powerful radicals (e.g. $HO\cdot$, $Cl\cdot$) which could mainly be scavenged by cell walls/membranes, chlorines and H_2O_2 can penetrate them, persist much longer and thus effective to inhibit algae growth. We explored the impact of electrical field and electro-generated oxidants on algal inhibition, and they were both found to be effective. We investigated the production of electro-generated reactive species and their contributions to the inhibition of *Microcystis aeruginosa* (*M. aeruginosa*) in simulated surface water with low Cl^- concentrations (< 18 mg/L). During the electrolysis at current density of 20 mA/cm^2, when initial Cl^- concentrations increased from 0-18 mg/L (0-5.07×10^{-4} mol/L), the chlorines increased from 0 to 3.62×10^{-6} mol/L, and the H_2O_2 concentration decreased from 3.68×10^{-6} to 1.15×10^{-6} mol/L (H_2O_2 and ClO^- react fast). The electro-generated chlorine species were more effective than H_2O_2 at low Cl^- concentration (18 mg/L, typical Cl^- concentration in the drinking water sources of the middle and lower reaches of the Yangtze River, China). In addition, we developed a kinetic

model that simulates the production of oxidants (correlated with other important parameters, such as the current density) at 18 mg/L Cl^- and the model gave a decent prediction for other Cl^- levels.

6.2 Introduction

Microcystis blooms commonly occur in eutrophic freshwater all over the world due to nutrient contamination [187,195] and global warming [179,180] The occurrence of *Microcystis* blooms pose threats to drinking water safety and ecosystem health [165,179,183,192]. Algal cells can release organic matters, including microcystins, odor, and taste compounds into the water bodies during their growth and lysis [194]. Conventional coagulation methods are still considered as the major processes for algae removal in drinking water treatment. However, due to the small size and low specific gravity of algae, it is difficult to remove algae effectively [163,182]. In addition, algal cells can clog water treatment plants facilities which further increases the difficulties of treatment [190]. Therefore, it is necessary to develop effective techniques to inhibit and inactivate algae during the pre-oxidation process in drinking water treatment.

Electrochemical oxidation process represents a promising technology for algae control in drinking water treatment [164,172,173,176,177,178]. The electrochemical treatment of microorganisms involves two major mechanisms: (1) oxidation by electro-generated oxidants, including long lifetime oxidants such as chlorines (including Cl_2, HClO, and ClO^-) and hydrogen peroxide (H_2O_2), and radicals (e.g. $HO\cdot$) [161,175,188];

(2) the effect of electrical field on cell membranes [176,177,181]. It was reported that when the algae exposed to an external electrical field, permanent or transient pores in the membrane of the cells can be induced, and electro-generated oxidants could go inside the cell more easily [163]. Consequently, comparing with traditional disinfection methods, electrochemical oxidation is considered more effective.

Researchers have observed that some algal cells can survive from electrochemical treatment and are still functional to grow [172,173,191]. To be effective, the oxidants that generated from anode should have long half-lives and continually inhibit the growth of algae [185]. Radicals can be generated at anode surface and indeed, they are powerful active oxidants. However, it has been shown radicals react badly with algae and the reason is they are too reactive and directly react (scavenged) with the cell walls and membranes rather than kill the cells. On the contrary, chlorines and H_2O_2 are more effective due to their long half-lives, which can be up to hours in the absence of sunlight [184,159]. External electrical field creates pores (holes) on cell membranes and increases their conductivity. This effect favors better chlorines and H_2O_2 transportation inside the cells [159,177,186].

Ti/RuO_2 anode is a suitable anode for algae treatment. It is a mixed metal oxide (MMO) electrode that focuses on chlorines and H_2O_2 generation [167,191,172]. The overpotential for oxygen evolution of Ti/RuO_2 is 1.1 V (vs. Ag/AgCl) [167] , equivalent to 1.297 V vs. NHE, which is higher than oxygen-forming standard reduction potential (1.23 V) but still relatively low. Anodes with high overpotentials are indeed more powerful but less conductive. From the electron efficiency perspective for algae treatment, Ti/RuO_2

anode can utilize electrons more effectively to generate Cl_2 (E^0= 1.36 V) and H_2O_2 (E^0= 1.77 V).

At relatively high Cl^- concentrations (35-600 mg/L), microorganism inactivation by the MMO anode is mainly due to the electrochemically generated chlorines [167,185]. The electrochemical production of chlorine species through the addition of high concentrations of Cl^- (35-600 mg/L) has been well reported [163,167,177]. The typical Cl^- concentration in drinking water resources in the middle and lower reaches of the Yangtze River, China is 10-30 mg/L (specifically 18 mg/L in Donghu Lake in Wuhan, China). At such low Cl^- concentrations, the capability of electrochemically generated oxidants in algal inhibition is questionable because much less chloride is available to produce chlorines. Furthermore, H_2O_2 can also be generated at this Cl^- concentrations. The individual contributions of chlorines and H_2O_2 in algal inhibition are not well understood.

In this study, the electrochemical system equipped with a Ti/RuO_2 anode which focus on generating chlorines (i.e. Cl_2, HOCl, and OCl^-) and H_2O_2 from Cl^- and water was used. We explored the impact of electrical field and electro-generated oxidants on algal inhibition in this system. We investigated the contributions of electro-generated chlorines and H_2O_2 on the inhibition of *Microcystis aeruginosa* (*M. aeruginosa*) growth at low Cl^- concentrations (< 18 mg/L). The production of chlorines and H_2O_2 at the anode was studied under various operational conditions. A kinetic model was developed to simulate the oxidants production in this complex system. Fitted kinetic parameters at 18 mg/L Cl^- were

used to predict oxidant concentrations of other Cl^- conditions. The contribution of chlorines and H_2O_2 for algal inhibition were also explored.

6.3 Materials and Methods

6.3.1 Experimental apparatus

A batch-type reactor was set up for the electrochemical treatments, and a schematic diagram is shown in Appendix. Glass beakers with 100-mL volumes were used as reactors and equipped with a Ti-RuO_2 anode and stainless-steel cathode, which was the same as our previous work [173]. The dimensions of the electrodes were approximately 2.5 cm×7.5 cm. The area immersed in the algal solution was 13.75 cm^2. The electrodes were 4 cm apart. Agitation during electrolysis was provided by a magnetic stirrer (Jiangsu Honghua, Model 85-2, China), and the agitation rate was 200 rpm. A direct-current power source (Guangdong Yishite, ModelWYK-305B2, China, 30 V/5 A) was employed to provide the electric power during the electrochemical experiments. The electrolyte was BG-11 medium, and its composition [190] is shown in Appendix. The room temperature was controlled at approximately 20 °C.

6.3.2 Algal Cultivation

Algal culture before electrochemical treatment. *M. aeruginosa* (FACHB-905) was obtained from the Wuhan Institute of Hydrology, Chinese Academy of Sciences.

Exponentially growing cultures of *M. aeruginosa* were used for the experiments. Algal growth medium BG-11 was added to erlenmeyer flasks equipped with gauze stoppers, which were then autoclaved (Shanghai Boxun, Mode BMX-30R, China) (121 °C, 30 min). Stock cultures (containing 18 mg/L Cl^-) were prepared daily by transferring a known number of algae cells from a culture in the log growth phase to a freshly sterilized flask containing BG-11 media. The algae seeds were cultured in an illumination incubator (Shanghai Boxun, Model SPX-250B-G, China). The light was provided by an incandescent lamp with an automated 14 h/10 h light/dark cycle. The light intensity during the light phase was 30 μEinstein/(m^2·s). The temperature was controlled at 25±1 °C.

Algal culture after electrochemical treatment. To determine whether the remaining algae cells had the potential to survive and grow, the algal solution was poured into a 100-mL conical flask with a gauze stopper, which was placed in an illumination incubator for 8 days of cultivation. Twelve-milliliter aliquots were removed from the conical flask at 0, 2, 4, 6 and 8 days and then analyzed. Control samples without electrochemical treatment were also exposed to the same conditions as the test samples.

Cl^- concentration adjustment. The original Cl^-concentration in the BG-11 medium was 18 mg/L, and the Cl^- concentration was adjusted to 0, 6 and 12 mg/L using equimolar $Ca(NO_3)_2·4H_2O$ and $Mn(NO_3)_2·4H_2O$ to replace $CaCl_2·2H_2O$ and $MnCl_2·2H_2O$ in BG-11, respectively. The modified BG-11 medium was used for algal cultivation as controls. We found that the optical density at 680 nm (OD_{680}) and chlorophyll fluorescence of the resulting cultivated algae were the same as those obtained using the original BG-11

medium. Consequently, we concluded that the altered BG-11 medium had no impact on the growth of algae.

6.3.3 Experimental Procedure

(1) Mechanisms of algal inhibition by electrochemical oxidation

Since we realize the oxidants and electrical field are both important in algae growth inhibition, we developed experiments of three cases to investigate their impacts respectively. In **case 1**, algae were treated directly with an electrochemical system which is at the presence of electro-generated oxidants and electrical field. In **case 2**, we electrolyzed BG-11 medium individually and then mixed with algae solution which isolated the impact of electro-generated oxidants on algae. In **case 3,** we directly added the same amount (as Case 1 & 2) external oxidants to the algal solution for comparison. Detailed procedures are shown below:

Case 1: 100 mL algal solution in BG-11 medium (cell density 5×10^5 cells/mL) was electrochemically treated at electrolysis time of 5, 10, 15, and 20 min with a current density of 20 mA/cm^2.

Case 2: 95 mL of BG-11 medium was electrochemically treated at electrolysis time of 5, 10, 15, and 20 min with a current density of 20 mA/cm^2, and then mixed thoroughly

for 1 min with 5 mL of *M. aeruginosa* solution (cell density 1×10^7 cells/mL). After the mixture, the cell density was 5×10^5 cells/mL which is consistent with Case 1.

Case 3: We measured the amount of chlorine and H_2O_2 that produced in case 2 at electrolysis time of 5, 10, 15, and 20 min with a current density of 20 mA/cm^2 and added to 100 ml algal solution in BG-11 medium (cell density 5×10^5 cells/mL). The production rates of chlorine and H_2O_2 in case 2 were calculated in section 3.4. NaClO (mass fraction 10%, AR) and H_2O_2 (mass fraction 30%, AR) were diluted and added to the algal solution to provide chlorine and H_2O_2. The algal solutions were allowed to react for 30 min to ensure adequate reaction of the generated oxidants with the algae cells.

(2) Production of chlorines and H_2O_2

95 mL of BG-11 medium was electrochemically treated under different current densities (0-20 mA/cm^2), electrolysis times (0-20 min) and initial Cl^- concentrations (0-18 mg/L) using a Ti/RuO_2 anode. The concentrations of chlorines and H_2O_2 were measured immediately.

(3) The algal inhibition efficiencies

In order to study the algal inhibition efficiencies under different operational conditions, 95 mL of BG-11 medium was electrolyzed under different current densities (0-20 mA/cm^2), electrolysis times (0-20 min) and initial Cl^- concentrations (0-18 mg/L), and

then mixed with 5 mL of *M. aeruginosa* solution (cell density, 1×10^7 cells/mL). The solutions were mixed thoroughly for 1 min and then allowed to react for 30 min to ensure adequate reaction between the oxidants electro-generated and algae cells.

All experiments were carried out in triplicate, and the mean values and standard deviations were calculated for each treatment.

6.3.4 Analysis Method

Cell density. *M. aeruginosa* cells were counted in the counting chamber of a compound microscope (Shanghai Yongheng, Mode 44X3A, China). Cell counts were determined based on the method of Burriniet al. (2000).

Optical density. The $OD_{680}$of algae cell solutions were measured on an ultraviolet spectrophotometer (PE, Lambda 25, America). The OD_{680} variation in the algal solutions over 8 days cultivation was used as an indirect index of cell viability [168,171]. Large increases in the $OD_{680}$with time indicated good growth of algae.

Chlorophyll-*a*. The chlorophyll-*a* concentration was used as an indicator of the biomass of *M. aeruginosa* and as an indirect measure of cell integrity. Samples were filtered through GF/C filters under low vacuum, and the chlorophyll was extracted using 5 mL of 90% acetone. The OD of the extracts at 663, 645, 630 and 750 nm were determined

using an ultraviolet spectrophotometer (PE, Lambda 25, USA). The chlorophyll-*a* concentration was determined using the method described in our previous work [175].

Chlorophyll fluorescence. Chlorophyll fluorescence can serve as a reliable, noninvasive indicator of algal photosynthetic activity [171]. The maximum quantum yield of photosystem II (PS II) (Φ, also called F_v/F_m) can reflect the cell viability [170]. The effective quantum yield of PS II(Y(II)) represents the capacity for the photon energy absorbed by PS II to be utilized in photochemical reactions under light-adapted conditions. The non-regulated energy dissipation of PS II(Y(NO)) is an important indicator of optical damage [171]. Chlorophyll fluorescence parameters are sensitive bioindicators of the damage to algae; decreases in Φ and Y(II) to almost 0 and increases in Y(NO) to 1 mean that the algae cells have been irreversibly damaged [168,171]. The chlorophyll fluorescence parameters were recorded on a prototype of a PAM chlorophyll fluorometer (Heinz Walz GmbH, Multi-Color-PAM, Germany) at 20 °C. The chlorophyll fluorescence parameters were immediately determined after each sampling. Initially, the algal solution samples were kept in the dark for 5 min before analysis.

Chlorines. The electrochemically generated chlorines (including Cl_2, HClO, and ClO^-) were determined in mg/L (as total Cl_2) using the N, N-diethyl-p-phenylenediamine (DPD) colorimetric method. DPD is oxidized to form a red-violet product, the concentrations of which were measured on a spectrophotometer (PE, Lambda 25, USA) at 515 nm [169,177]. This method is valid for chlorines concentrations at (0.42-21.1) $\times 10^{-6}$ mol/L.

H_2O_2. The concentration of electrochemically generated H_2O_2 was measured using a photometric method in which DPD was oxidized by a modified peroxidase-catalyzed reaction (POD) [154,176]. This method is based on the principle that H_2O_2 reacts with DPD only in the presence of POD. The reaction of H_2O_2 produces a colored compound that exhibits a relatively high absorbance at 551 nm, which is measured on a spectrophotometer (PE, Lambda 25, USA). This method is valid for H_2O_2 concentrations at (0.01-3) $\times 10^{-6}$ mol/L.

O_3. The O_3 concentration was measured using the indigo method on a spectrophotometer (PE, Lambda 25, USA) at 600 nm. This method is based on the quantitative decolorization of indigo trisulfonate as a result of its reaction with O_3 [167] and is valid for O_3 concentrations at (0.2-300) $\times 10^{-6}$ mol/L.

6.4 Results and Discussion

6.4.1 Analysis of electro-generated oxidants

The reduction potentials of the oxidants that potentially generated from anode in our study are listed in Table 6. Since overpotential for oxygen evolution is reported 1.297 V (vs. NHE), oxidants generated from Ti/RuO_2 anode are mainly Cl_2 (E^0= 1.36 V) and H_2O_2 (E^0= 1.77 V). The O_3 (E^0= 2.08 V) concentration was measured and found to be insignificant. Other oxidants ($ClO_3\cdot$, $SO_4^{-}\cdot$, $NO_3\cdot$and $HO\cdot$) which have higher standard reduction potentials will be more difficult to generate (neglected for this anode).

Table 6 - Reduction potential of related oxidants

Oxidants	Reduction potential (V) (vs. NHE)	Reference
O_2	1.23	[189]
Cl_2	1.36	[153]
H_2O_2	1.77	[189]
O_3	2.08	[189]
$ClO_3\cdot$	2.35	[194]

$SO_4^{-}\cdot$	2.43	[194]
$NO_3\cdot$	2.45	[194]
$HO\cdot$	2.74	[189,157]

The main electrochemical reactions involved in this study included:

- The formation of H_2O_2 [172,169,161].

$$2H_2O \rightarrow H_2O_2 + 2H^+ + 2e^- \quad (54)$$

- The oxidation of chloride to form chlorines; chlorines produces hypochlorous acid and hypochlorite ions, which is a pH dependent reaction [169,161].

$$2Cl \rightarrow^{-} Cl_2(g) + 2e^{-} \quad (55)$$

$$Cl_2(g) + H_2O \rightarrow HClO + H^{+} + Cl^{-} \quad (56)$$

$$HClO \rightarrow ClO^{-} + H^{+} \quad (57)$$

6.4.2 Mechanisms of algal inhibition by electrochemical treatment

Figure 1 shows the OD_{680} variations in the algal solutions after treatment in three cases: case 1: algae were treated by electro-generated oxidants and electrical field (Figure 1a), case 2: algae were treated only by electro-generated oxidants (Figure 1b), and case 3: algae were treated by external oxidants (Figure 1c).

The results showed that the electrolysis time of 10 min is enough for algal inhibition in case 1. However, electrolysis time of 15 min is needed case 2. The different electrolysis time required for algal inhibition in Figure 1a and Figure 1b indicated that electrical field contributed to algal inhibition, although it is hard to make a quantitative calculation. Similar results were also reported in literature [174,176,163,181]. Figure 1b also showed

that the generated oxidants from electrodes can inhibit the growth of *M. aeruginosa* at a low Cl^- concentration by electrolysis time of 15-20 min. Thus, the electric field and generated oxidants were both important contributors to algal inhibition. And solely relying on the effect of electro-generated oxidants was also effective for algal inhibition.

Compare the results in Figure 1b and Figure 1c, it could be found that case 2 and case 3 almost had the same OD_{680} variations trend, which meant the main oxidants produced in case 2 are chlorines and H_2O_2. The small differences in OD_{680} values could be caused by a small number of other oxidants generated in our study.

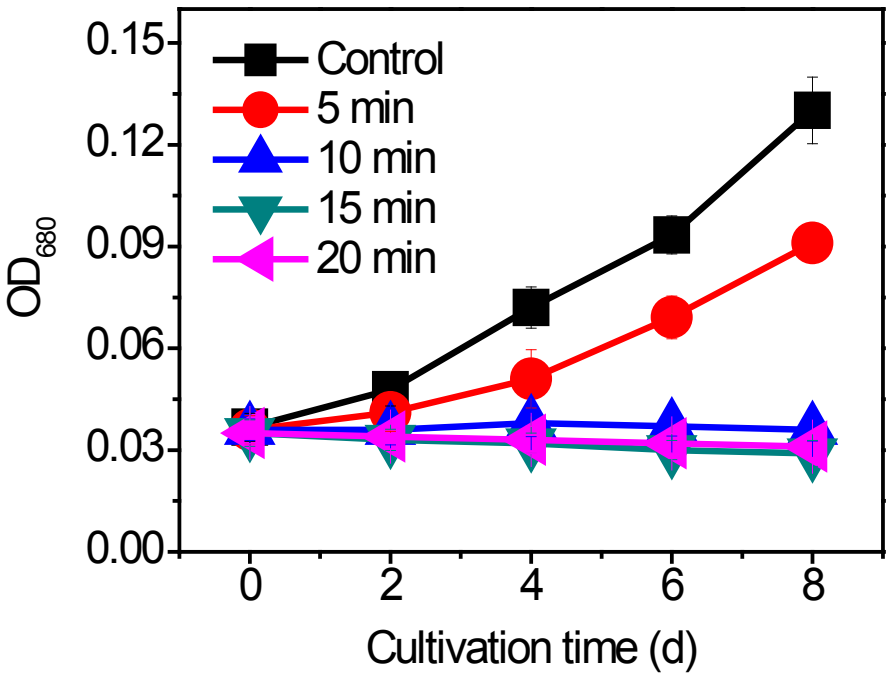

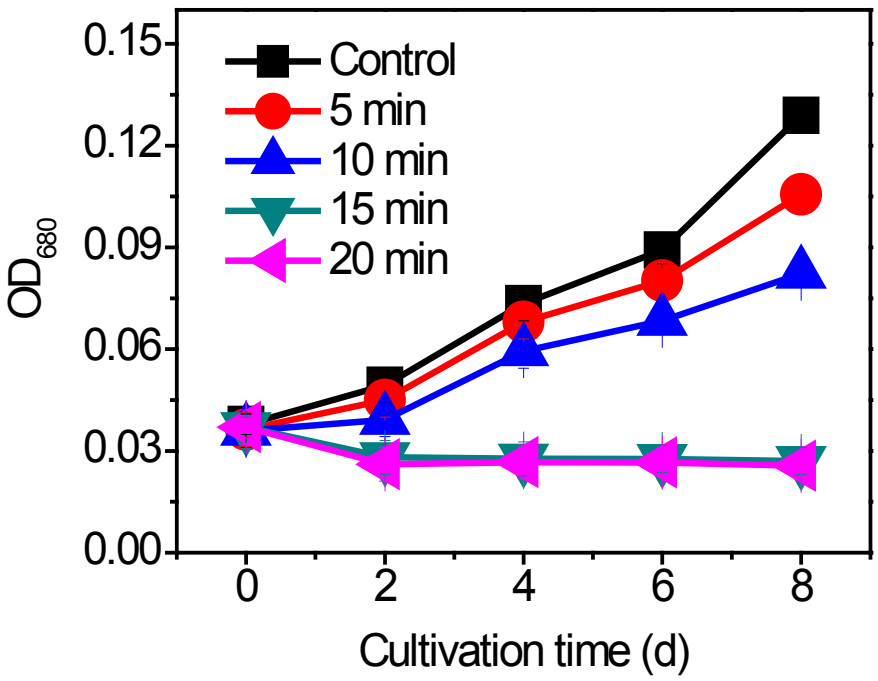
0.15
0.12
0.09
0.06
0.03
0.00
OD680
Control
5 min
10 min
15 min
20 min
0
2
4
6
8
Cultivation time (d)

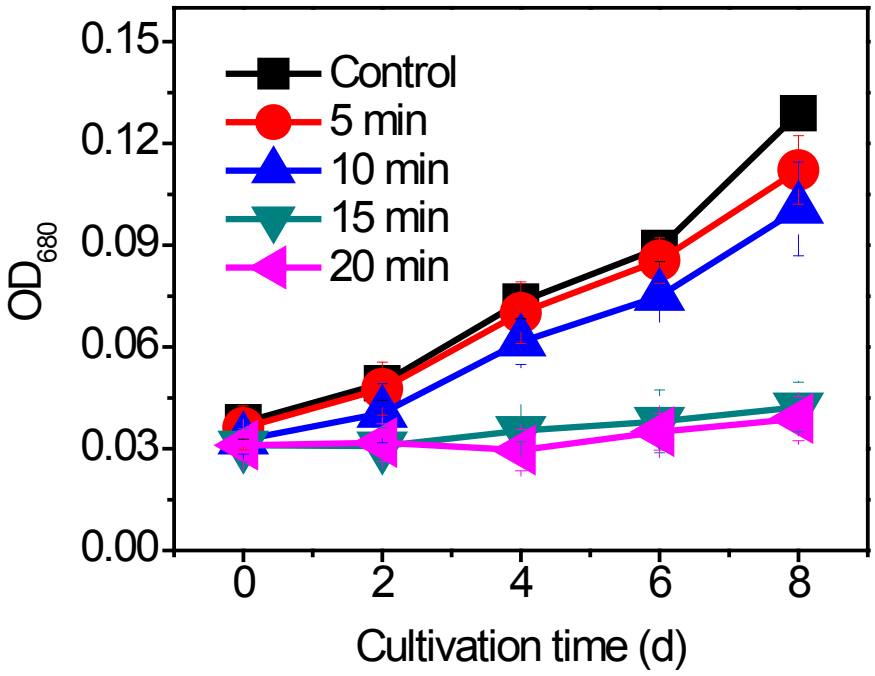

Figure 15 - OD_{680} variations in algal solutions with the cultivation time after (a) case 1: 100 ml algal solution in BG-11 medium (cell density 5×10^5 cells/mL) was electrochemically treated; (b) case 2: 95 mL of BG-11 medium had been electrochemically treated and then mixed with 5 mL of *M. aeruginosa* solution (cell density 1×10^7 cells/mL) (current density, 20 mA/cm^2; Cl^- concentration, 18 mg/L); (c) case 3: the same amount of chlorines and H_2O_2 produced in case 2 were added to 100 ml algal solution in BG-11 medium (cell density 5×10^5 cells/mL).

6.4.3 Production of chlorines and H_2O_2

The electro-generated chlorines and H_2O_2 productions at different operating conditions are shown in Table 7.

The concentrations of chlorine species (as total Cl_2) increased with current density, electrolysis time and initial Cl^- concentration. From Table 7, 3.62×10^{-6} mol/L chlorines were detected in the solution with an initial Cl^- concentration of 18 mg/L at a current

density of 20 mA/cm^2 after 15 min of electrochemical treatment. Jeong et al. (2009) reported that 9.80×10^{-4} mol/L chlorines (as total Cl_2) were produced with an initial Cl^- concentration of 600 mg/L at a current density of 17 mA/cm^2 after 10 min. These results show that a higher initial Cl^- concentration causes a higher conversion of chlorines. The concentration of chlorines increased with the electrolysis time during 0-15 min, but no further significant increase was observed after 15 min. Chlorine species can react with oxygen species (e.g., H_2O_2, see the reaction (48)). Thus, the electrochemically generated chlorines might react to form other byproducts with increasing electrolysis time.

$$H_2O_2 + ClO^- \rightarrow Cl^- + H_2O + O_2 \quad (58)$$

The maximum concentration of chlorines (as total Cl_2) was 3.67×10^{-6} mol/L (Table 7). Generally, the recommended concentration of residual chlorines for disinfection is (7.04-14.08) $\times10^{-6}$ mol/L [152]. More than 96% of the algae present during algal blooms can be killed using a chlorines concentration of 5.63×10^{-5} mol/L in drinking water treatment plants [186].

Table 7 - Concentrations of chlorines and H_2O_2 under different operating conditions (current density, 20 mA/cm^2; electrolysis time, 15 min; and Cl^- concentration, 18 mg/L, unless otherwise stated)

Operating parameter		Chlorines (10^{-6}mol/L, as Cl_2)	H_2O_2 (10^{-6}mol/L)
Current density (mA/cm^2)	0	*N.D.*	*N.D.*
	4	0.54±0.12	0.54±0.05
	8	1.33±0.15	1.35±0.09
	12	2.52±0.20	1.58±0.05
	16	3.22±0.21	1.40±0.08

	20	3.62±0.18	1.15±0.05
Electrolysis time (min)	0	*N.D.*	*N.D.*
	1	0.50±0.12	0.29±0.05
	2	0.88±0.15	0.55±0.06
	5	1.75±0.20	1.10±0.05
	10	2.70±0.21	1.36±0.09
	15	3.62±0.18	1.15±0.05
	20	3.67±0.12	1.08±0.05

	0	*N.D.*	3.68±0.16
Cl^- concentration (mg/L)	6	0.80±0.15	3.13±0.15
	12	2.31±0.02	1.91±0.18
	18	3.62±0.18	1.15±0.05

Note: *N.D.* indicates that chlorines or H_2O_2 was not detectable or was not statistically significant.

H_2O_2 is an efficient oxidant at cyanobacterial oxidation [159,166]. The H_2O_2 concentrations increased with current density at the beginning, since increased current density means more electrons flow and more reactions taking place. Then H_2O_2 concentrations decreased due to the instantaneous reaction between H_2O_2 and ClO^- (reaction (50)) because more chlorines were generated with increasing current density [160]. The decrease in H_2O_2 concentration after 10 min of electrochemical treatment was attributed to the increased decomposition of H_2O_2 (such as via reaction with ClO^-). The H_2O_2 concentration decreased rapidly as the Cl^- concentration increased from 0 to 18 mg/L,

which might also be attributed to the reaction between H_2O_2 and ClO^- (reaction (5)) since more chlorines were generated with increasing Cl^- concentration [155].

6.4.4 Modeling of the production of chlorines and H_2O_2

Several electrochemical oxidation kinetics models have been developed to describe the production of oxidants in chloride contained solution [176,191]. However, these models were developed for a relatively high Cl^- concentrations solution, in which chlorines were the major oxidants. In our study, at a relatively low Cl^- concentration, we found chlorines and H_2O_2 were both important oxidants. We developed a model to simulate the production of chlorines and H_2O_2 from Ti/RuO_2 anode at 18 mg/L Cl^-. The parameters obtained from the simulation were used to predict oxidants generation at other Cl^- conditions (compared for model validation).

According to the standard reduction potentials of oxidants and our experimental results, chlorines and H_2O_2 were the major electro-generated oxidants and the correlation of their reaction rates are described in Eqs. (53) and (54).

$$r_{chlorines} = \frac{\eta_{chlorines} \cdot J \cdot S}{F \cdot V} \cdot [Cl^-] - k_{obs} \cdot [ClO^-] \cdot [H_2O_2] \quad (59)$$

$$r_{H_2O_2} = \frac{\eta_{H_2O_2} \cdot J \cdot S}{2 \cdot F \cdot V} - k_{obs} \cdot [ClO^-] \cdot [H_2O_2] \quad (60)$$

Where η is the fraction of electrons in the current that attributes to this reaction. η has units of L/mol in eq. (53) and is dimensionless (since H_2O is the reactant for H_2O_2 generation) in eq. (54). J is the current density (mA/cm^2), S is the anode surface area (cm^2), V is the reactor volume (cm^3), and F is Faraday's constant (96485 C/mol). The reaction between chlorines (ClO^-) and H_2O_2 has a second-order observed rate constant, k_{obs} (L/mol·s). The pH of the algal solution was buffered at 7.0, and the pka of HClO is 7.54. The simulation results are plotted in Figure 15a. Fitted parameters are listed in Table 8.

Table 8 - Parameters used in the experiments and modeling

Parameter	Symbol	Value	Unit
Algal inhibition efficiency	θ	variable	
Reactive quantum yield of PS II	Φ	variable	

Effective quantum yield of PS II	Y(II)	variable	
Non-regulated energy dissipation of PS II	Y(NO)	variable	
Reaction rate of chlorines	$r_{chlorines}$	variable	mol/(L·s)
Reaction rate of H_2O_2	$r_{H_2O_2}$	variable	mol/(L·s)
Fraction of electrons from the current that flow to produce chlorines	$\eta_{chlorines}$	0.460 (fitted)	L/mol
Fraction of electrons from the current that flow to produce H_2O_2	$\eta_{H_2O_2}$	2.90×10^{-4} (fitted)	

Current density	J	0.02	A/cm^2
Anode surface area	S	13.75	cm^2
Reactor volume	V	0.1	L
Faraday's constant	F	96485	C/mol
Observed second-order rate constant between ClO^- and H_2O_2	k_{obs}	4777 (fitted)	L/(mol·s)
Initial Cl^- concentration	$[Cl^-]$	variable	mol/L
ClO^- concentration	$[ClO^-]$	variable	mol/L

H_2O_2concentration	$[H_2O_2]$	variable	mol/L

The production rate of chlorines (values of $\frac{\eta_{chlorines} \cdot J \cdot S}{F \cdot V} \cdot [Cl^-]$ in eq. (59)) and production rate of H_2O_2 ($\frac{\eta_{H_2O_2} \cdot J \cdot S}{2 \cdot F \cdot V}$ in eq. (54)) were calculated to be 6.65×10^{-9} and 4.13×10^{-9} mol/(L·s) at a current density of 20 mA/cm^2, respectively. The production rate of chlorines (6.65×10^{-9}mol/(L·s)) was greater than the production rate of H_2O_2 (4.13×10^{-9}mol/(L·s)) because reaction (54) (E^0= 1.36 V) occurs more easily than reaction (53) (E^0=1.77 V).

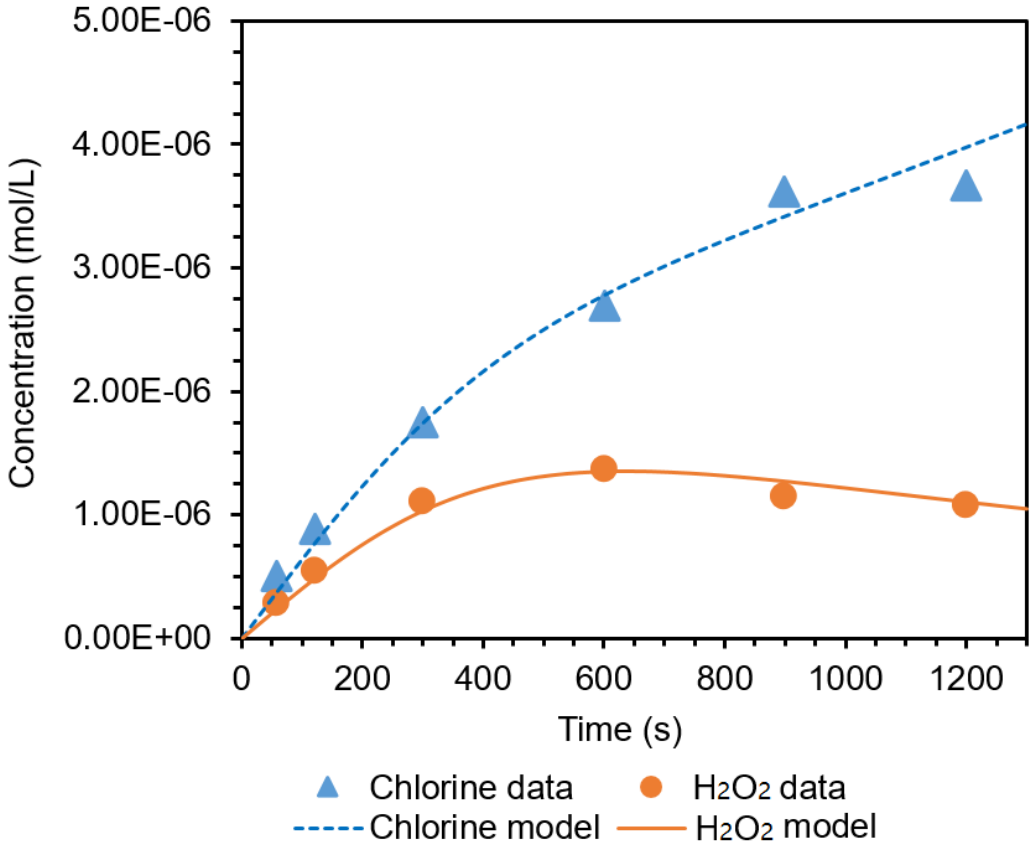

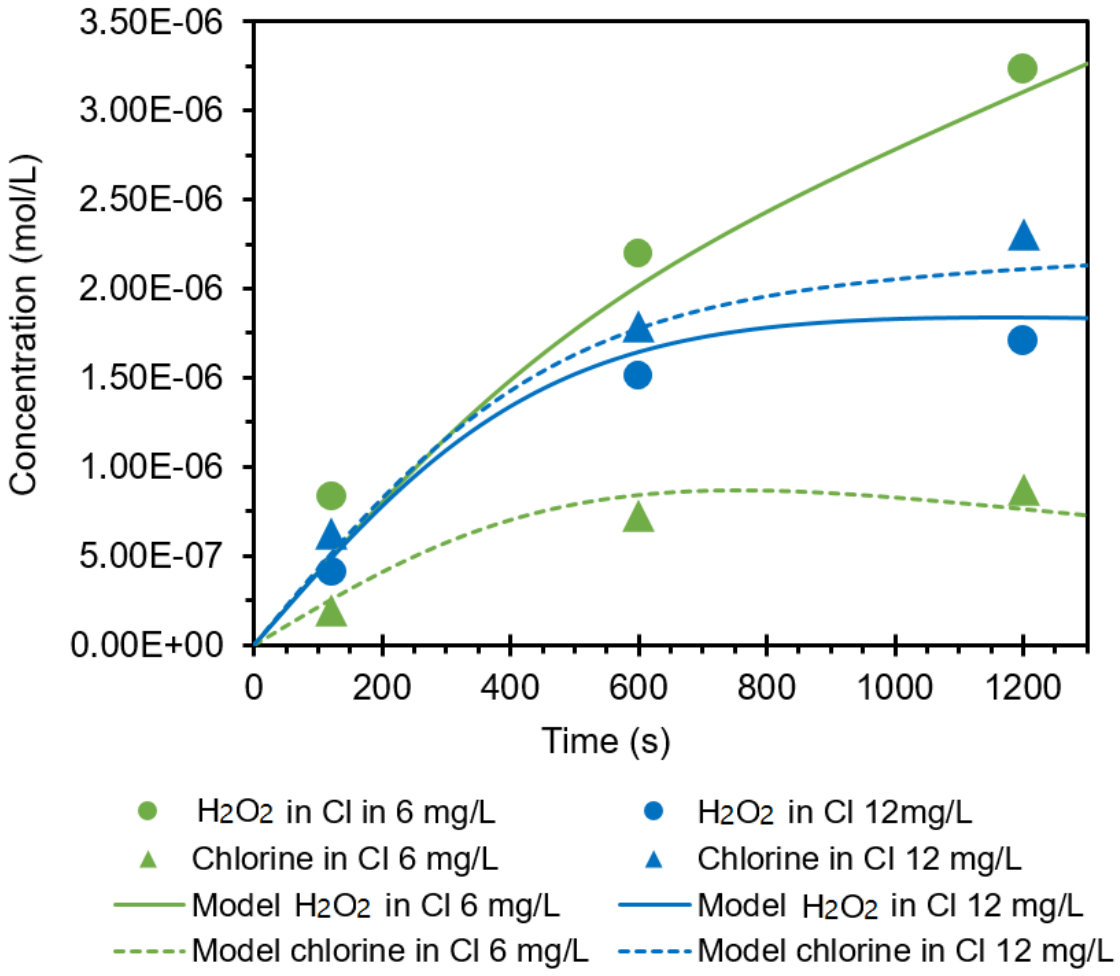

Figure 16 - (a) Concentration profiles of chlorines and H_2O_2 with a Cl^- concentration of 18 mg/Lata current density of 20 mA/cm^2. (b)Concentrations of chlorines and H_2O_2predicted by the model with different Cl^-concentrations at a current density of 20 mA/cm^2. The dots indicate the experimental results, and the lines represent the computer model fits.

Based on independent parameters obtained from the simulation, we predicted the concentration of chlorines and H_2O_2 at other Cl^- levels (6 mg/L and 12 mg/L), and the results are shown in Figure 16b. The predicted values were relatively close (on the same 10^{-6}mol/L magnitude) to the experimental results, which also validates the rationality of our modeling approach and its simulated parameters.

6.4.5 The relationship between the algal inhibition efficiency and oxidants production

The Φ, OD_{680}, Y(II) and Y(NO) variations in algal solutions after treatment by oxidants electro-generated under different current density, electrolysis time and Cl^- concentration are shown in Figure 17. The results clearly indicated that the algal inhibition efficiency was influenced by current density, electrolysis time and initial Cl^- concentration. The growth of algae was inhibited by electro-generated oxidants at current densities larger than 16 mA/cm^2 (Figure 17a). Algal inhibition increased over an electrolysis time of 0-20 min, and only electrolysis times longer than 15 min were effective (Figure 17b). The algal inhibition efficiency increased with initial Cl^- concentrations (Figure 17c). Effective algal inhibition was attained above 12 mg/L Cl^- (production of chlorines exceeded 3.01×10^{-6}mol/L) (Figure 17c and Table 7). These results indicated that the electro-generated oxidants were also effective for algal inhibition at low Cl^- concentrations.

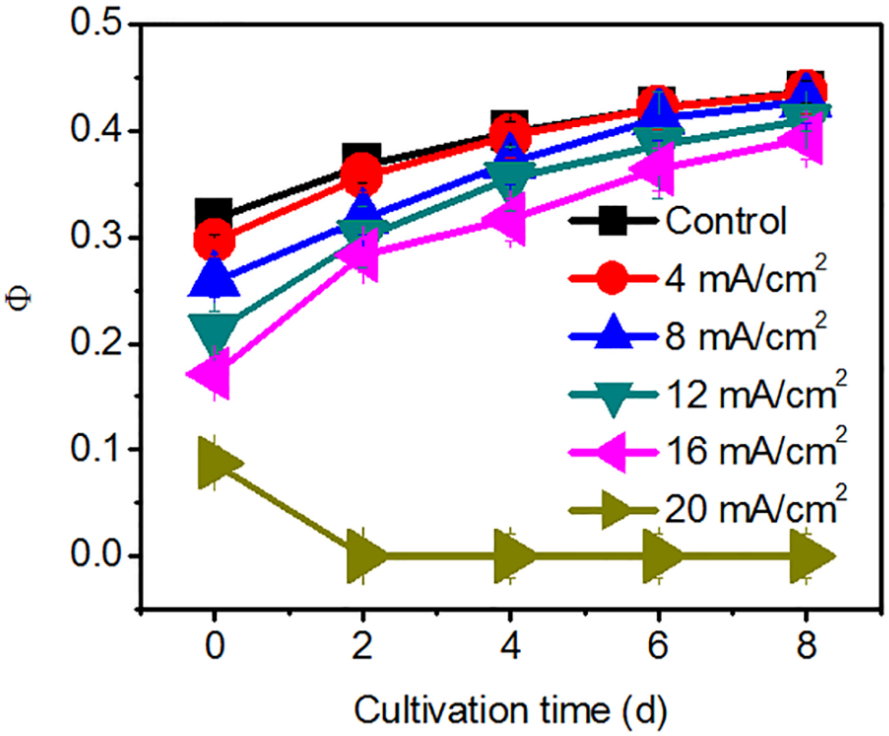
0.5
0.4
0.3
0.2
0.1
0.0
Φ
0
2
4
6
8
Cultivation time (d)
Control
4 mA/cm2
8 mA/cm2
12 mA/cm2
16 mA/cm2
20 mA/cm2

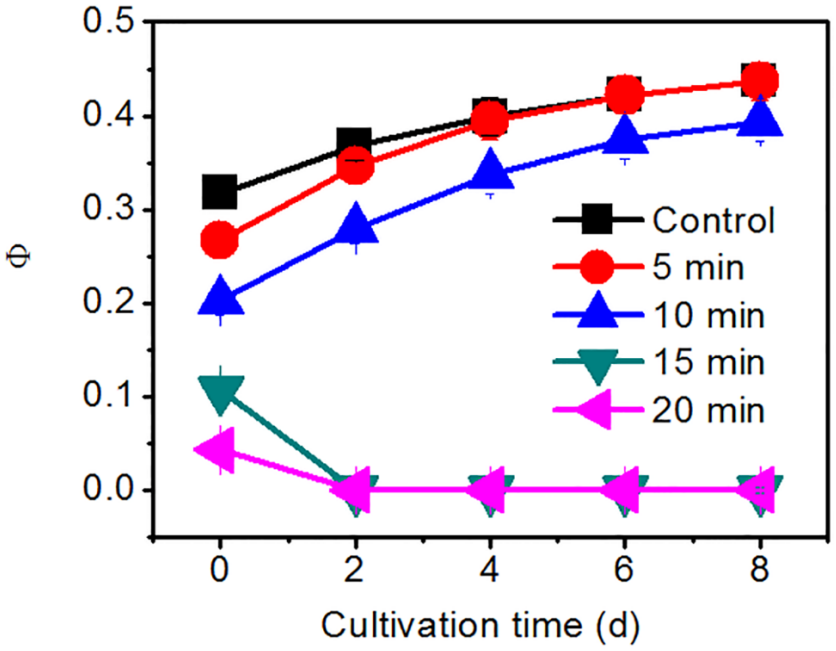
0.5
0.4
0.3
0.2
0.1
0.0
Φ
0
2
4
6
8
Cultivation time (d)
Control
5 min
10 min
15 min
20 min

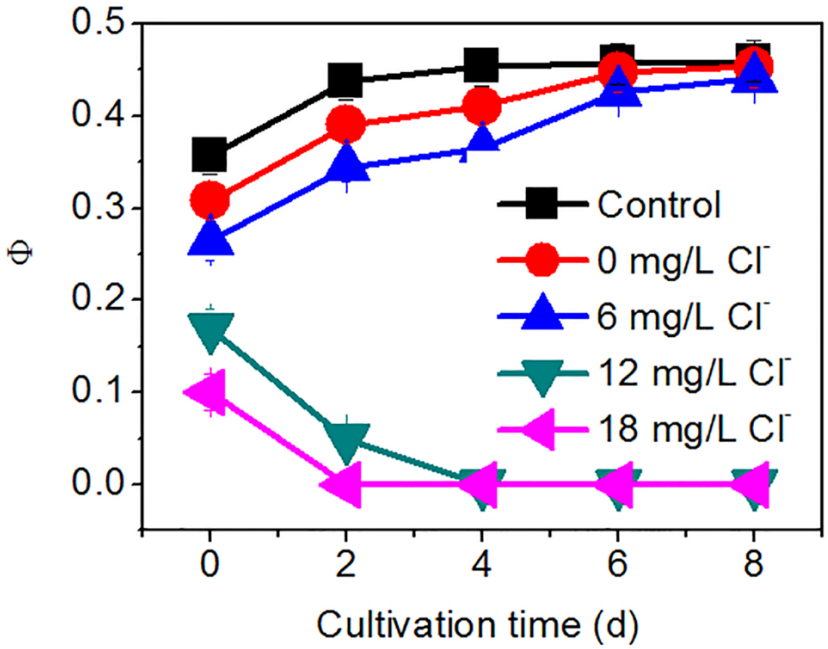

Figure 17 - Variations in the chlorophyll fluorescence parameters Φ of algal solutions with the cultivation time after electrochemical treatment under different conditions: (a) electrolysis time of 15 min and 18 mg/L Cl^-, (b) current density of 20 mA/cm^2 and 18 mg/L Cl^-, and (c) current density of 20 mA/cm^2 and electrolysis time of 15 min

To elucidate the relationship between the algal inhibition efficiency and oxidants production, the total concentrations of chlorines and H_2O_2, chlorines concentration and H_2O_2 concentration were plotted against the algal inhibition efficiency θ, respectively (Figure 18). The algal inhibition efficiency θ was defined based on Φ as follows [158]:

$$\theta = (\Phi_0 - \Phi)/\Phi_0 \quad (61)$$

where Φ is the reactive quantum yield of the electrolyzed sample after electrochemical treatment, and Φ_0 is the reactive quantum yield of the control sample.

As shown in Figure 18, the total concentrations of chlorines and H_2O_2 were positively correlated with ln(θ) (R^2=0.9807), which demonstrated that these two oxidants played important roles in algal inhibition. The algal inhibition efficiency was positively correlated with the concentration of chlorines (R^2=0.9578), but no correlation was found between the algal inhibition efficiency and H_2O_2 concentration (R^2=0.5198).

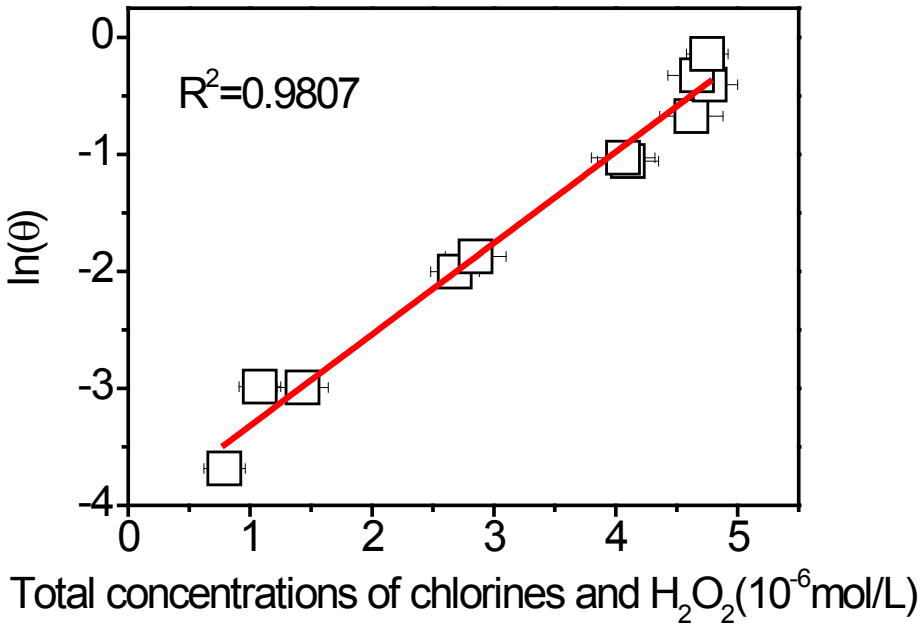

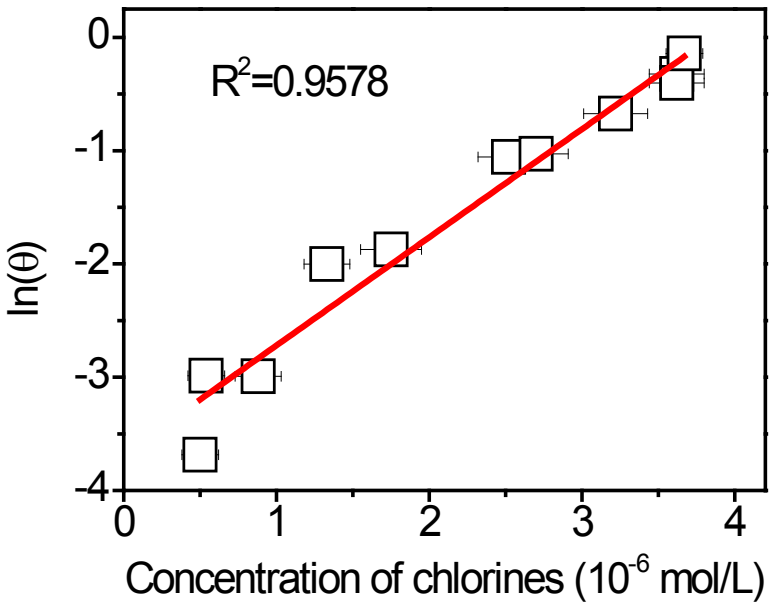
R2=0.9578
ln(θ)
0
-1
-2
-3
-4
0
1
2
3
4
Concentration of chlorines (10-6 mol/L)

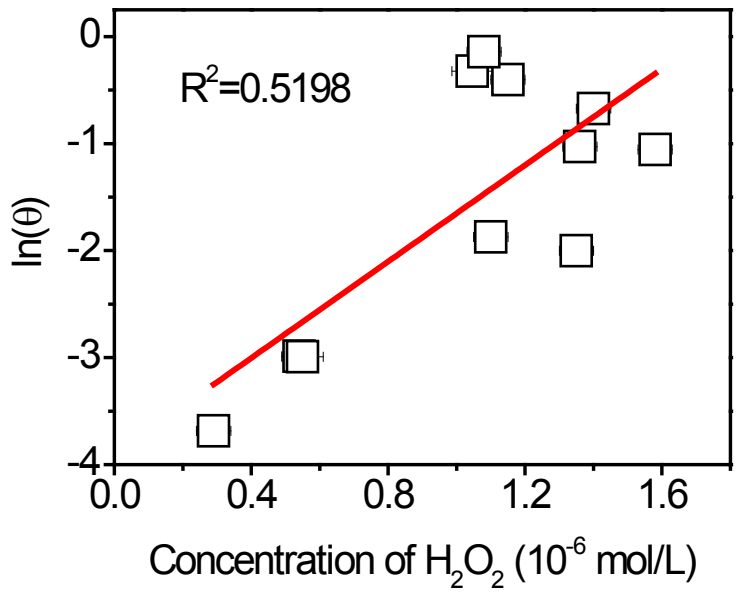

Figure 18 - Correlation between the algal inhibition efficiency ln(θ) and (a)total concentration of chlorines and H_2O_2; (b) concentration of chlorines; (c) concentration of H_2O_2 (Cl^- concentration, 18 mg/L).

To further investigate the relative contributions of chlorines and H_2O_2 to the algal inhibition efficiency, multiple linear regression correlations were established by analyzing the concentration of chlorines andH_2O_2 and the algal inhibition efficiencies at 18 mg/L Cl^-as follows:

$$\ln(\theta)=a\cdot[\text{chlorines}] + b\cdot[H_2O_2] +c \quad (62)$$

where θ is the algal inhibition efficiency, [chlorines]is the concentration of chlorines (10^{-6}mol/L), [H_2O_2] is the H_2O_2 concentration (10^{-6}mol/L), a is the coefficient for [chlorines], b is the coefficient for [H_2O_2], and c is the constant.

The fitting parameters a, b and c in Eq. (56) were 0.8772, 0.6655 and -4.2192. The correlation has a good regression with a high R^2 of 0.9935. A partial correlation coefficient describes the relationship between X and Y when removing the effect of a control variable Z and can be used to test conditional independence [162]. Partial correlation coefficients of [chlorines]and [H_2O_2] with ln(θ) were also calculated to reflect the independent contributions of [chlorines] and [H_2O_2] to ln(θ), and the calculated values were 0.9867 and 0.8112, respectively. Thus, the contribution of chlorines to the algal inhibition efficiency was higher than that of H_2O_2 at an initial Cl^-concentration of 18 mg/L. Therefore, at the low concentrations of Cl^- present in natural water, chlorines play a key role in algal inhibition, and the effect of H_2O_2 on algal inhibition is relatively small.

6.5 Conclusions

The contributions of electrochemically generated chlorines (Cl_2, ClO^- , and HClO) and H_2O_2 to the inhibition of *M. aeruginosa* at relatively low initial Cl^- concentrations using a Ti/RuO_2 anode were investigated, and the following conclusions can be drawn.

(1) Electrical field and electro-generated oxidants were both important contributors to algal inhibition during electrochemical oxidation treatment. The Ti/RuO_2 anode mainly generates chlorines and H_2O_2 from Cl^- and water.

(2) The concentration of chlorines increased with current density, electrolysis time and initial Cl^- concentration. The concentration of H_2O_2 increased with current density and electrolysis time to a maximum value and then decreased. ClO^- was supposed to be the major scavenger of H_2O_2 during the reaction since the concentration of H_2O_2 decreased with increasing Cl^-concentration. In specific, when the initial Cl^-concentration increased from 0 to 18 mg/L, the concentration of chlorines increased from 0 to 3.62×10^{-6} mol/L and the H_2O_2 concentration decreased from 3.68×10^{-6} to 1.17×10^{-6} mol/L, respectively.

(3) A kinetic model was developed to simulate the concentrations of electro-generated chlorines and H_2O_2 at 20 mA/cm^2 and 18 mg/L Cl^-. Our model also made decent predictions of other Cl^- concentrations by comparing with experimental data which validated the rationality of this modeling approach.

(4) The algal inhibition efficiency caused by oxidants electro-generated was positively correlated with the concentration of chlorines, but not correlated with H_2O_2 concentration. The electro-generated chlorine species were more effective than H_2O_2 at an initial Cl^- concentration of 18 mg/L.

6.6 The Treatment of Deuterated Contaminants with UV/H_2O_2 and Rate Constants Estimation Using Kinetic Isotope Effect

Deuterated pharmaceuticals are able to evade from metabolic clearance processes in the body because the metabolic clearance processes depend on breaking carbon-hydrogen bonds. Deuterium is a heavier isotope of hydrogen and this makes the bonds more difficult to break due to the kinetic isotope effect. It has been reported the deuterated compounds have a smaller second-order rate constant with hydroxyl radical than undeuterated compounds. [196-198] Hydroxyl radical attacks organic compounds through four major pathways: H-atoms abstraction, addition to an unsaturated alkene, addition to aromatic compounds and interactions with nitrogen, sulfur, and phosphorus functional groups. [199-201] Among these four pathways, D-abstraction will be affected the most. Therefore, the calculation of deuterated compounds second-order rate constants starts from D-atom abstraction.

6.6.1 Correlation between rate constants and aqueous phase free energy of activation

Activated-complex theory or transition state theory treats a transition state as a chemical species in thermal equilibrium with its surroundings. Accordingly, the kinetic reaction rate constant for a given elementary reaction relates linearly to the free energy

change in the transition from reactants to transition states. This relation specifically for D-atom abstraction, after putting natural logarithms on both sides expressed,

$$\ln k_D = -\rho \cdot \Delta G_{aq}^{act} + \sigma \tag{63}$$

Where k_D is the reaction rate constant for the D-atom abstraction reaction from one C-D bond by hydroxyl radical, $M^{-1}S^{-1}$; ρ denotes a coefficient for the difference in the free energy of activation; σ is a coefficient and ΔG_{aq}^{act} is the aqueous phase standard free energy of activation, kcal/mol.

6.6.2 The aqueous phase free energy of activation-experimental

The aqueous phase free energy of activation can be measured and calculated experimentally. Under the thermodynamic equilibrium assumption between reactants and transition states, thermodynamic parameters in the aqueous phase can be obtained using the following equation,

$$E_a = \Delta H_{aq,\exp}^{act} + RT \tag{64}$$

$$A = (ek_B T / h)\exp(-\Delta S^{act}_{aq,\exp} / R) \tag{65}$$

$$\Delta G^{act}_{aq,\exp} = \Delta H^{act}_{aq,\exp} - T \cdot \Delta S^{act}_{aq,\exp} \tag{66}$$

Where E_a and A are the experimentally obtained Arrhenius activation energy, kcal/mol and frequency factor, $M^{-1}s^{-1}$, respectively. $\Delta G^{act}_{aq,\exp}$, $\Delta H^{act}_{aq,\exp}$ and $\Delta S^{act}_{aq,\exp}$ are the experimentally obtained standard state free energy, enthalpy and entropy of activation and R is the gas constant.

6.6.3 The aqueous phase free energy of activation-theoretical

The aqueous phase free energy can also be calculated by quantum mechanics approaches. The theoretically calculated aqueous phase standard free energy of activation $\Delta G^{act}_{aq,cal}$, at a given temperature T is the sum of standard state gaseous phase free energy of activation $\Delta G^{act}_{gas,cal}$ and the solvation free energy of activation $\Delta G^{act}_{sol,cal}$.

$$\Delta G^{act}_{aq,cal} = \Delta G^{act}_{gas,cal} + \Delta G^{act}_{sol,cal} \tag{67}$$

The calculations of free energy of activation in the gas phase and free energy of solvation have been established and Gaussian-n-series should be sufficient. By plotting the $\Delta G^{act}_{aq,\exp}$ and $\Delta G^{act}_{aq,cal}$ with experimentally obtained reaction rate constants, a linear correlation between $\ln k_H$ and $\Delta G^{act}_{aq,cal}$ $\Delta G^{act}_{aq,\exp}$ is expected.

6.6.4 Evaluate the impact of deuterium on organic degradation kinetics

Hydroxyl radical mainly has three different way of 'attacking' the organic contaminants in the aqueous phase (since the kinetic of hydroxyl radical react with a functional group is still unclear in the field): 1). Hydrogen abstraction, 2). Addition to the double bond, and 3). Addition to the ring. In this work, we are trying to reveal the impact of deuterium on the degradation kinetics. Theoretically, an additional neutron in the atom nuclear just simply double the weight of the atom. In classical theory, it only affects the vibrational frequency of the hydrogen atom in the molecular. A higher weight of the atom (i.e. switch hydrogen with deuterium) will lower the zero point energy (ZPE) of the compound and lower the vibrational frequency of this compound. A smaller vibrational frequency will yield a smaller second-order rate constant of hydroxyl radical react with organic contaminants via hydrogen abstraction (since in classic theory, the hydrogen abstraction is an effect on hydrogen stretching mode). The impact of deuterium on the double bond and ring structure is limited because the additional energy is only affected by the atom repulsion force and the vacancy of the bonds. Such differences can be observed from the computing of non-deuterated/deuterated zero point energy, shows in Table 1. In this work, we selected 4 different compounds to represent different kinetics: chloroform

($CHCl_3$) and bromoethane (C_2H_5Br) for hydrogen abstraction, phenol (C_6H_6O) for addition to the ring, and trichloroethylene (C_2HCl_3) for addition to the double bond.

Table 9 - Zero-point energies comparison of 4 different compounds (deuterated/non-deuterated version). The computation of ZPEs used B3LYP method and 6-311G* basis sets in Gaussian.

Chemicals	ZEP (kJ/mol)	Δ(kJ/mol) & %	Chemicals	ZEP (kJ/mol)	Δ(kJ/mol) & %
$CHCl_3$	79.9272	9.5426	C_6H_6O	271.1635	50.9008
$CDCl_3$	70.381	11.944%	C_6D_6O	220.2627	18.7713%
C_2H_5Br	175.071	43.239	C_2HCl_3	57.5451	0.1762
C_2D_5Br	131.832	24.698%	C_2DCl_3	57.3689	0.306%

From the table, we can clearly observe all deuterated compounds have smaller zero-point energy comparing with non-deuterated version. According to the classic theory, a

primary kinetic isotope effect (KIE) is a KIE where the isotopically labeled atom is directly involved in bond cleavage or formation. For most organics, the reaction coordinate can be thought of as stretching vibrational mode at the GS becoming a translational mode at the TS. Thus the GS-ZPE of the stretching mode is lost and only the much lower frequencies of vibrations orthogonal to the reaction coordinate are present at the TS. So, a first-order approximation of the sources of KIEs is just the difference in GS-ZPE between the two isotopes:

$$\mathrm{KIE} \approx \exp\left(\frac{\Delta \mathrm{ZPE}}{\mathrm{RT}}\right) \tag{68}$$

However, clearly, this equation can only be adapted to explain the kinetics of hydrogen abstraction not for any additions. According to the computational results, we found a KIE of chloroform to be 47.068 and KIE for bromoethane to be more than 3×10^7, which are obviously wrong for this approximation. Our experiments result also support that a large overestimation of such KIE approach. In Figure 19, the chloroform and chloroform-D are degraded with UV/H_2O_2 system. We established a pseudo-steady-state model to fit the data and find the second-order rate constants of the parent compound with hydroxyl radicals.

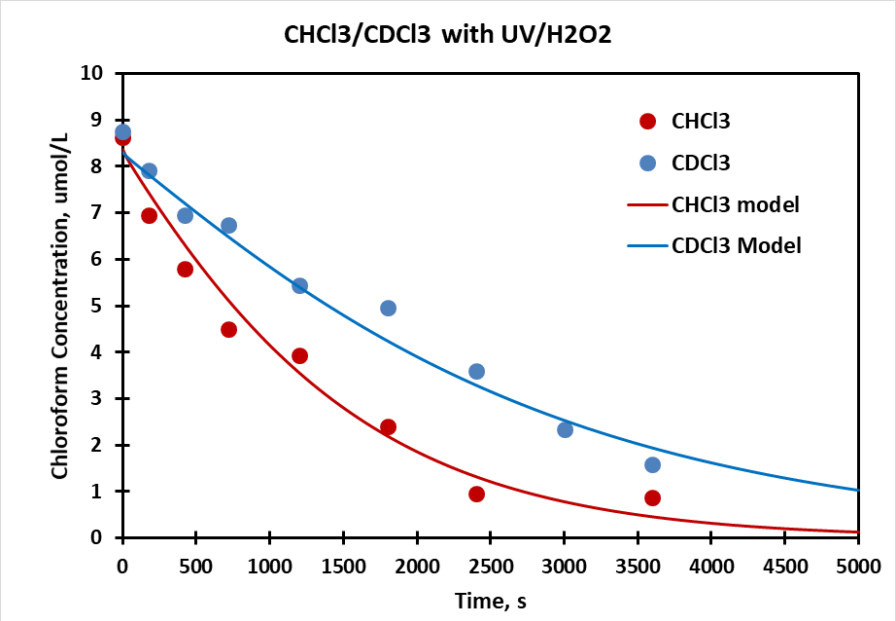

Figure 19 - Chloroform and chloroform-D degradation in UV/H_2O_2 system. The kinetic model is a pseudo-steady-state dynamic kinetic model with all elementary reactions.

From the model fitting, we obtained the second-order reaction rate constants for chloroform $7.16 \times 10^7\ L/(mol \cdot s)$ and chloroform-D $3.59 \times 10^7\ L/(mol \cdot s)$, respectively. The experiment results indicate a KIE=1.994 which is different from model prediction. However, when we consider adding the transition state energy difference as a correction for the difference of ZPE, it gave a better result. It was calculated the difference of transition state energy between chloroform and chloroform-D is 7.1732 kJ/mol. By taking into account this modification, the KIE for chloroform is 2.602 based on equation [61], which is a far more reasonable than the calculation (prediction) without transition state energy modification.

Another interesting phenomenon we observed from experiments is that deuterated phenol is actually faster degraded than phenol in UV/H_2O_2 system. The results are plotted in Figure 21.

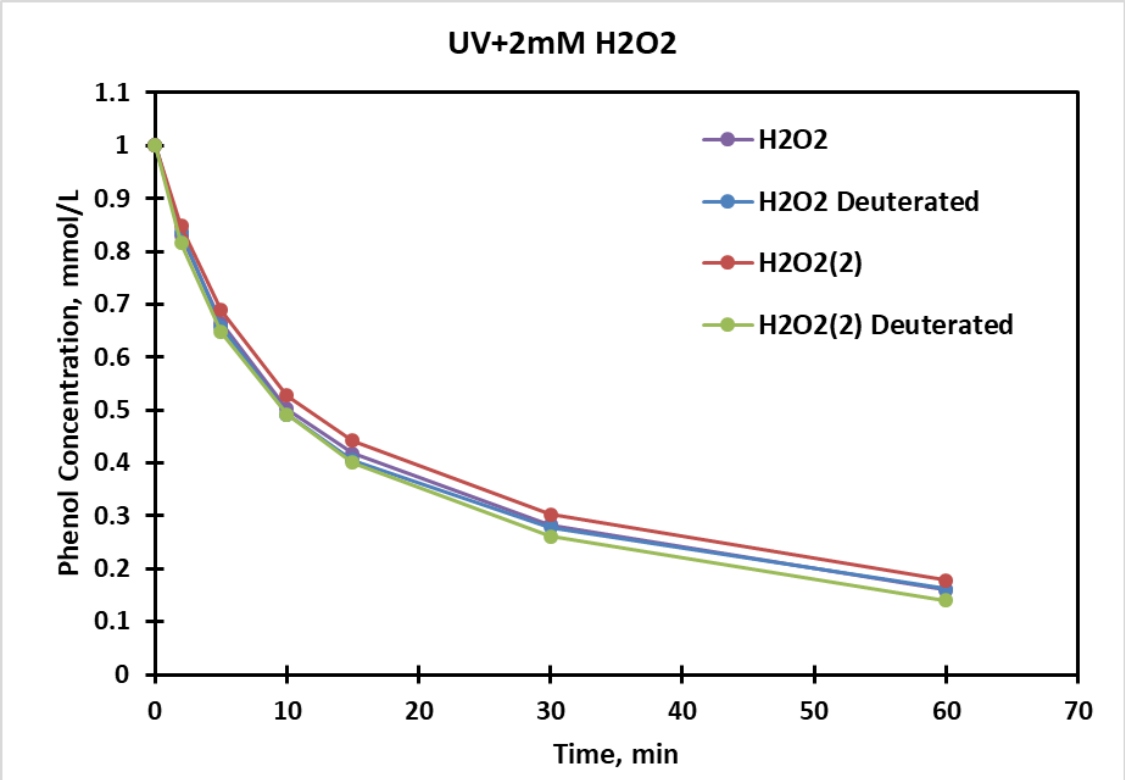

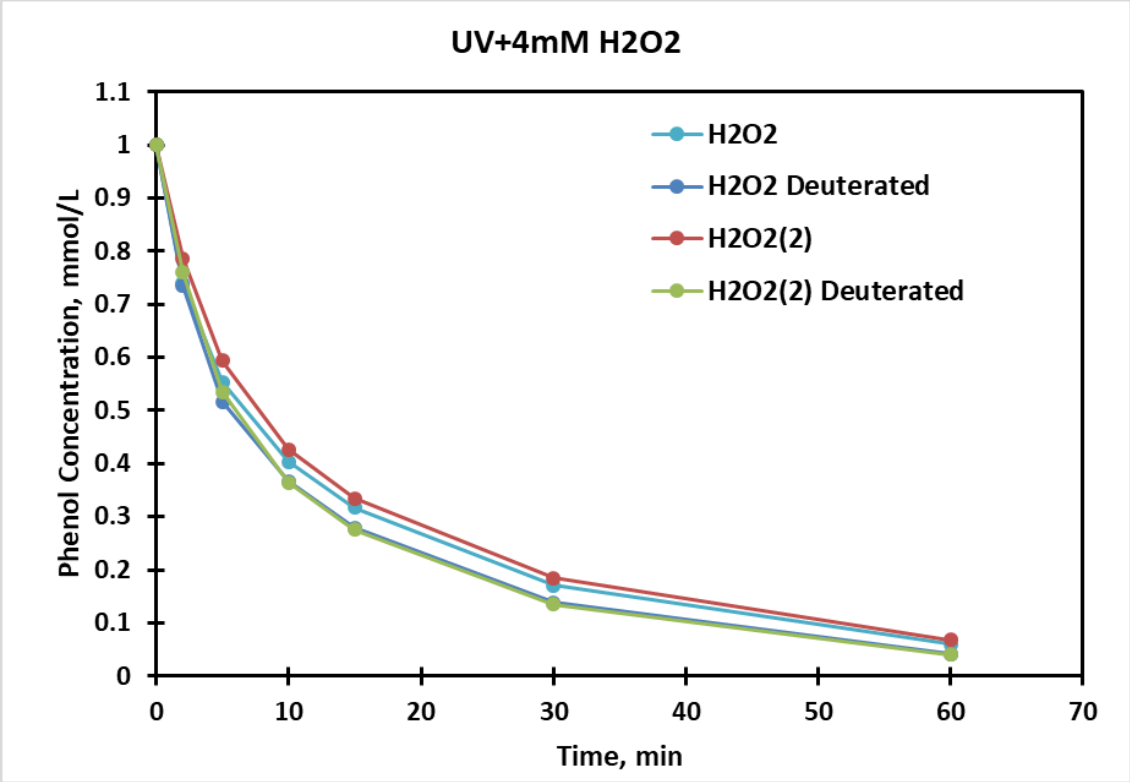
UV+4mM H2O2
Phenol Concentration, mmol/L
Time, min
H2O2
H2O2 Deuterated
H2O2(2)
H2O2(2) Deuterated
1.1
1
0.9
0.8
0.7
0.6
0.5
0.4
0.3
0.2
0.1
0
0
10
20
30
40
50
60
70

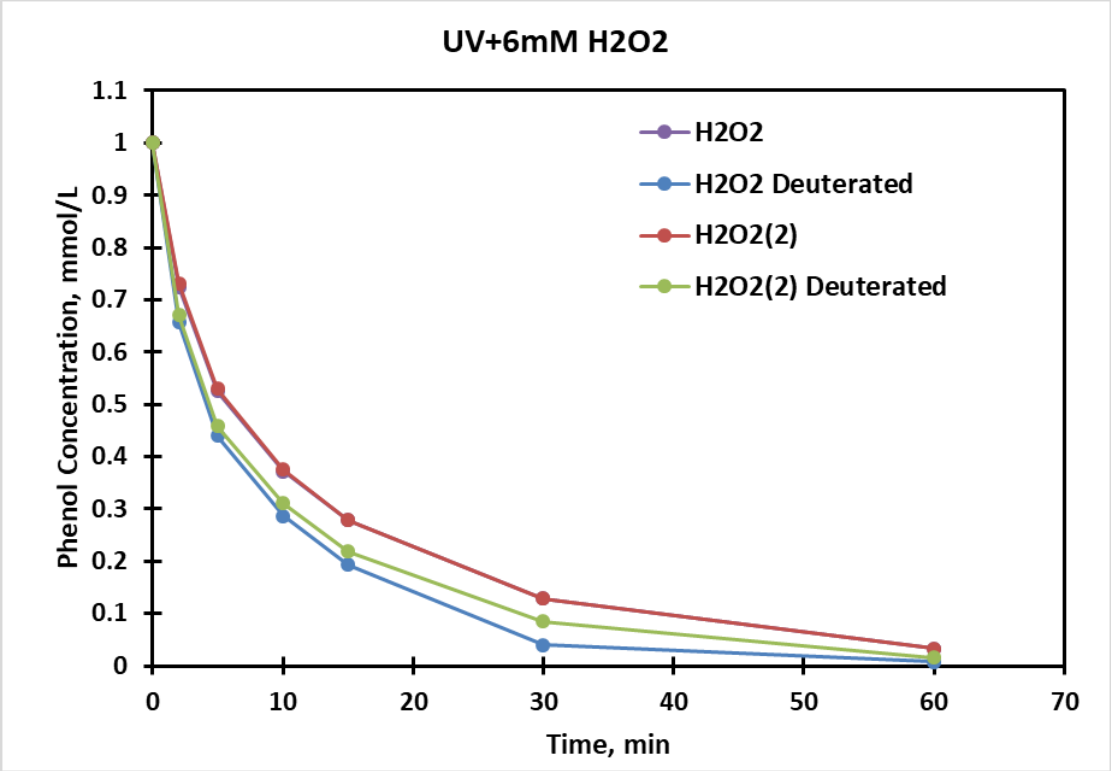

Figure 20 - Phenol degradation in UV/H_2O_2 system. The experiments are repeated once (each data points are triple sampled for accuracy.

From the results, we can clearly observe that when the hydrogen peroxide concentration increased, a more significant difference between phenol and deuterated phenol degradation. The results appear to contradict the KIE hypothesis because deuterated phenol do has a smaller ZPE than phenol. But since the KIE can only explain hydrogen abstraction, a more feasible explanation of this phenomenon is still under developing. One possible explanation is that the reaction kinetics between hydroxyl radical and phenol is not via hydroxyl radical addition to the ring, which is a completely different hypothesis than the original. We have computational results to support this new hypothesis. In figure 3, the Gaussian pathway calculation indicates that hydroxyl attacking the hydrogen on oxygen is far easier than attacking the hydrogen on carbon. Therefore, the conclusion drawn from the

calculation is that the major pathway for hydroxyl radical with phenol is still hydrogen abstraction. The reason for such hydrogen abstraction contradicts the classic theory is still unclear.

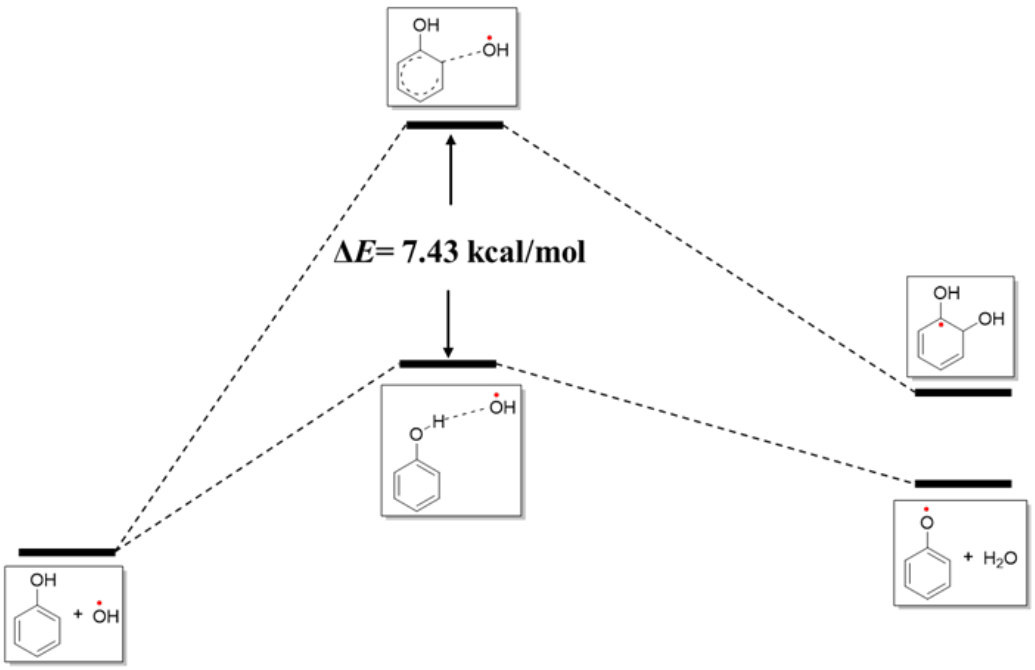

Figure 21 - A density functional group (DFT) calculation on two possible pathways of hydroxyl radical and phenol.

CHAPTER 7. MAJOR CONCLUSIONS AND FUTURE WORKS

7.1 Major Conclusions

The key conclusions of this dissertation include:

1. The development of anode materials regarding the generation of hydroxyl radicals and lifetime have been refined to focus on three properties: 1) enlarge the band gap can increase the oxygen evolution potential and thus favors the production hydroxyl radicals; 2) Titanium nanotubes have large band gap and reasonable conductivity. The nanotubes structure can delay the recombination rate of excitons and thus increase the quantity of viable hydroxyl radicals; 3). SnO_2-Sb has a large band gap and good conductivity but poor stability. Aged SnO_2-Sb coating layer exhibits better crystallinity and can extensively increase the lifetime of the anode.
2. The mass transfer has a big impact on the overall oxidation efficiency. Especially when operated in high current density (current density > limiting current), the mass transfer is the determining factor of the system. The impact was quantitatively evaluated by established a dimensionless coefficient, effectiveness factor Ω between 0 to 1 where 0 is maximum mass transfer resistant and 1 is no mass transfer impact.
3. When operated in high current density mode and mass transfer is the determining factor, it has been valid the overall EE/O will not significantly increase as the elevating initial target contaminants concentrations because in such operational

conditions, the generated hydroxyl radicals on the surface is overall dosed and the limiting factor is the quantity of organics can be transported from the bulk solution to the anode surface.

4. A three-dimensional electrochemical oxidation system configuration can significantly lower the applied (cell) voltage and hence lower the overall energy requirement. Proton exchange membrane acts as the electrolyte in the system and established a proton bridge which allows a closed circuit for conduction. The meshed electrode can use the sol-gel method and dip-coating techniques to fabricate outer coating layer however it is important to keep the exposure for water to move through freely.
5. It is not the better the anode materials (regarding the quantity of hydroxyl radicals' production), the better the treatment efficiency. Cases such as algae contaminated wastewater disinfection, a less inactive (less good) anode have oxygen evolution overpotential ranges 1.2 V to 1.9 V/SHE which can mainly focus on active chlorines and hydrogen peroxide generation is more sufficient because comparing with radicals, these oxidants persist much longer.
6. Deuterated compounds can be degraded by AOPs (i.e. hydroxyl radicals) typically have larger second-order rate constants comparing with their normal hydrogen version compounds. The conclusion is valid for those hydroxyl radicals' attack organics via hydrogen abstraction. The deuterated compounds of these hydrogen abstraction destructions can be evaluated by kinetic isotope effect where most of the rate constants of hydrogen version compounds with hydroxyl radicals are already available.

7.2 Future Works

Based on the current conclusions from studies, future work to advance the understanding of electrochemical oxidation and the development of electrochemical advanced oxidation processes for wastewater treatment may include the following:

1. Currently developed anode materials exhibit good oxidation efficiency in bench scale, however, the actual accelerate lifetime test is lack of performing. The pilot and industrial scale electrochemical facilities utilize large size of electrodes, hence the resistance of the electrode especially when constructed in electrode packs, although the applied voltage is large enough for hydroxyl radicals generation, the current density is small. Advanced configuration approach is required to develop to overcome the possible low oxidation efficiency issue.
2. Advanced anode materials can be further developed regarding the large band gap, enhanced lifetime and stability. Develop first-principle electrochemical oxidation kinetics model which can simulate the electrode materials, applied voltage, current density etc. regarding the oxidants production from the anode (heterogeneous electrochemical surface reactions).
3. Further, improve the three-dimensional electrochemical system by solving the meshed electrodes and proton exchange membrane adherence issue which may have the potential to extensively enhance the production of hydroxyl radicals. Investigate the correlation between the meshed grids regarding surface area per volume and the overall oxidation efficiency.

4. Conduct AOP degradation experiments on more deuterated compounds, especially on those compounds that are not degraded via hydrogen abstraction to further investigate the isotope effect regarding their degradation kinetics and toxicity.

APPENDIX A. SUPPORTING INFORMATION FOR CHAPTER 4

Text S1. Instrumental analysis.

The ofloxacin was determined using an HPLC – DAD system (Agilent Technologies, series 1200) equipped with a C18 column (Extend, 3.5 μm, 4.63 × 150 mm) and operated at a flow rate of 1 mL min^{-1}. An isocratic method, with 15% HPLC-grade acetonitrile and 85% ultrapure water acidified with 5 mM H_3PO_4 was used as the mobile phase. The ofloxacin concentration was determined using a UV detector monitor and an absorbance at λ = 287 nm. The sample injection volume was 10 μL.

The F^- concentration was measured using an ion chromatography equipped with a Dionex Ionpac AS11 – HC 4 × 250 mm column. Samples were filtered using 0.22 μm syringe filters (Millipore) and the samples were placed into the Dionex autosampler. Standard solutions were injected with every run to ensure the correct operation of the system. The gradient elution was performed using $NaHCO_3$ (1 mM) + Na_2CO_3 (8 mM) solution at 0.8 mL min^{-1}. Mineralization was monitored by measuring the dissolved organic carbon (DOC) by direct injection of the filtered samples (0.22 μm PTFE filters, Panreac) into a Shimadzu – L CSH/CSN TOC analyzer calibrated with standard solutions of Potassium hydrogen phthalate.

The mass of parent OFL in solution and its breakdown products were identified by LC/MS (Agilent, Palo Alto, CA) by selected ion monitoring (SIM) and positive electrospray ionization (ESI) mode. Accordingly, the protonated molecular ion $[M+H]^+$

was selected as the precursor ion for analysis. The nebulizer pressure and the capillary voltages were 35 psig and 4500V, respectively, and the scan range was 50-500 Daltons. The LC flow rate was 0.5mL/min. Water containing 0.1% formic acid was used as eluent A and acetonitrile was used as eluent B. The concentrations of metal ions (Pb, Sn, and Sb) leaching during electrochemical degradation were measured by an inductively coupled plasma mass spectrometry (ICP-MS, Perkin Elmer Optima NexIonTM 300D) and the experimental error is less than 10%. The detection limits were 0.0497 mg/L for Pb, 0.0048 mg/ L for Sn and 0.0039 mg /L for Sb.

Text S2. Residual analysis.

It is important to know the metal ions concentration in the residual because we need to know whether our fabricate anode foul significantly and whether our treated water becomes more toxic. The metal ion concentrations in the residual (i.e. Pb, Sn, and Sb) were measured by an inductively coupled plasma mass spectrometry (ICP – MS, Perkin Elmer Optima NexIonTM 300D) with errors less than 10%. The detected concentrations from residual for single run (i.e. current density 30 mA/cm^2 for 2 h) were 0.0497 mg/L for Pb, 0.0048 mg/L for Sn and 0.0039 mg/L for Sb.

Text S3. Model fitting.

To calculate the unknown surface reaction rate, k_s, and the surface roughness factor, θ, we use our model to fit observed pseudo first-order rate constants, k. To get the best fitting results, we minimize the objective function (OF) using the generalized reduced gradient nonlinear algorithm (GRG).

$$OF = \sqrt{\frac{1}{n-1} \cdot \sum_{i=1}^{n} \left(\frac{C_{data,i} - C_{model,i}}{C_{data,i}}\right)^2} \tag{69}$$

In which, n is the number of the data points, $C_{data,i}$ represent the value from data and $C_{model,i}$ represent the value from the model. Our fitting results from Figure 11 and Figure S6 show that our model fits the observed data well (OF > 0.05).

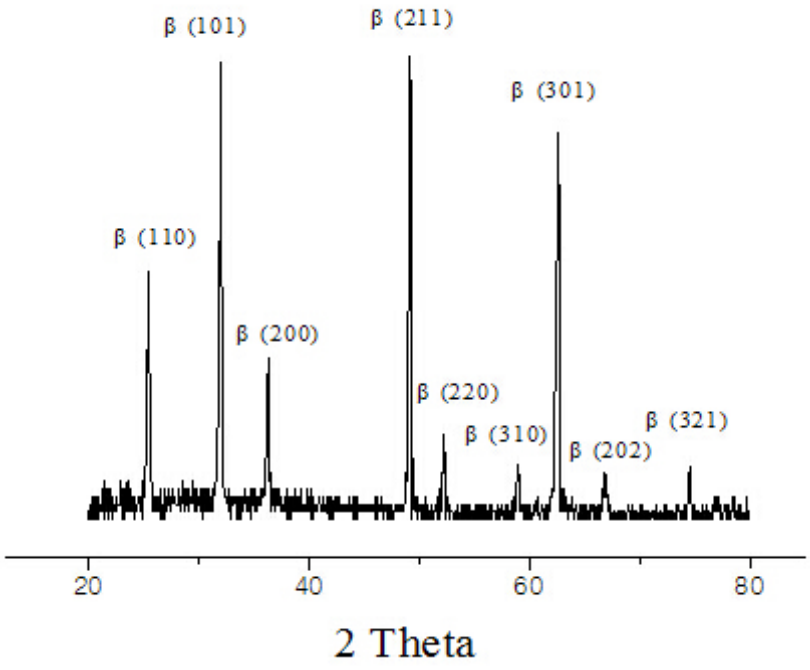

Figure 22 - The X-Ray Diffraction pattern of TiO_2 based SnO_2 – Sb/FR – PbO_2 electrode.

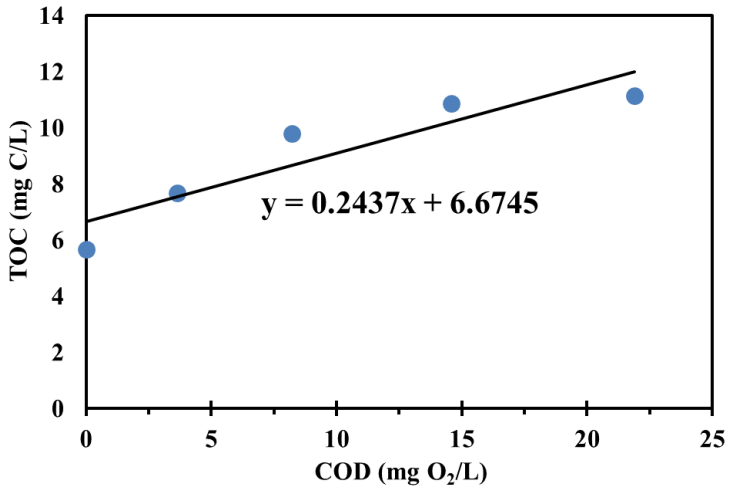

Figure 23 - The TOC vs. COD for TiO_2 based SbO_2 – Sb/FR – PbO_2 electrode. Current density 30 mA/cm^2, initial ofloxacin concentration 20 mg/L, electrolyte 0.05 M Na_2SO_4

solution, pH value 6.25, temperature 25 ℃, reaction time 2 h, electrode spacing 1 cm, reactor total volume 310 mL, flow rate 400 mL/min.

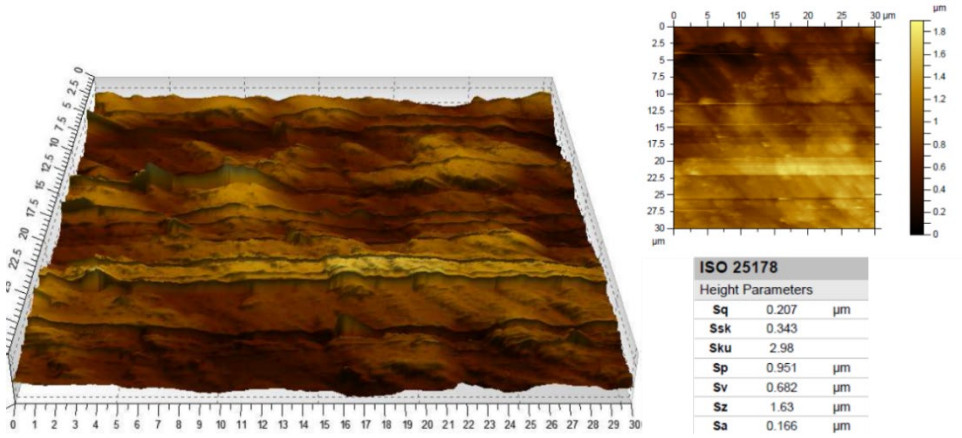

Figure 24 - AFM image for the surface of TiO_2 based SbO_2 – Sb/FR – PbO_2 electrode. Scanning area 30 µm^2, 3 random spots are scanned and the average arithmetic means height is 0.18 µm. The scanning accuracy is 256×256.

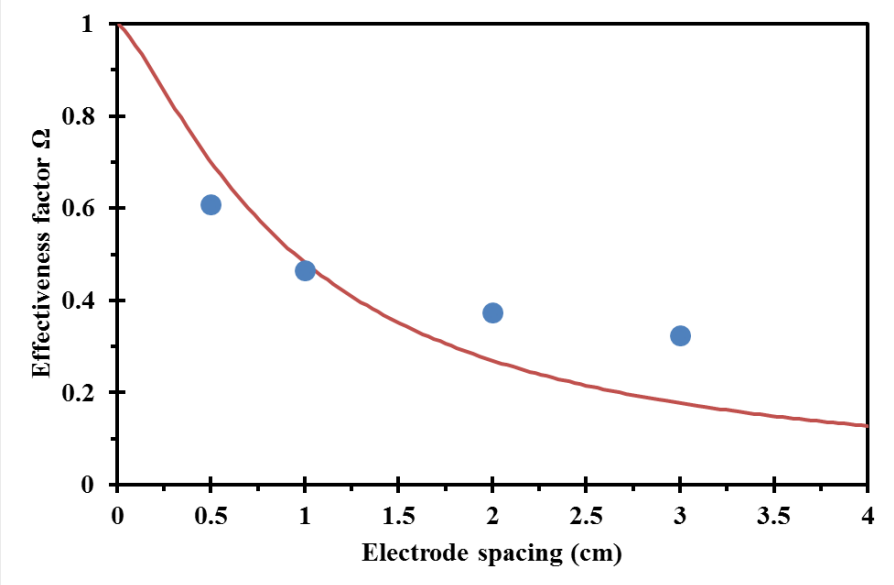

Figure 25 - Effectiveness factor in different electrode spacing and the best model fitted. Current density 30 mA/cm^2, voltage 5 – 9.2 v, initial ofloxacin concentration 20 mg/L, electrolyte 0.05 M Na_2SO_4 solution, pH value 6.25, temperature 25 ℃ and fluid velocity 0.033 m/s.

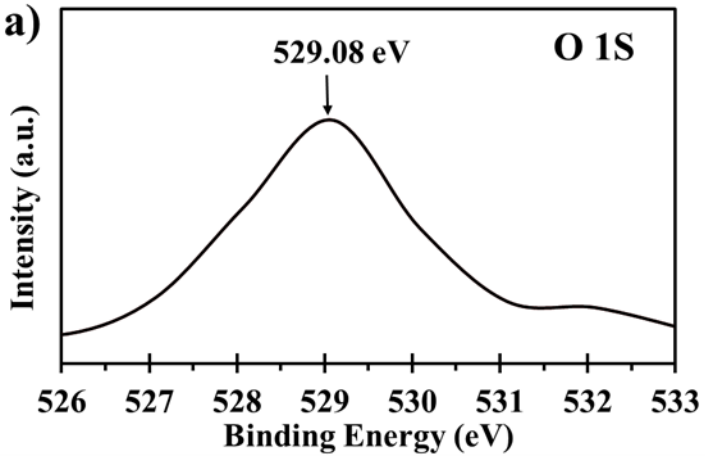

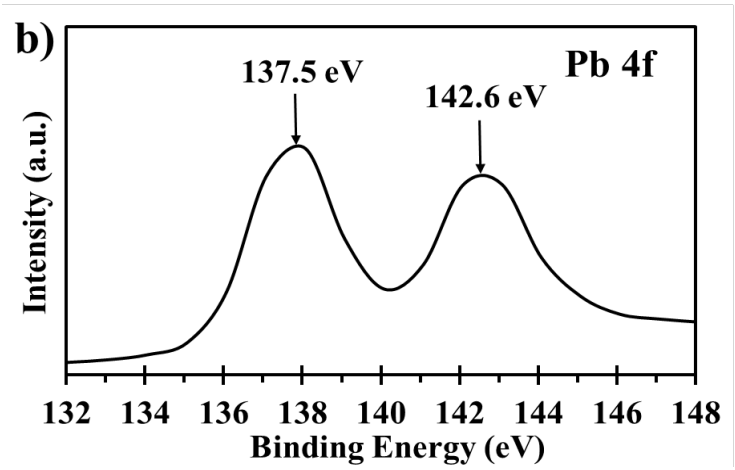

Figure 26 - XPS of the TiO_2 based SnO_2-Sb/FR-PbO_2 electrode, a). O 1s peak, b). Pb 4f peak.

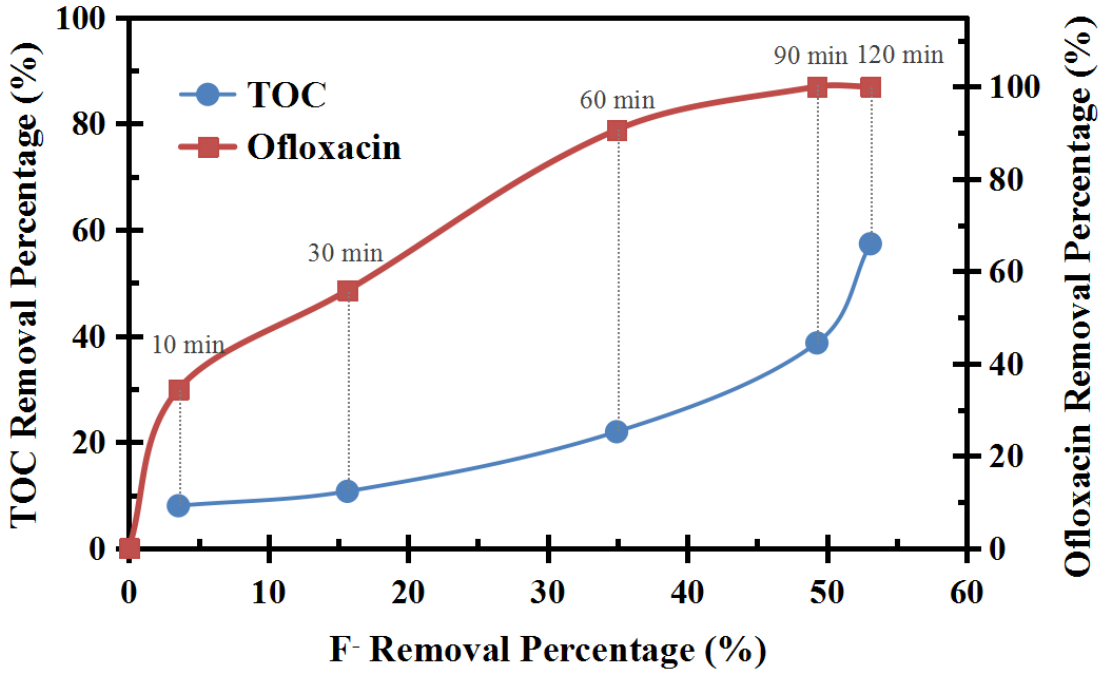

Figure 27 - The F^- vs. TOC mineralization and ofloxacin degradation profile for TiO_2 based SnO_2-Sb/FR-PbO_2 electrode. Current density 50 mA/cm^2, initial ofloxacin

concentration 20 mg/L, electrolyte 0.05 M Na_2SO_4 solution, pH value 6.25, temperature 25 ℃, reaction time 2 h, electrode spacing 1 cm, reactor total volume 310 mL, flow rate 400 mL/min.

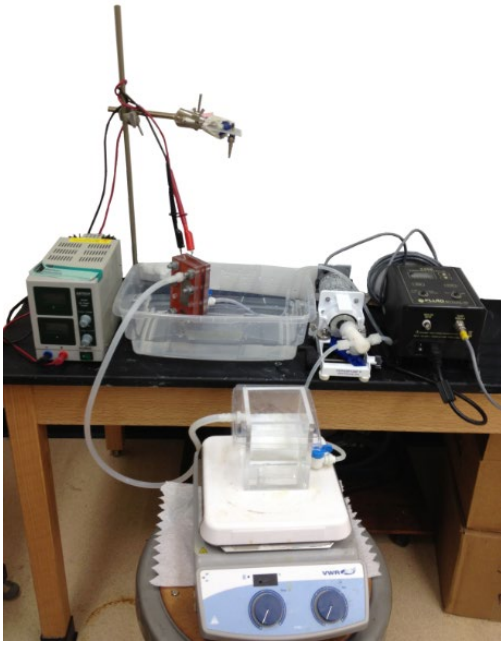

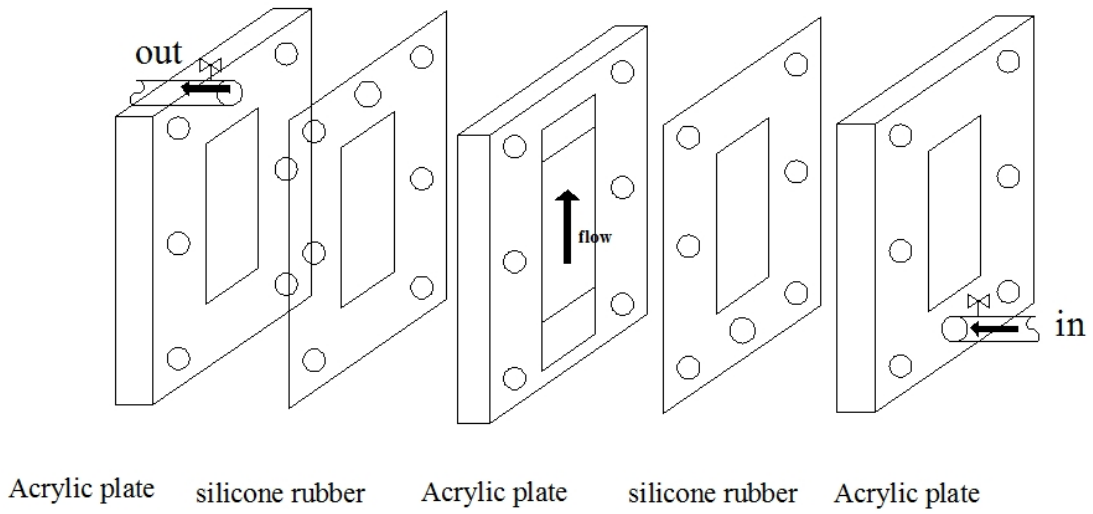

Figure 28 - (a) Schematic diagram of the experimental differential column batch reactor (DCBR) setup and (b) exploded view of the flow cell.

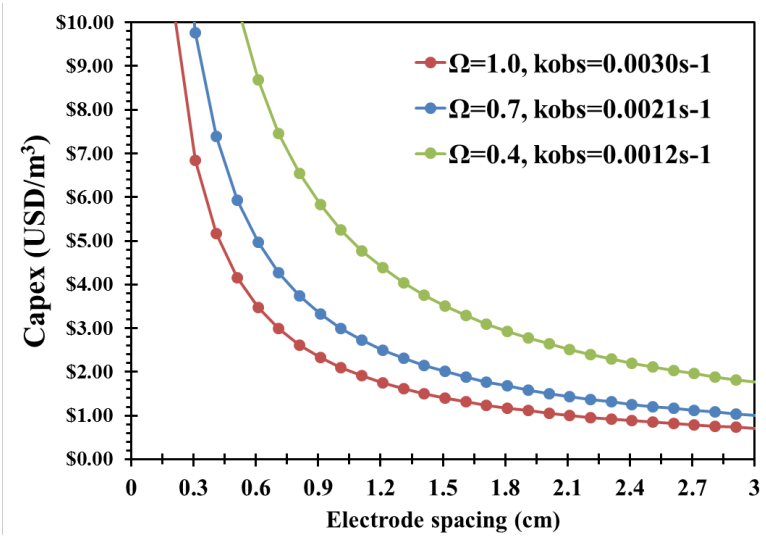

Figure 29 - capital cost vs. different electrode spacing. For the same treatment objective, the higher the effectiveness factor, the smaller the reactor size it requires

thus its capital cost decreases. The capital cost increases when the electrode spacing decreases thus more electrodes required in the reactor.

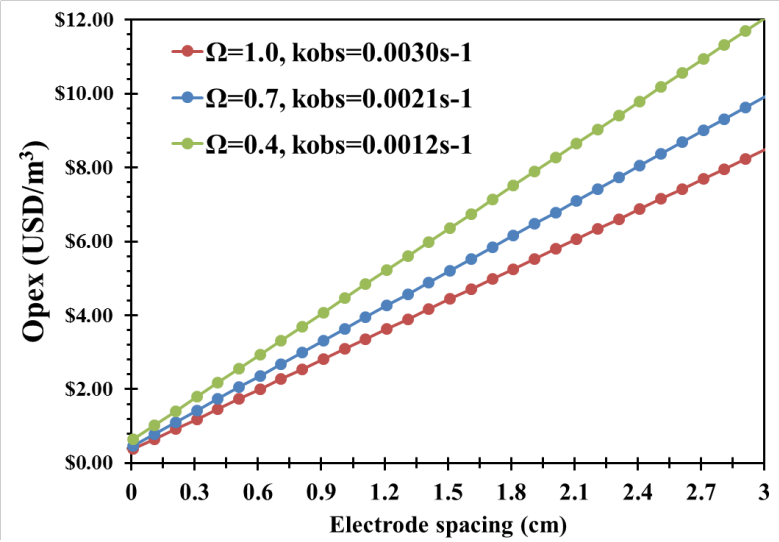

Figure 30 - operational cost vs. different electrode spacing. For the same treatment objective, the higher the effectiveness factor, the fewer energy it requires thus its operational cost decrease. The operational cost increases when the electrode spacing increases thus higher voltage required to maintain the current density.

larger the electrode spacing, the higher the voltage it requires to maintain the same current density thus higher operational cost.

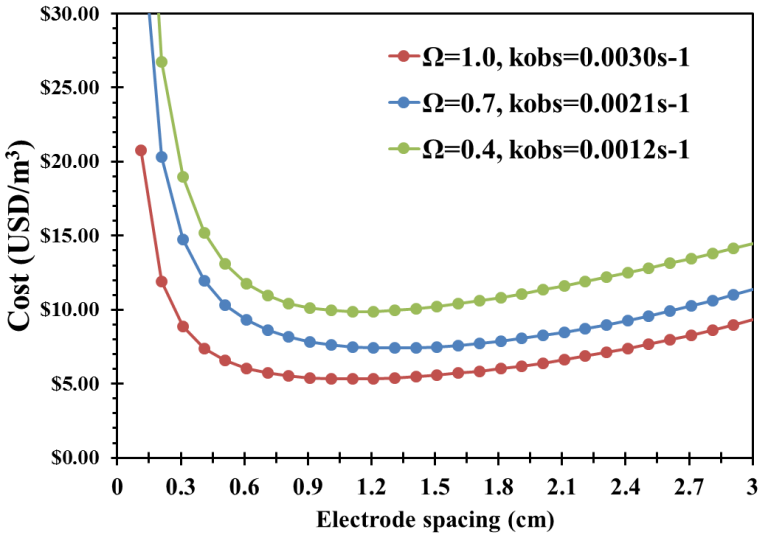

Figure 31 - total cost vs. different electrode spacing. The total cost is the sum of its capital cost and operational cost. The preliminary design of an electrochemical reactor and its total cost can be roughly estimated based on its effectiveness factor. Use effectiveness factor Ω for preliminary design and total cost estimation. In here, the treatment objective is 99% removal, the flow rate is 1000 m^3/day and the fluid velocity is 0.0116 m/s. The flow channel has an eddy promoter and its electrode spacing and obstacle distance ratio is 1/3. The electricity price is $0.0512/kWh and the pumping power is 8.53 kW. The electrode price is $300/$m^2$ and its lifetime is 2000 h.

APPENDIX B. SUPPORTING INFORMATION FOR CHAPTER 5

Text S1. Lifetime estimation

An empirical equation for the prediction of anode lifetime was reported as follows:

$$T_1 \times j_1^n = T_2 \times j_2^n \tag{70}$$

Where T_1 is the accelerate lifetime obtained at a high current density (j_1) and T_2 is the actual lifetime obtained at operational current density (j_1). n is an adjustable parameter.[3, 4] The test experiment was carried out in 0.5 M H_2SO_4 solution During the experiments, the lifetime was determined as 3 hours at $j = 1000\, mA/cm^2$ and 8 hours at $j = 400\, mA/cm^2$. Hence the power parameter was fitted and calibrated as 1.07. Accordingly, the actual lifetime was estimated of 128, 415, 871 and 4880 h at operational current density 30, 10, 5 and 1 mA/cm^2.

Text S2. Objective function

To get the best fitting results, we minimize the objective function (OF) using the generalized reduced gradient nonlinear algorithm (GRG).

$$OF = \sqrt{\frac{1}{n-1} \cdot \sum_{i=1}^{n} \left(\frac{C_{data,i} - C_{mod\,el,i}}{C_{data,i}}\right)^2} \quad (71)$$

In which, n is the number of the data points, $C_{data,i}$ represent the value from data and $C_{model,i}$ represent the value from the model. Our fitting results from Figure 3 show that our model fits the observed data well (OF < 0.07).

Text S3. Simulation parameters

$[HCO_3^-]$ = 3 mM; [NOM] = 2 mg/L; $[Cl^-]$ = 0.001 M;

pH = 7; $k_{BA} = 5.9\times10^{-9}$ L/(mol·S)

Same 2.2 W input energy gives UV light intensity = 1.64×10^{-6} Einstein s^{-1} L^{-1};

Initial Concentrations [R] (Benzoic Acid in this case) = 20, 200, 2000 mg/L;

Quantum yield:

UV/H_2O_2 = 0.5, UV/HOCl = 0.9, UV/Persulfate = 0.7,

UV/TiO_2 = 0.04 (light transmission efficiency = 0.4);

Chemical production energy:

H_2O_2 = 4.9 kWh/lb, persulfate = 4.9 kWh/lb, HOCl = 5.1 kWh/lb, O_3 = 5 kWh/lb;

Note: TiO_2 and electrodes production energies are not included in simulation

EAOPs assumptions & parameters:

J = 30 mA/cm^2, 2D anode size A = 10 cm^2, 3D anode size A= 7.18 cm^2 (80 meshed Ti gauze)

Sc = 2727, Sh = 194, $D_l = 9\times10^{-6}$ cm^2/s, d = 1 cm

Note: pumping energy is small compare to electricity and neglected in simulation

Q = 20 mL/min, Re = 18.51, $k_f = 2.35\times10^{-6}$ m/s

Q = 500 mL/min, Re = 462.96, $k_f = 6.88\times10^{-6}$ m/s

Q = 2000 mL/min, Re = 2037.04, $k_f = 1.13\times10^{-5}$ m/s (Re < 2100 in laminar flow)

Text S4. H_2O_2/O_3 process modeling approach

(1) Model type: pseudo-steady-state kinetic model

$$[HO\cdot]_{ss} = \frac{k_L a\left(\frac{P_{O_3}}{H_{O_3}}\right)}{k_1[H_2O_2]_0 + k_2[HCO_3^-]_0 + k_3[NOM]_0 + k_4[R]_0} \quad (72)$$

where,

O_3 dissolved rate is 0.2 g/hr, and O_3 transfer efficiency is 30%

$$k_L a\left(\frac{P_{O_3}}{H_{O_3}}\right) = \frac{(0.2\text{g/hr})/(3600\text{s/hr})}{(48\text{g/mol})(1\text{L})} = 1.158\times10^{-6}\ M\cdot s^{-1}$$

(2) Simulation condition

$[HCO_3^-]$ = 3mM; [NOM] = 2 mg/L; [R] = 200 mg/L; $[H_2O_2] = 1.142\times10^{-6}$ M

$[Cl^-]$ = 0.001 M (Note: Cl^- has no impact); pH = 7

(3) EE/O Calculation

$$EE/O = \frac{\frac{k_L a \times \frac{P_{O_3}}{H_{O_3}} \times V \times M_{O_3} \times \frac{0.0022\ \text{lb}}{\text{gram}} \times E_{O3} \times t}{\eta} + C_{H2O2} \times V \times E_{H2O2} \times \frac{0.0022\ \text{lb}}{\text{gram}}}{V \times \log\left(\frac{C_i}{C_f}\right)} \quad (73)$$

where

k_{La} = overall mass transfer coefficient for ozone, s^{-1}

P_{O3} = partial pressure of ozone in inlet gas, atm

H_{O3} = Henry's law constant for ozone, atm·L/mole

V = reactor volume, 1 L

M_{O3} = molecular weight of ozone, 48 g/mole

E_{O3} = energy use to produce O_3, 5 kWh/lb

t = reaction time for batch reactor, minute

η = transfer efficiency of ozone contactor, dimensionless

C_{H2O2} = total concentration of H_2O_2 added into the reactor, mg/L

E_{H2O2} = energy use to produce H_2O_2, 4.9 kWh/lb;

C_i = influent concentration of the target compound, mg/L

C_f = effluent concentration of the target compound, mg/L

Text S5. UV/H_2O_2 process modeling approach

(1) Model type: pseudo-steady-state kinetic model

$$[\mathrm{HO}\cdot]_{ss,0} = \frac{2\Phi_{H_2O_2} P_{\text{U-V}} f_{H_2O_2} (1\text{-}10^{A})}{k_1[H_2O_2]_0 + k_2[\mathrm{HCO_3^-}]_0 + k_3[\mathrm{NOM}]_0 + k_4[R]_0} \quad (74)$$

where,

$\phi_{H_2O_2}$ is the quantum yield of H_2O_2 (0.5); $\varepsilon_{H_2O_2}$ is the extinction coefficient of H_2O_2 (19.6 $M^{-1}cm^{-1}$); ε_R is the extinction coefficient of benzoic acid (730 $M^{-1}cm^{-1}$); ε_{NOM} is the extinction

coefficient of NOM (0.0315 $(mg/L)^{-1}cm^{-1}$); L is the effective pathlength (6 cm^{-1}).

$$A = \left(\varepsilon_{H_2O_2} C_{H_2O_2} + \varepsilon_R C_R + \varepsilon_{NOM} C_{NOM}\right) L \quad (75)$$

$$f_{H_2O_2} = \frac{\varepsilon_{H_2O_2} C_{H_2O_2}}{\varepsilon_{H_2O_2} C_{H_2O_2} + \varepsilon_R C_R + \varepsilon_{NOM} C_{NOM}} \quad (76)$$

(2) Simulation condition

UV intensity = 1.64×10^{-6} Einstein s^{-1} L^{-1};

$[HCO_3^-]$ = 3mM; [NOM] = 2 mg/L; [R] = 200 mg/L; $[Cl^-]$ = 0.001 M (Note: Cl^- has no impact);

pH 7; H_2O_2 dosage ranges from 0 mg/L to 200 mg/L;

(3) EE/O Calculation

$$\text{EE/O} = \frac{\text{P}\times\text{t} + \text{V}\times\text{C}_{\text{H2O2}} \times \frac{0.0022\ \text{lb}}{\text{gram}} \times E_{\text{H2O2}}}{\text{V}\times\log\left(\frac{C_i}{C_f}\right)} \quad (77)$$

where P = total lamp power, kW

C_{H2O2} = total concentration of H_2O_2 added into the reactor, mg/L

E_{H2O2} = energy use to produce H_2O_2, 4.9 kWh/lb

V = reactor volume, 10^{-3} m^3 (1 L)

t = reaction time for the batch system, hr

C_i = influent concentration of the target compound, mg/L

C_f = effluent concentration of the target compound, mg/L

Text S6. UV/Persulfate process modeling approach

(1) Model type: dynamic kinetic model

Activation step: $r_{UV,PS} = 2\phi_{PS} P_{UV} f_{PS}(1 - 10^{-A})$

where,

ϕ_{PS} is the quantum yield of persulfate (PS) (0.7); ε_{PS} is the extinction coefficient of PS (20.7

$M^{-1}cm^{-1}$); $\varepsilon_R$is the extinction coefficient of benzoic acid (730 $M^{-1}cm^{-1}$); ε_{NOM} is the

extinction coefficient of NOM (0.0315 $(mg/L)^{-1}cm^{-1}$); L is the effective pathlength (6 cm^{-1}).

$$A = (\varepsilon_{PS}C_{PS} + \varepsilon_R C_R + \varepsilon_{NOM}C_{NOM})L \quad (77)$$

$$f_{PS} = \frac{\varepsilon_{PS}C_{PS}}{\varepsilon_{PS}C_{PS} + \varepsilon_R C_R + \varepsilon_{NOM}C_{NOM}} \quad (78)$$

(2) Simulation condition

UV intensity = 1.64×10^{-6} Einstein s^{-1} L^{-1};

$[HCO_3^-]$ = 3mM; [NOM] = 2 mg/L; [R] = 200 mg/L; $[Cl^-]$ = 0.001 M

pH 7; PS dosage ranges from 0 mg/L to 200 mg/L;

(3) EE/O Calculation

$$EE/O = \frac{P\times t + V\times C_{PS} \times \frac{0.0022\ lb}{gram} \times E_{PS}}{V\times \log\left(\frac{C_i}{C_f}\right)} \quad (79)$$

where P = total lamp power, kW

C_{PS} = total concentration of PS added into the reactor, mg/L

E_{PS} = energy use to produce PS, 4.9 kWh/lb

V = reactor volume, 10^{-3} m^3 (1 L)

t = reaction time for the batch system, hr

C_i = influent concentration of the target compound, mg/L

C_f = effluent concentration of the target compound, mg/L

Text S7. UV/HOCl process modeling approach

(1) Model type: dynamic kinetic model

Activation step:

$$r_{Cl\cdot} = \phi_{HOCl} P_{UV} f_{HOCl} (1 - 10^{-A}) + \phi_{OCl^-} P_{UV} f_{OCl^-} (1 - 10^{-A}) \quad (80)$$

$$r_{HO\cdot} = \phi_{OCl^-} P_{UV} f_{OCl^-} (1 - 10^{-A}) \quad (81)$$

where,ϕ_{HOCl} is the quantum yield of HOCl (0.9); ϕ_{OCl^-} is the quantum yield of OCl^- (0.8);

ε_{HOCl} is the extinction coefficient of HOCl (59 $M^{-1}cm^{-1}$); ε_{OCl^-} is the extinction coefficient of

OCl^- (66 $M^{-1}cm^{-1}$); $\varepsilon_R$is the extinction coefficient of benzoic acid (730 $M^{-1}cm^{-1}$); ε_{NOM} is the

extinction coefficient of NOM (0.0315 $(mg/L)^{-1}cm^{-1}$); L is the effective pathlength ($6cm^{-1}$).

$$A = (\varepsilon_{HOCl}C_{HOCl} + \varepsilon_{OCl^-}C_{OCl^-} + \varepsilon_R C_R + \varepsilon_{NOM}C_{NOM})L \quad (82)$$

$$f_{HOCl} = \frac{\varepsilon_{HOCl}C_{HOCl}}{\varepsilon_{HOCl}C_{HOCl} + \varepsilon_{OCl^-}C_{OCl^-} + \varepsilon_R C_R + \varepsilon_{NOM}C_{NOM}} \quad (83)$$

$$f_{OCl^-} = \frac{\varepsilon_{OCl^-}C_{OCl^-}}{\varepsilon_{HOCl}C_{HOCl} + \varepsilon_{OCl^-}C_{OCl^-} + \varepsilon_R C_R + \varepsilon_{NOM}C_{NOM}} \quad (84)$$

(2) Simulation condition

UV intensity = 1.64×10^{-6} Einstein s^{-1} L^{-1};

[HCO_3^-] = 3mM; [NOM] = 2 mg/L; [R] = 200 mg/L; [Cl^-] = 0.001 M

pH 7; PS dosage ranges from 0 mg/L to 200 mg/L;

(3) EE/O Calculation

$$EE/O = \frac{P \times t + V \times C_{HOCl} \times \frac{0.0022\ lb}{gram} \times E_{HOCl}}{V \times \log\left(\frac{C_i}{C_f}\right)} \quad (85)$$

where P = total lamp power, kW

C_{HOCl} = total concentration of HOCl added into the reactor, mg/L

E_{HOCl} = energy use to produce PS, 5.1 kWh/lb

V = reactor volume, 10^{-3} m^3 (1 L)

t = reaction time for the batch system, hr

C_i = influent concentration of the target compound, mg/L

C_f = effluent concentration of the target compound, mg/L

Text S8. UV/TiO_2 process modeling approach

(1) Model type: pseudo-steady-state kinetic model

$$[\mathrm{HO}\cdot]_{\mathrm{ss},0} = \frac{2\Phi_{\mathrm{TiO_2}} P_{\mathrm{U\text{-}V}} f_{\mathrm{TiO_2}} (1\text{-}10^{A})}{k_2[\mathrm{HCO_3^-}]_0 + \mathrm{k_3}[\mathrm{NOM}]_0 + \mathrm{k_4}[R]_0} \quad (86)$$

where,

$\phi_{Ti_{O_2}}$ is the quantum yield of TiO_2 (0.04); $\varepsilon_R$is the extinction coefficient of benzoic acid (730

$M^{-1}cm^{-1}$); ε_{NOM} is the extinction coefficient of NOM (0.0315 $(mg/L)^{-1}cm^{-1}$); L is the effective

pathlength (6 cm^{-1}).

$A = (\varepsilon_R C_R + \varepsilon_{NOM} C_{NOM})L$, $f_{TiO_2} = 0.4$

Energy to produce titanium dioxide = 24.8 GJ/ton = 6888.889 kWh/ton = 3.444 kWh/lb (neglect the type of TiO2 such as anatase or rutile or mixture)

(2) Simulation condition

UV intensity = 1.64×10^{-6} Einstein s^{-1} L^{-1};

$[HCO_3^-]$ = 3mM; [NOM] = 2 mg/L; [R] = 200 mg/L; $[Cl^-]$ = 0.001 M (Note: Cl^- has no impact);

pH 7; TiO_2 dosage is 300 mg/L= 3.756×10^{-3} mol/L

(Here we do not consider the recycle, separation and reuse process of TiO2 powder)

(3) EE/O Calculation

$$EE/O = \frac{P \times t + V \times C_{TiO_2} \times \frac{0.0022\ \text{lb}}{\text{gram}} \times E_{TiO_2}}{V \times \log\left(\frac{C_i}{C_f}\right)} \quad (87)$$

where P = total lamp power, kW

C_{TiO2} = total concentration of TiO_2 added into the reactor, mg/L

E_{TiO2} = energy use to produce TiO_2, 3.44 kWh/lb

V = reactor volume, 10^{-3} m^3 (1 L)

t = reaction time for the batch system, hr

C_i = influent concentration of the target compound, mg/L

C_f = effluent concentration of the target compound, mg/L

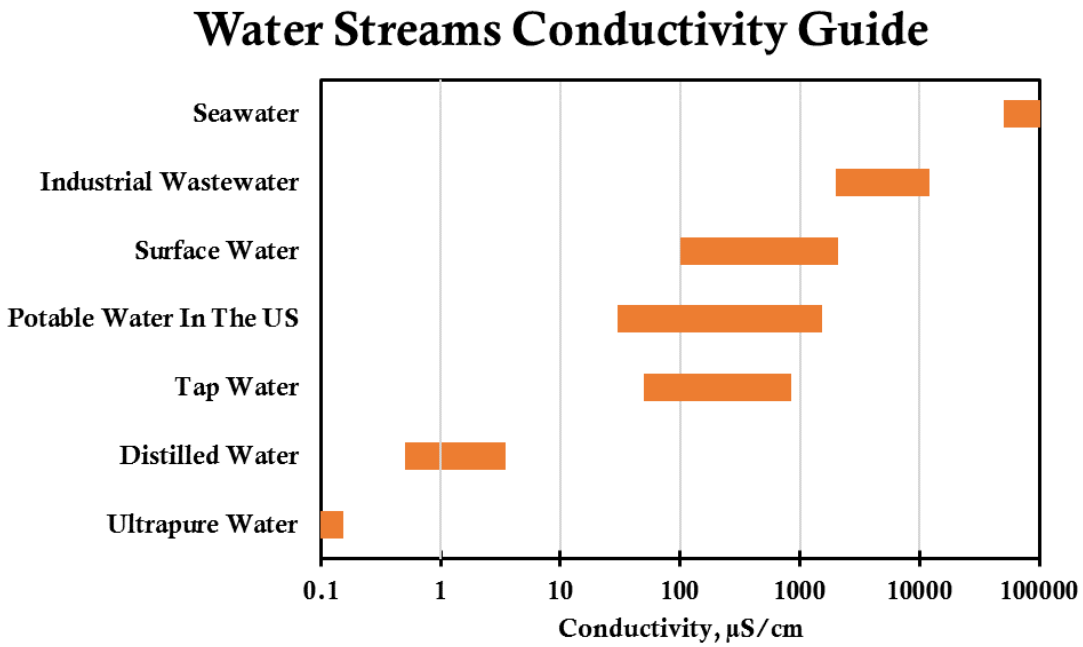

Figure 32 - A typical US water streams conductivity guide.[1,2] Our surface water was sampled from Lake Lanier, Buford, GA in April 2018. The conductivity was determined as 112.5 µS/cm. Five different ion strength were electrolyzed with 0.001, 0.005, 0.01, 0.05 and 0.1 M Na2SO4 and their conductivity was determined as 260, 1074, 1964, 8740 and 16210 µS/cm. Electrolytes $NaClO_4$ and NaCl were also tested

and the conductivities are 140, 530, 960, 4450, 8590 µS/cm and 160, 587, 1095, 5290, 10250 µS/cm, respectively.

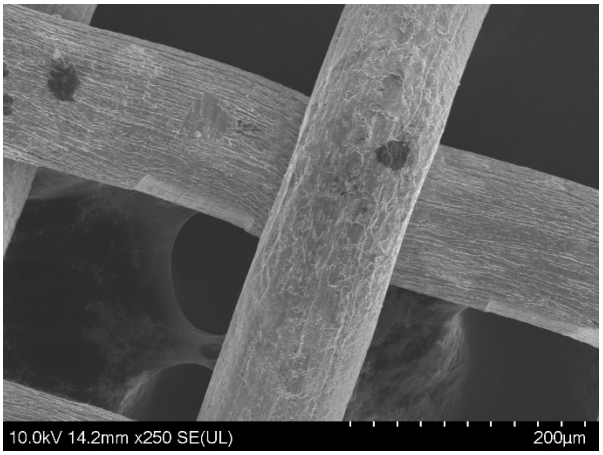

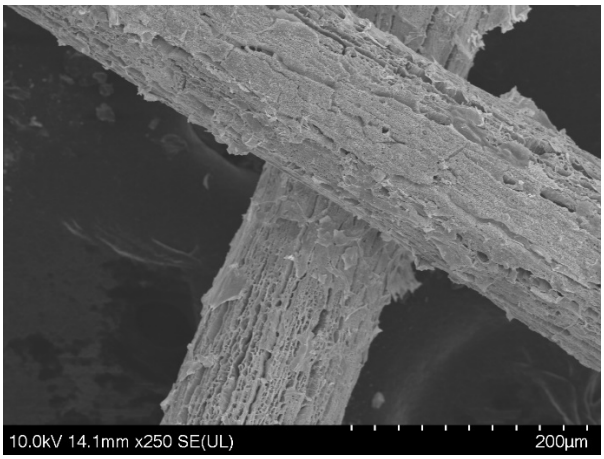

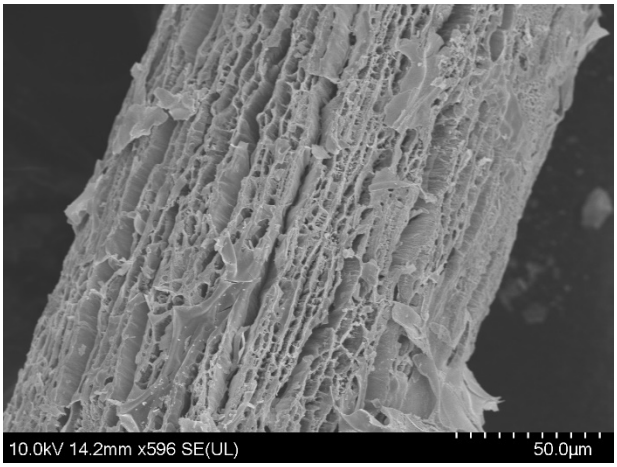

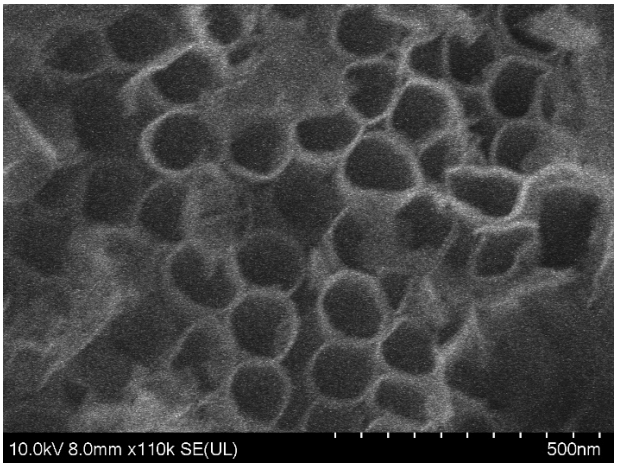

Figure 33 - (a) SEM of meshed Ti substrate (gauze type wire) in 200 µm. (b) Blue TiO_2 nanotubes grown on meshed Ti substrate (after cathodization enhancement) in 200 µm. (c) Meshed blue TiO_2 nanotubes view in 50 µm, surface enhancement can be clearly observed. More cracks observed on nanotubes array because the surface of

the substrate is not slab type and nanotubes cracks when they grew long. (d) Nanotubes view in 500 nm, the diameter of the nanotubes is estimated 18-22 nm.

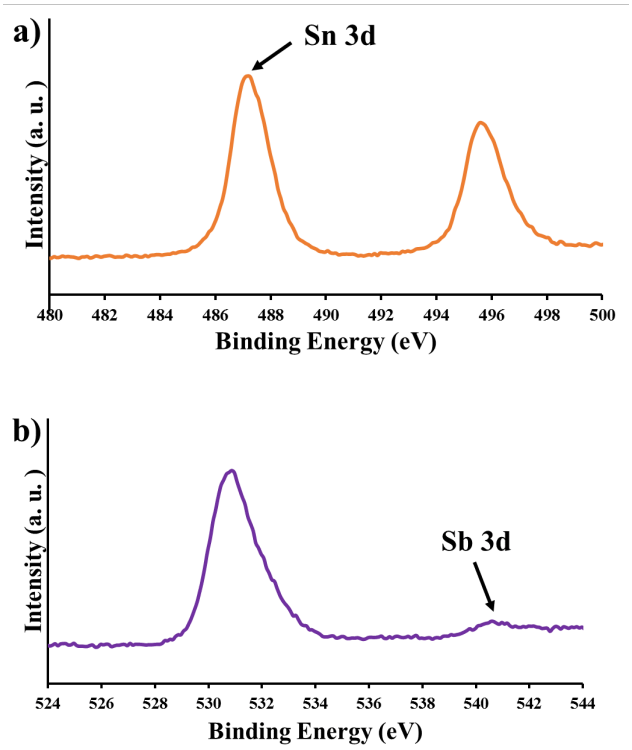

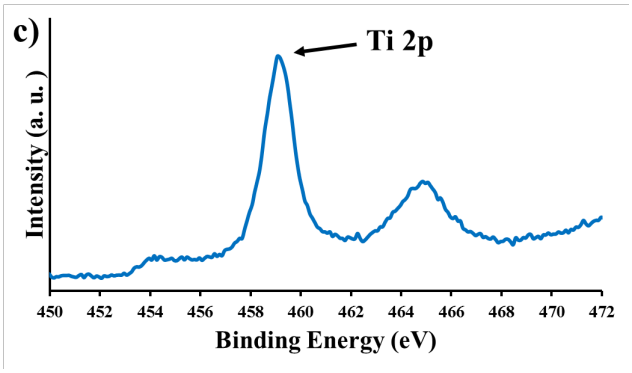

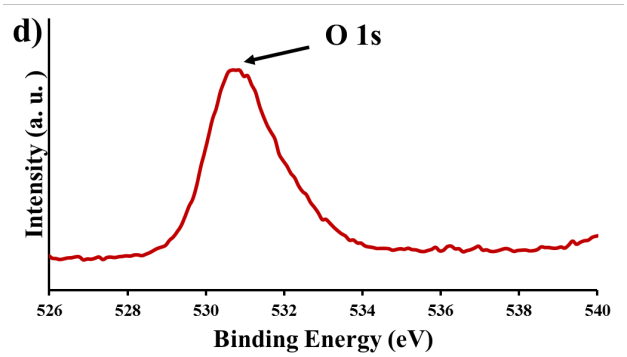

Figure 34 - XPS of the blue TiO2 nanotubes/SnO_2-Sb anode. (a) Sn 3d peak. (b) Sb 3d peak. The weak absorption indicates the aging process leveraged crystallinity. Sb bonded with Sn crystal well. (c) Ti 2p peak. (d) O1s peak.

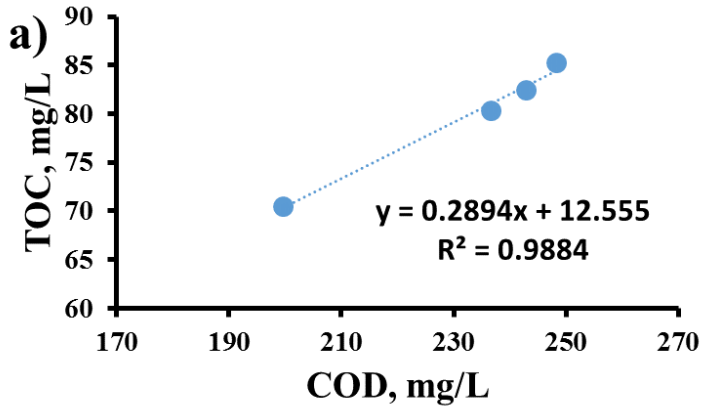

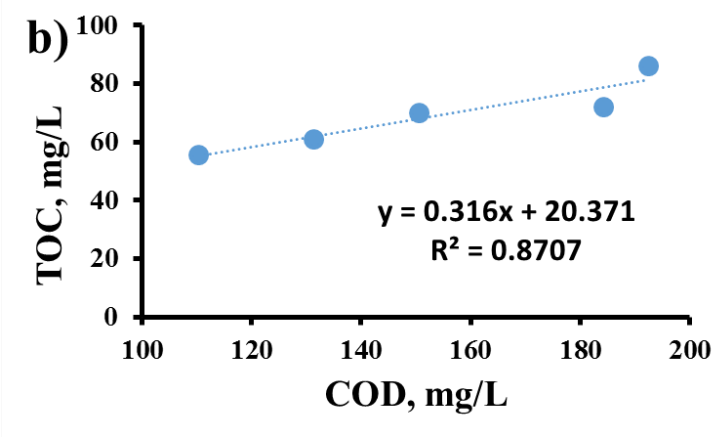

Figure 35 - The TOC vs. COD for benzoic acid degradation. (a) two-dimensional system. (b) three-dimensional system. Current density 30 mA/cm^2, initial concentration 1 mM, experiments carried out in surface water, initial pH value 4.9, temperature 25 ℃, reaction time 4 h, two-dimensional system electrode spacing 1 cm.

Table 10 - Electrochemical oxidation for the degradation of benzoic acid EE/O analysis in EAOPs. Two different initial concentrations in two different water bodies (according to Appendix classification).

Electrolyte Conc.	BA Conc.	Two-Dimensional System	Three-Dimensional System

	Na_2SO_4 mol/L	mg/L	V	mA/cm^2	kWh/m^3	V	mA/cm^2	kWh/m^3
Surface Water	~0.0004 (113µS/cm)	24 (0.2mM)	60	10.5	17.38	15.2	10.5	8.68
Surface Water	0.0004	122 (1mM)	60	10.5	20.03	ND	ND	ND
Industrial Water	0.1 (16210µS/cm)	24	7.3	30.4	1.75	5.3	30.4	2.90
Industrial Water	0.1	122	8	30	2.07	ND	ND	ND

Table 11 - Standard reduction potentials of some reactive oxidant species (ROS) generated from the anode.

Loss Electron Oxidation (LEO)	Oxidation Potential vs. NHE
$\boldsymbol{2H_2O \rightarrow 4H^+ + 4e^- + O_2}$	$E^0 = -1.23\ V$
$\boldsymbol{2H_2O \rightarrow HO_2 \cdot + 3H^+ + 3e^-}$	$E^0 = -1.70\ V$
$\boldsymbol{2H_2O \rightarrow H_2O_2 + 2H^+ + 2e^-}$	$E^0 = -1.77\ V$
$\boldsymbol{2SO_4^{2-} \rightarrow S_2O_8^{2-} + 2e^-}$	$E^0 = -2.01\ V$
$\boldsymbol{H_2O + O_2 \rightarrow O_3 + 2H^+ + 2e^-}$	$E^0 = -2.07\ V$
$\boldsymbol{Cl^- \rightarrow Cl \cdot + e^-}$	$E^0 = -2.43\ V$
$\boldsymbol{SO_4^{2-} \rightarrow SO_4^- \cdot + e^-}$	$E^0 = -2.60\ V$
$\boldsymbol{H_2O \rightarrow HO \cdot + H^+ + e^-}$	$E^0 = -2.74\ V$

REFERENCES

1. Corcoran, Emily, ed. *Sick water?: the central role of wastewater management in sustainable development: a rapid response assessment*. UNEP/Earthprint, 2010.
2. Qu, Xiaolei, Pedro JJ Alvarez, and Qilin Li. "Applications of nanotechnology in water and wastewater treatment." *Water research* 47.12 (2013): 3931-3946.
3. Pruden, Amy. "Balancing water sustainability and public health goals in the face of growing concerns about antibiotic resistance." (2013): 5-14.
4. Ayres, Robert U. "Industrial metabolism." *Technology and environment* 1989 (1989): 23-49.
5. Szejtli, József. "Utilization of cyclodextrins in industrial products and processes." *Journal of Materials Chemistry* 7.4 (1997): 575-587.
6. El Haggar, Salah. *Sustainable industrial design and waste management: cradle-to-cradle for sustainable development*. Academic Press, 2010.
7. Luo, Yunlong, et al. "A review on the occurrence of micropollutants in the aquatic environment and their fate and removal during wastewater treatment." *Science of the Total Environment* 473 (2014): 619-641.
8. Crittenden, John C., et al. *MWH's water treatment: principles and design*. John Wiley & Sons, 2012.
9. Martinez-Huitle, Carlos A., and Sergio Ferro. "Electrochemical oxidation of organic pollutants for the wastewater treatment: direct and indirect processes." *Chemical Society Reviews*35.12 (2006): 1324-1340.
10. Martínez-Huitle, Carlos A., and Enric Brillas. "Decontamination of wastewaters containing synthetic organic dyes by electrochemical methods: a general review." *Applied Catalysis B: Environmental* 87.3-4 (2009): 105-145.
11. Cheng, Min, et al. "Hydroxyl radicals based advanced oxidation processes (AOPs) for remediation of soils contaminated with organic compounds: a review." *Chemical Engineering Journal* 284 (2016): 582-598.
12. Sahni, Mayank, and Bruce R. Locke. "Quantification of hydroxyl radicals produced in aqueous phase pulsed electrical discharge reactors." *Industrial & engineering chemistry research* 45.17 (2006): 5819-5825.
13. Reddy, P. Manoj Kumar, et al. "Degradation and mineralization of methylene blue by dielectric barrier discharge non-thermal plasma reactor." *Chemical Engineering Journal* 217 (2013): 41-47.
14. Pignatello, Joseph J., Esther Oliveros, and Allison MacKay. "Advanced oxidation processes for organic contaminant destruction based on the Fenton reaction and related

chemistry." *Critical reviews in environmental science and technology* 36.1 (2006): 1-84.
15. Pera-Titus, Marc, et al. "Degradation of chlorophenols by means of advanced oxidation processes: a general review." *Applied Catalysis B: Environmental* 47.4 (2004): 219-256.
16. Neyens, E., and J. Baeyens. "A review of classic Fenton's peroxidation as an advanced oxidation technique." *Journal of Hazardous materials* 98.1-3 (2003): 33-50.
17. Radjenovic, Jelena, and David L. Sedlak. "Challenges and opportunities for electrochemical processes as next-generation technologies for the treatment of contaminated water." *Environmental science & technology* 49.19 (2015): 11292-11302.
18. Kerwick, M. I., et al. "Electrochemical disinfection, an environmentally acceptable method of drinking water disinfection?." *Electrochimica Acta* 50.25-26 (2005): 5270-5277.
19. Anipsitakis, George P., Dionysios D. Dionysiou, and Michael A. Gonzalez. "Cobalt-mediated activation of peroxymonosulfate and sulfate radical attack on phenolic compounds. Implications of chloride ions." *Environmental science & technology* 40.3 (2006): 1000-1007.
20. Atkinson, Alan, et al. "Advanced anodes for high-temperature fuel cells." *Materials For Sustainable Energy: A Collection of Peer-Reviewed Research and Review Articles from Nature Publishing Group*. 2011. 213-223.
21. Fernando, Xavier N. *Radio over fiber for wireless communications: from fundamentals to advanced topics*. John Wiley & Sons, 2014.
22. Luttge, Regina. *Microfabrication for industrial applications*. William Andrew, 2011.
23. Lofrano, Giusy, et al. "Chemical and biological treatment technologies for leather tannery chemicals and wastewaters: a review." *Science of the Total Environment* 461 (2013): 265-281.
24. Martinez-Huitle, Carlos A., and Sergio Ferro. "Electrochemical oxidation of organic pollutants for the wastewater treatment: direct and indirect processes." *Chemical Society Reviews*35.12 (2006): 1324-1340.
25. Wuana, Raymond A., and Felix E. Okieimen. "Heavy metals in contaminated soils: a review of sources, chemistry, risks and best available strategies for remediation." *Isrn Ecology* 2011 (2011).
26. Martinez-Huitle, Carlos A., and Sergio Ferro. "Electrochemical oxidation of organic pollutants for the wastewater treatment: direct and indirect processes." *Chemical Society Reviews*35.12 (2006): 1324-1340.
27. Chen, Guohua. "Electrochemical technologies in wastewater treatment." *Separation and purification Technology* 38.1 (2004): 11-41.

28. Zhang, Jiujun, ed. *PEM fuel cell electrocatalysts and catalyst layers: fundamentals and applications*. Springer Science & Business Media, 2008.
29. Plechkova, Natalia V., and Kenneth R. Seddon. "Applications of ionic liquids in the chemical industry." *Chemical Society Reviews* 37.1 (2008): 123-150.
30. Vogel, Steven. *Cats' paws and catapults: Mechanical worlds of nature and people*. WW Norton & Company, 2000.
31. Weinberg, N. L., and H. R. Weinberg. "Electrochemical oxidation of organic compounds." *Chemical Reviews* 68.4 (1968): 449-523.
32. Bockris, John O'M., and Shahad UM Khan. *Surface electrochemistry: a molecular level approach*. Springer Science & Business Media, 2013.
33. Moreira, Francisca C., et al. "Electrochemical advanced oxidation processes: a review on their application to synthetic and real wastewaters." *Applied Catalysis B: Environmental*202 (2017): 217-261.
34. Martínez-Huitle, Carlos A., et al. "Single and coupled electrochemical processes and reactors for the abatement of organic water pollutants: a critical review." *Chemical reviews*115.24 (2015): 13362-13407.
35. Sirés, Ignasi, et al. "Electrochemical advanced oxidation processes: today and tomorrow. A review." *Environmental Science and Pollution Research* 21.14 (2014): 8336-8367.
36. Kapałka, Agnieszka, György Fóti, and Christos Comninellis. "Kinetic modelling of the electrochemical mineralization of organic pollutants for wastewater treatment." *Journal of Applied Electrochemistry* 38.1 (2008): 7-16.
37. Oturan, Mehmet A., and Jean-Jacques Aaron. "Advanced oxidation processes in water/wastewater treatment: principles and applications. A review." *Critical Reviews in Environmental Science and Technology* 44.23 (2014): 2577-2641.
38. Daneshvar, Nezamaddin, Darioush Salari, and A. R. Khataee. "Photocatalytic degradation of azo dye acid red 14 in water on ZnO as an alternative catalyst to TiO2." *Journal of photochemistry and photobiology A: chemistry* 162.2-3 (2004): 317-322.
39. Pignatello, Joseph J., Esther Oliveros, and Allison MacKay. "Advanced oxidation processes for organic contaminant destruction based on the Fenton reaction and related chemistry." *Critical reviews in environmental science and technology* 36.1 (2006): 1-84.
40. Malato, Sixto, et al. "Decontamination and disinfection of water by solar photocatalysis: recent overview and trends." *Catalysis Today* 147.1 (2009): 1-59.
41. Sirés, Ignasi, et al. "Electrochemical advanced oxidation processes: today and tomorrow. A review." *Environmental Science and Pollution Research* 21.14 (2014): 8336-8367.

42. Comninellis, Christos, et al. "Advanced oxidation processes for water treatment: advances and trends for R&D." *Journal of Chemical Technology & Biotechnology: International Research in Process, Environmental & Clean Technology* 83.6 (2008): 769-776.
43. Sopaj, Flamur, et al. "Influence of the anode materials on the electrochemical oxidation efficiency. Application to oxidative degradation of the pharmaceutical amoxicillin." *Chemical Engineering Journal* 262 (2015): 286-294.
44. Martínez-Huitle, Carlos A., et al. "Single and coupled electrochemical processes and reactors for the abatement of organic water pollutants: a critical review." *Chemical reviews*115.24 (2015): 13362-13407.
45. Meyer, Jens, et al. "Transition metal oxides for organic electronics: energetics, device physics and applications." *Advanced Materials* 24.40 (2012): 5408-5427.
46. Panizza, Marco, and Giacomo Cerisola. "Influence of anode material on the electrochemical oxidation of 2-naphthol: Part 1. Cyclic voltammetry and potential step experiments." *Electrochimica Acta* 48.23 (2003): 3491-3497.
47. Hayfield, P. C. S. *Development of a New Material: Monolithic Ti4O7 Ebonex Ceramic*. Royal Society of Chemistry, 2007.
48. Senevirathne, Keerthi, et al. "Electrocatalytic activity and durability of Pt/NbO2 and Pt/Ti4O7 nanofibers for PEM fuel cell oxygen reduction reaction." *Electrochimica Acta* 59 (2012): 538-547.
49. Brownson, Dale AC, Dimitrios K. Kampouris, and Craig E. Banks. "An overview of graphene in energy production and storage applications." *Journal of Power Sources* 196.11 (2011): 4873-4885.
50. Panizza, Marco, and Giacomo Cerisola. "Direct and mediated anodic oxidation of organic pollutants." *Chemical reviews*109.12 (2009): 6541-6569.
51. Iizuka, Kosuke, et al. "Photocatalytic reduction of carbon dioxide over Ag cocatalyst-loaded ALa4Ti4O15 (A= Ca, Sr, and Ba) using water as a reducing reagent." *Journal of the American Chemical Society* 133.51 (2011): 20863-20868.
52. Wuana, Raymond A., and Felix E. Okieimen. "Heavy metals in contaminated soils: a review of sources, chemistry, risks and best available strategies for remediation." *Isrn Ecology* 2011 (2011).
53. Marrone, Philip A., and Glenn T. Hong. "Corrosion control methods in supercritical water oxidation and gasification processes." *The Journal of Supercritical Fluids* 51.2 (2009): 83-103.
54. Pearton, S. J., et al. "Wide band gap ferromagnetic semiconductors and oxides." *Journal of Applied Physics* 93.1 (2003): 1-13.
55. Bonaccorso, Francesco, et al. "Graphene photonics and optoelectronics." *Nature photonics* 4.9 (2010): 611.

56. Manifacier, J. C., et al. "Optical and electrical properties of SnO2 thin films in relation to their stoichiometric deviation and their crystalline structure." *Thin Solid Films* 41.2 (1977): 127-135.
57. Kötz, R., S. Stucki, and B. Carcer. "Electrochemical waste water treatment using high overvoltage anodes. Part I: Physical and electrochemical properties of SnO 2 anodes." *Journal of applied electrochemistry* 21.1 (1991): 14-20.
58. Lipp, L., and D. Pletcher. "The preparation and characterization of tin dioxide coated titanium electrodes." *Electrochimica Acta* 42.7 (1997): 1091-1099.
59. Bagastyo, Arseto Y., et al. "Electrochemical oxidation of electrodialysed reverse osmosis concentrate on Ti/Pt–IrO2, Ti/SnO2–Sb and boron-doped diamond electrodes." *Water research* 47.1 (2013): 242-250.
60. Quintana, Maria, et al. "Comparison of dye-sensitized ZnO and TiO2 solar cells: studies of charge transport and carrier lifetime." *The Journal of Physical Chemistry C* 111.2 (2007): 1035-1041.
61. Mor, Gopal K., et al. "A review on highly ordered, vertically oriented TiO2 nanotube arrays: Fabrication, material properties, and solar energy applications." *Solar Energy Materials and Solar Cells* 90.14 (2006): 2011-2075.
62. Smith, J. R., F. C. Walsh, and R. L. Clarke. "Electrodes based on Magnéli phase titanium oxides: the properties and applications of Ebonex® materials." *Journal of applied electrochemistry* 28.10 (1998): 1021-1033.
63. Troster, I., L. Schafer, and Matthias Fryda. "Recent developments in production and application of DiaChem-electrodes for wastewater treatment." *New Diam. Front. C. Tec* 12.2 (2002): 89-97.
64. Swain, Greg M., Alfred B. Anderson, and John C. Angus. "Applications of diamond thin films in electrochemistry." *Mrs Bulletin* 23.9 (1998): 56-60.
65. Mraz, R., and J. Krýsa. "Long service life IrO 2/Ta 2 O 5 electrodes for electroflotation." *Journal of Applied Electrochemistry* 24.12 (1994): 1262-1266.
66. Yeo, In-Hyeong, and Dennis C. Johnson. "Electrocatalysis of Anodic Oxygen-Transfer Reactions Effect of Groups III A and VA Metal Oxides in Electrodeposited β-Lead Dioxide Electrodes in Acidic Media." *Journal of the Electrochemical Society* 134.8 (1987): 1973-1977.
67. Correa-Lozano, B., Ch Comninellis, and A. De Battisti. "Preparation of SnO 2-Sb 2 O 5 films by the spray pyrolysis technique." *Journal of Applied Electrochemistry* 26.1 (1996): 83-89.
68. Weres, Oleh, and Michael R. Hoffmann. "Electrode, electrode manufacturing process and electrochemical cell." U.S. Patent No. 5,419,824. 30 May 1995.
69. Martin, Heidi B., et al. "Hydrogen and oxygen evolution on boron-doped diamond electrodes." *Journal of the Electrochemical Society* 143.6 (1996): L133-L136.

70. Chen, Xueming, et al. "High-performance Ti/BDD electrodes for pollutant oxidation." *Environmental science & technology*37.21 (2003): 5021-5026.
71. Cussler, Edward Lansing. *Diffusion: mass transfer in fluid systems*. Cambridge university press, 2009.
72. Xiong, Y. A., et al. "Treatment of dye wastewater containing acid orange II using a cell with three-phase three-dimensional electrode." *Water research* 35.17 (2001): 4226-4230.
73. Normann, Richard A., Patrick K. Campbell, and Kelly E. Jones. "Three-di
74. Zhao, Hua-Zhang, et al. "Removal of Acid Orange 7 in simulated wastewater using a three-dimensional electrode reactor: Removal mechanisms and dye degradation pathway." *Chemosphere* 78.1 (2010): 46-51.
75. Baker, Bernard S., and Hossein G. Ghezel-Ayagh. "Fuel cell system." U.S. Patent No. 4,532,192. 30 Jul. 1985.
76. T. Lin, S. Yu, W. Chen, Occurrence, removal and risk assessment of pharmaceutical and personal care products (PPCPs) in an advanced drinking water treatment plant (ADWTP) around Taihu Lake in China, Chemosphere 152 (2016) 1-9.
77. J. Roberts, A. Kumar, J. Du, C. Hepplewhite, D.J. Ellis, A.G. Christy, S.G. Beavis, Pharmaceuticals and personal care products (PPCPs) in Australia's largest inland sewage treatment plant, and its contribution to a major Australian river during high and low flow, Sci. Total Environ. 541 (2016) 1625-1637.
78. C.I. Kosma, D.A. Lambropoulou, T.A. Albanis, Investigation of PPCPs in wastewater treatment plants in Greece: occurrence, removal and environmental risk assessment, Sci. Total Environ. 466-467 (2014) 421-438.
79. C. Liu, V. Nanaboina, G. Korshin, Spectroscopic study of the degradation of antibiotics and the generation of representative EfOM oxidation products in ozonated wastewater, Chemosphere (2011).
80. B. Pan, P. Wang, M. Wu, J. Li, D. Zhang, D. Xiao, Sorption kinetics of ofloxacin in soils and mineral particles, Environ. Pollut. 171 (2012) 185-190.
81. J. Radjenovic, M. Petrovic, D. Barcelo, Fate and distribution of pharmaceuticals in wastewater and sewage sludge of the conventional activated sludge (CAS) and advanced membrane bioreactor (MBR) treatment, Water Res. 43 (2009) 831-841.
82. K.H. Wammer, A.R. Korte, R.A. Lundeen, J.E. Sundberg, K. McNeill, W.A. Arnold, Direct photochemistry of three fluoroquinolone antibacterials: norfloxacin, ofloxacin, and enrofloxacin, Water Res. 47 (2013) 439-448.
83. E.M. Van Wieren, M.D. Seymour, J.W. Peterson, Interaction of the fluoroquinolone antibiotic, ofloxacin, with titanium oxide nanoparticles in water: adsorption and breakdown, Sci. Total Environ. 441 (2012) 1-9.

84. A. Dirany, I. Sires, N. Oturan, A. Ozcan, M.A. Oturan, Electrochemical treatment of the antibiotic sulfachloropyridazine: kinetics, reaction pathways, and toxicity evolution, Environ. Sci. Technol. 46 (2012) 4074-4082.
85. M. Chen, W. Chu, Photocatalytic degradation and decomposition mechanism of fluoroquinolones norfloxacin over bismuth tungstate: Experiment and mathematic model, Appl. Catal. B:Environ. 168-169 (2015) 175-182.
86. T.S. Chen, K.L. Huang, J.L. Chen, An electrochemical approach to simultaneous determination of acetaminophen and ofloxacin, Bull. Environ. Contam. Toxicol. 89 (2012) 1284-1288.
87. M. Imamura, S. Shibamura, I. Hayakawa, Y. Osada, Inhibition of DNA gyrase by optically active ofloxacin, Antimicrob. Agents Chemother. 31 (1987) 325-327.
88. C. Carlesi Jara, D. Fino, V. Specchia, G. Saracco, P. Spinelli, Electrochemical removal of antibiotics from wastewaters, Appl. Catal. B:Environ. 70 (2007) 479-487.
89. C. Borras, C. Berzoy, J. Mostany, J.C. Herrera, B.R. Scharifker, A comparison of the electrooxidation kinetics of p-methoxyphenol and p-nitrophenol on Sb-doped SnO_2 surfaces: Concentration and temperature effects, Appl. Catal. B:Environ. 72 (2007) 98-104.
90. X. Guo, D. Minakata, J. Crittenden, Computer-based first-principles kinetic Monte Carlo simulation of polyethylene glycol degradation in aqueous phase UV/H_2O_2 advanced oxidation process, Environ. Sci. Technol. 48 (2014) 10813-10820.
91. X. Guo, D. Minakata, J. Crittenden, On-the-Fly Kinetic Monte Carlo Simulation of Aqueous Phase Advanced Oxidation Processes, Environ. Sci. Technol. 49 (2015) 9230-9236.
92. X. Guo, D. Minakata, J. Niu, J. Crittenden, Computer-based first-principles kinetic modeling of degradation pathways and byproduct fates in aqueous-phase advanced oxidation processes, Environ. Sci. Technol. 48 (2014) 5718-5725.
93. I. Michael, E. Hapeshi, C. Michael, D. Fatta-Kassinos, Solar Fenton and solar TiO_2 catalytic treatment of ofloxacin in secondary treated effluents: evaluation of operational and kinetic parameters, Water Res. 44 (2010) 5450-5462.
94. E. Hapeshi, A. Achilleos, M.I. Vasquez, C. Michael, N.P. Xekoukoulotakis, D. Mantzavinos, D. Kassinos, Drugs degrading photocatalytically: Kinetics and mechanisms of ofloxacin and atenolol removal on titania suspensions, Water Res. 44 (2010) 1737-1746.
95. G. Márquez, E.M. Rodríguez, F.J. Beltrán, P.M. Álvarez, Determination of Rate Constants for Ozonation of Ofloxacin in Aqueous Solution, Ozone: Sci. Eng. 35 (2013) 186-195.
96. E. Brillas, I. Sires, M.A. Oturan, Electro-Fenton process and related electrochemical technologies based on Fenton's reaction chemistry, Chem. Rev. 109 (2009) 6570-6631.

97. G. Zhao, S. Shen, M. Li, M. Wu, T. Cao, D. Li, The mechanism and kinetics of ultrasound-enhanced electrochemical oxidation of phenol on boron-doped diamond and Pt electrodes, Chemosphere 73 (2008) 1407-1413.
98. I.D. Santos, M. Dezotti, A.J.B. Dutra, Electrochemical treatment of effluents from petroleum industry using a Ti/RuO_2 anode, Chem. Eng. J. 226 (2013) 293-299.
99. G.S. Cordeiro, R.S. Rocha, R.B. Valim, F.L. Migliorini, M.R. Baldan, M.R.V. Lanza, N.G. Ferreira, Degradation of profenofos in an electrochemical flow reactor using boron-doped diamond anodes, Diamond Relat. Mater. 32 (2013) 54-60.
100. L. Vazquez-Gomez, A. de Battisti, S. Ferro, M. Cerro, S. Reyna, C.A. Martínez-Huitle, M.A. Quiroz, Anodic Oxidation as Green Alternative for Removing Diethyl Phthalate from Wastewater Using Pb/PbO_2 and Ti/SnO_2 Anodes, CLEAN - Soil, Air, Water 40 (2012) 408-415.
101. A. Mukimin, K. Wijaya, A. Kuncaka, Oxidation of remazolbrilliant bluer (RB.19) with in situ electro-generated active chlorine using Ti/PbO_2 electrode, Sep. Purif. Technol. 95 (2012) 1-9.
102. H. Lin, J. Niu, J. Xu, Y. Li, Y. Pan, Electrochemical mineralization of sulfamethoxazole by Ti/SnO_2-Sb/Ce-PbO_2 anode: Kinetics, reaction pathways, and energy cost evolution, Electrochim. Acta 97 (2013) 167-174.
103. G. Zhao, J. Gao, S. Shen, M. Liu, D. Li, M. Wu, Y. Lei, Ultrasound enhanced electrochemical oxidation of phenol and phthalic acid on boron-doped diamond electrode, J. Hazard. Mater. 172 (2009) 1076-1081.
104. D. Lawless, N. Serpone, D. Meisel, Role of hydroxyl radicals and trapped holes in photocatalysis. A pulse radiolysis study, J. Phys. Chem. 95 (1991) 5166-5170.
105. Q. Xiao, Z. Si, J. Zhang, C. Xiao, X. Tan, Photoinduced hydroxyl radical and photocatalytic activity of samarium-doped TiO(2) nanocrystalline, J. Hazard. Mater. 150 (2008) 62-67.
106. G.V. Buxton, C.L. Greenstock, W.P. Helman, A.B. Ross, W. Tsang, Critical Review of rate constants for reactions of hydrated electronsChemical Kinetic Data Base for Combustion Chemistry. Part 3: Propane, J. Phys. Chem. Ref. Data 17 (1988) 513.
107. J.M. Peralta-Hernández, C. de la Rosa-Juárez, V. Buzo-Muñoz, J. Paramo-Vargas, P. Cañizares-Cañizares, M.A. Rodrigo-Rodrigo, Synergism between anodic oxidation with diamond anodes and heterogeneous catalytic photolysis for the treatment of pharmaceutical pollutants, Sustain. Environ. Res. (2016).
108. F. Beck, W. Kaiser, H. Krohn, Boron doped diamond (BDD)-layers on titanium substrates as electrodes in applied electrochemistry, Electrochim. Acta 45 (2000) 4691-4695.
109. H. An, Q. Li, D. Tao, H. Cui, X. Xu, L. Ding, L. Sun, J. Zhai, The synthesis and characterization of Ti/SnO_2–Sb_2O_3/PbO_2 electrodes: The influence of morphology

caused by different electrochemical deposition time, Appl. Surf. Sci. 258 (2011) 218-224.

110. S. Song, J. Fan, Z. He, L. Zhan, Z. Liu, J. Chen, X. Xu, Electrochemical degradation of azo dye C.I. Reactive Red 195 by anodic oxidation on Ti/SnO_2–Sb/PbO_2 electrodes, Electrochim. Acta 55 (2010) 3606-3613.

111. M.M. Halmann, Photodegradation of Water Pollutants, CRC Press, Baca Raton, New York, 1996, pp. 285.

112. C. Zhong, K. Wei, W. Han, L. Wang, X. Sun, J. Li, Electrochemical degradation of tricyclazole in aqueous solution using Ti/SnO_2–Sb/PbO_2 anode, J. Electroanal. Chem. 705 (2013) 68-74.

113. Y. Chen, J.C. Crittenden, S. Hackney, L. Sutter, D.W. Hand, Preparation of a Novel TiO_2-Based p−n Junction Nanotube Photocatalyst, Environ. Sci. Technol. 39 (2005) 1201-1208.

114. S. Herna´ndez, D. Hidalgo, A. Sacco, A. Chiodoni, A. Lamberti, V. Cauda, E. Tressoa, G. Saracco, Comparison of photocatalytic and transport properties of TiO_2 and ZnO nanostructures for solar-driven water splitting Phys. Chem. Chem. Phys. 17 (2015) 7775-7786.

115. C.G. Zoski, Handbook of Electrochemistry, Elsevier, Amsterdam,Boston, 2007, pp. 11-13.

116. A.A. Sonin, M.S. Isaacson, Optimization of Flow Design in Forced Flow Electrochemical Systems, with Special Application to Electrodialysis, Ind. Eng. Chem. Process Des. Dev. 13 (1974) 241-248.

117. W. Djoudi, F. Aissani-Benissad, P. Ozil, Flow modeling in electrochemical tubular reactor containing volumetric electrode: Application to copper cementation reaction, Chem. Eng. Res. Des. 90 (2012) 1582-1589.

118. U.M. López-García, P.E. Hidalgo, J.C. Olvera, F. Castañeda, H. Ruiz, G. Orozco, The hydrodynamic behavior of a parallel-plate electrochemical reactor, Fuel 110 (2013) 162-170.

119. J.Y. Choi, Y.J. Lee, J. Shin, J.W. Yang, Anodic oxidation of 1,4-dioxane on boron-doped diamond electrodes for wastewater treatment, J. Hazard. Mater. 179 (2010) 762-768.

120. L. Ciríaco, C. Anjo, J. Correia, M.J. Pacheco, A. Lopes, Electrochemical degradation of Ibuprofen on Ti/Pt/PbO_2 and Si/BDD electrodes, Electrochim. Acta 54 (2009) 1464-1472.

121. A.J. Bard, R. Parsons, J. Jordan, Standard potentials in aqueous solution, CRC press, New York, 1985.

122. W.H. Koppenol, J.F. Liebman, The oxidizing nature of the hydroxyl radical. A comparison with the ferryl ion (FeO^{2+}), J. Phys. Chem. 88 (1984) 99-101.

123. M.J. Pacheco, A. Morão, A. Lopes, L. Ciríaco, I. Gonçalves, Degradation of phenols using boron-doped diamond electrodes: A method for quantifying the extent of combustion, Electrochim. Acta 53 (2007) 629-636.
124. M. Panizza, G. Cerisola, Direct and mediated anodic oxidation of organic pollutants, Chem. Rev. 109 (2009) 6541-6569.
125. T. Raju, C.A. Basha, Electrochemical cell design and development for mediated electrochemical oxidation-Ce(III)/Ce(IV)system, Chem. Eng. J. 114 (2005) 55-65.
126. J. Cao, H. Zhao, F. Cao, J. Zhang, C. Cao, Electrocatalytic degradation of 4-chlorophenol on F-doped PbO_2 anodes, Electrochim. Acta 54 (2009) 2595-2602.
127. J. Radjenovic, D.L. Sedlak, Challenges and Opportunities for Electrochemical Processes as Next-Generation Technologies for the Treatment of Contaminated Water, Environ. Sci. Technol. 49 (2015) 11292-11302.
128. A. Anglada, A.M. Urtiaga, I. Ortiz, Laboratory and pilot plant scale study on the electrochemical oxidation of landfill leachate, J. Hazard. Mater. 181 (2010) 729-735.
129. X. Zhu, J. Ni, J. Wei, X. Xing, H. Li, Y. Jiang, Scale-up of BDD anode system for electrochemical oxidation of phenol simulated wastewater in continuous mode, J. Hazard. Mater 184 (2010) 493-498.
130. I. Michael, E. Hapeshi, J. Acena, S. Perez, M. Petrovic, A. Zapata, D. Barcelo, S. Malato, D. Fatta-Kassinos, Light-induced catalytic transformation of ofloxacin by solar Fenton in various water matrices at a pilot plant: mineralization and characterization of major intermediate products, Sci. Total Environ. 461-462 (2013) 39-48.
131. John C. Crittenden, R. Rhodes Trussell, David W. Hand, Kerry J. Howe, G. Tchobanoglous, MWH's Water Treatment: Principles and Design, 3rd Ed., John Wiley &Sons, Inc., Hoboken, New Jersey, 2012.
132. I. Peternel, H. Kusic, V. Marin, N. Koprivanac, UV-assisted persulfate oxidation: the influence of cation type in the persulfate salt on the degradation kinetics of an azo dye pollutant, React. Kinet. Mech. Cat. 108 (2012) 17-39.
133. T.N. Das, Reactivity and Role of $SO_5^{\bullet-}$Radical in Aqueous Medium Chain Oxidation of Sulfite to Sulfate and Atmospheric Sulfuric Acid Generation, J. Phys. Chem. A 105 (2001) 9142-9155.
134. R.F.P. Ain A. Sonin, A hydrodynamic theory of desalination by electrodialysis, Desalination 5 (1968) 293-329.
135. A.A.S. Gershon Grossman, Experimental study of the effects of hydrodynamics and membrane fouling in electrodialysis, Desalination 10 (1972) 157-180.
136. H.S. Fogler, Elements of chemical reaction engineering, 2nd Ed., Prentice-HallInternational,Inc.,NewJersey, 1992.
137. Shao, Zongping, et al. "A thermally self-sustained micro solid-oxide fuel-cell stack with high power density." *Nature* 435.7043 (2005): 795.

138. Lu, Wen, et al. "Use of ionic liquids for π-conjugated polymer electrochemical devices." *Science* 297.5583 (2002): 983-987.
139. Atkinson, Alan, et al. "Advanced anodes for high-temperature fuel cells." *Materials For Sustainable Energy: A Collection of Peer-Reviewed Research and Review Articles from Nature Publishing Group*. 2011. 213-223.
140. Strathmann, Heiner. "Electrodialysis, a mature technology with a multitude of new applications." *Desalination* 264.3 (2010): 268-288.
141. Anglada, Angela, Ane Urtiaga, and Inmaculada Ortiz. "Contributions of electrochemical oxidation to waste-water treatment: fundamentals and review of applications." *Journal of Chemical Technology & Biotechnology* 84.12 (2009): 1747-1755.
142. Elimelech, Menachem, and William A. Phillip. "The future of seawater desalination: energy, technology, and the environment." *science* 333.6043 (2011): 712-717.
143. Klavarioti, Maria, Dionissios Mantzavinos, and Despo Kassinos. "Removal of residual pharmaceuticals from aqueous systems by advanced oxidation processes." *Environment international* 35.2 (2009): 402-417.
144. Dirany, Ahmad, et al. "Electrochemical treatment of the antibiotic sulfachloropyridazine: kinetics, reaction pathways, and toxicity evolution." *Environmental science & technology*46.7 (2012): 4074-4082.
145. Bedner, Mary, and William A. MacCrehan. "Transformation of acetaminophen by chlorination produces the toxicants 1, 4-benzoquinone and N-acetyl-p-benzoquinone imine." *Environmental science & technology* 40.2 (2006): 516-522.
146. Cheng, Shaoan, Hong Liu, and Bruce E. Logan. "Increased power generation in a continuous flow MFC with advective flow through the porous anode and reduced electrode spacing." *Environmental science & technology* 40.7 (2006): 2426-2432.
147. Armand, Michel, and J-M. Tarascon. "Building better batteries." *nature* 451.7179 (2008): 652.
148. Peck, Robert L. "Ionic semiconductor materials and applications thereof." U.S. Patent No. 5,055,171. 8 Oct. 1991.
149. Inzelt, G., et al. "Electron and proton conducting polymers: recent developments and prospects." *Electrochimica Acta*45.15-16 (2000): 2403-2421.
150. Comninellis, Christos. "Electrocatalysis in the electrochemical conversion/combustion of organic pollutants for waste water treatment." *Electrochimica Acta* 39.11-12 (1994): 1857-1862.
151. Panizza, M., and Gr Cerisola. "Application of diamond electrodes to electrochemical processes." *Electrochimica Acta*51.2 (2005): 191-199.
152. Acero, J. L., Rodriguez, E., Meriluoto, J. 2005. Kinetics of reactions between chlorine and the cyanobacterial toxins microcystins. Water Res. 39, 1628-1638.

153. Al-Hamaiedeh, D. H. 2013. Electrochemical-active chlorine generation by circulating the electrolyte through an electrolytic Cell. Environ. Eng. Sci. 30, 82-88.
154. Bader, H., Sturzenegger, V., Hoigne, J. 1988. Photometric method for the determination of low concentrations of hydrogen peroxide by the peroxidase catalyzed oxidation of N, N-,diethyl-P-phenylenedia- mine (DPD). Water Res. 22, 1109-1115.
155. Bergmann, M.E. H., Rollin, J. 2007. Product and by-product formation in laboratory studies on disinfection electrolysis of water using boron-doped diamond anodes. Catal. Today. 124, 198–203.
156. Burrini, D., Lupi, E., Klotzner, C., Santine, C., Lanciotti, E. 2000. Survey of microalgae and cyanobacteria in a drinking –water utility supplying the city of Florence, Italy. J. Water Supply: Res. T. 49, 139-147.
157. Buxton, G., Greenstock, C., Helman, P., Ross, A. 1988. Critical review of rate constants for reactions of hydrated electrons, hydrogen atoms and hydroxyl radicals ($OH•/O•^-$) in Aqueous Solution. J. Phys. Chem. Ref. Data 17, 513-518.
158. Chen, C., Yang, Z., Kong, F.X., Zhang, M., Yu, Y., Shi, X.L. 2016. Growth, physiochemical and antioxidant responses of overwintering benthic cyanobacteria to hydrogen peroxide. Environ. Pollut. 219, 649-655.
159. Drabkova, M., Admiraal, W., Marsalek, B. 2007. Combined exposure to hydrogen peroxide and light selective effects on cyanobacteria, green algae, and diatoms. Environ. Sci. Technol. 41, 309-314.
160. Duan, F., Li, Y. P., Cao, H.B., Wang, Y. Crittenden, J., Zhang, Y. 2015. Activated carbon electrodes: Electrochemical oxidation coupled with desalination for wastewater treatment. Chemosphere 125, 205-211.
161. Feng, C., Sugiura, N., Shimada, S., Maekawa, T. 2003. Development of a high performance electrochemical wastewater treatment system. J. Hazard. Mater. 103 (1-2), 65-78.
162. Fuente, A. de la, Bing, N., Hoeschele, I., Mendes P. 2004. Discovery of meaningful associations in genomic data using partial correlation coefficients. Bioinformatics 20, 3565-3574.
163. Gao, S.S., Du, M.A, Tian, J.Y., Yang, J.Y., Yang, J.X., Ma, F., Nan, J. 2010. Effects of chloride ions on electro-coagulation-flotation process with aluminum electrodes for algae removal. J. Hazard. Mater. 182, 827-834.
164. Ghernaout D., Ghernaout B. 2010. From chemical disinfection to electrodisinfection: the obligatory itinerary? Desalin Water Treat. 16, 156–175.
165. Huang, H.M., Xiao, X., Lin, F., Grossart, H.P., Nie., Z.Y., Sun, L.J., Xu, C., Shi, J.Y. 2016. Continuous-release beads of natural allele chemicals for the long-term control of cyanobacterial growth: Preparation, release dynamics and inhibitory effects. Water Res. 95, 113-123.

166. Huo, X.C., Chang, D.W., Tseng, J.H., Burch, M., Lin, T.F. 2015. Exposure of *microcystis aeruginosa* to hydrogen peroxide under light: kinetic modeling of cell rupture and simultaneous microcystin degradation. Environ. Sci. Technol. 49, 5502-5510.
167. Jeong, J., Kim, C., Yoon, J. 2009. The effect of electrode material on the generation of oxidants and microbial inactivation in the electrochemical disinfection processes. Water Res. 43, 895-901.
168. Kramer, D.M., Johnson, G., Kiirats, O., Edwards, G.E. 2004. New fluorescence parameters for the determination of QA redox state and excitation energy fluxes. Photosynth Res. 79, 209-218.
169. Li, H., Zhu, X., Ni, J. 2010. Inactivation of Escherichia coli in Na_2SO_4 electrolyte using boron-doped diamond anode. Electrochim. Acta. 56(1): 448-453.
170. Li, L., Shao, C., Lin, T.F., Shen, J.Y., Yu, S.L., Shang, R., Yin, D.Q., Zhang, K.J., Gao, N.Y. 2014. Kinetics of cell inactivation, toxin release, and degradation during permanganation of*Microcystis aeruginosa*. Environ. Sci. Technol. 48, 2885-2892.
171. Li, Y., Li, C., Zheng, Y., Wu, G., Wuyun, T, Xu, H., He, X., Jiang, G. 2011. Cadmium pollution enhanced ozone damage to winter wheat: biochemical and physiological evidences. J. Environ.Sci. 23, 255-265.
172. Liang, W.Y., Qu, J.H., Chen, L.B., Liu, H.J., Lei, P.J. 2005. Inactivation of *Microcystis aeruginosa* by continuous electrochemical cycling process in tube using Ti/RuO_2 electrodes. Environ. Sci. Technol. 39, 4633-4639.
173. Lin, L., Feng, C., Li, Q.Y., Wu, M., Zhao, L.Y. 2015. Effects of electrolysis by low-amperage electric current on the chlorophyll fluorescence characteristics of *Microcystis aeruginosa*. Environ. Sci. Pollut. R. 22, 14932-14939.
174. Liu, C., Xie, X., Zhao, W., Liu, N., Maraccine, A. P., Sassoubre, M. L., Boehm, B. A., Cui, Y. 2013. Conducting nanosponge electroporation for affordable and high-efficiency disinfection of bacteria and viruses in water. Nano Let. 13(9), 4288-4293.
175. Martinez-Huitle, C. A., Ferro, S. 2006. Electrochemical oxidation of organic pollutants for the wastewater treatment: direct and indirect processes. Chem. Soc. Rev. 35, 1324-1340.
176. Mascia, M., Monasterio, S., Vacca, A., Palmas, S. 2016. Electrochemical treatment of water containing *Microcystis aeruginosa* in a fixed bed reactor with three-dimensional conductive diamond anodes. J Hazard. Mater. 319: 111-120.
177. Mascia, M., Vacca, A., Palmas, S. 2013. Electrochemical treatment as a pre-oxidative step for algae removal using Chlorella vulgaris as a model organism and BDD anodes. Chem. Eng. J. 219, 512-519.
178. Nanayakkara, K.G.N., Zheng, Y.M., Alam, A.K.M.K., Zou, S., Chen, J.P. 2011. Electrochemical disinfection for ballast water management: Technology development and risk assessment. Mar. Pollut. Bull. 63, 119-123.

179. Paerl, H.W., Huisman, J. 2008. Blooms like it hot. Science 320, 57-58.
180. Paerl, H.W., Xu, H., McCarthy, M. J., Zhu, G.W., Qin, B.Q., Li, Y.P., Gardner, W.S. 2011. Controlling harmful cyanobacterial blooms in a hyper-eutrophic lake (Lake Taihu, China): The need for a dual nutrient (N & P) management strategy. Water Res. 45, 1973-1983.
181. Pliquett, U., Joshi, R.P., Sridhara, V., Schoenbach, K.H., 2007. High electrical field effects on cell membranes. Bioelectrochem. 70, 275-282.
182. Qi, J., Lan, H.C., Liu, R.P., Miao, S.Y., Liu, H.J., Qu, J.H. 2016. Prechlorination of algae-laden water: The effects of transportation time on cell integrity, algal organic matter release, and chlorinated disinfection byproduct formation. Water Res. 102 (1), 221-2128.
183. Qin, B.Q., Zhu, G.W., Gao, G., Zhang, Y.L., Li, W., Paerl., H.W., Carmichael W.W. 2010. A drinking water crisis in Lake Taihu, China: Linkage to climatic variability and lake management. Environ. Manage. 45, 105-112.
184. Saetae, P., Bunthawin, S., Ritchie, R. 2014. Environmental persistence of chlorine from prawn farm discharge monitored by measuring the light reactions of photosynthesis of phytoplankton. Aquac. Int. 22(2), 321-338.
185. Sarkka, H., Vepsalainen, M., Pulliainen, M., Sillanpaa, M. 2008. Electrochemical inactivation of paper mill bacteria with mixed metal oxide electrode. J. Hazard. Mater. 156, 208-213.
186. Shen, Q.H., Zhu, J.W., Cheng, L.H., Zhang, J.H., Zhang, Z., Xu, X.H. 2011. Enhanced algae removal by drinking water treatment of chlorination coupled with coagulation. Desalination 271, 236-240.
187. Shi, K., Zhang, Y., Xu, H., Zhu, G., Qin, B., Huang, C., Liu, X., Zhou, Y., Heng, L. 2015. Long-term satellite observations of microcystin concentrations in Lake Taihu during cyanobacterial bloom periods. Environ. Sci. Technol. 45, 6448-6456.
188. Vacca, A., Mascia, M., Palmas, S., Pozzo, A. Da, 2011. Electrochemical treatment of water containing chlorides under non-ideal flow conditions with BDD anodes, J. Appl. Electrochem. 41, 1087-1097.
189. Xie, R.Z., Meng, X.Y., Sun, P.Z., Niu, J.F., Jiang, W.J., Bottomley, L., Li, D., 2017. Chen Y.S, Crittenden J. Electrochemical oxidation of ofloxacin on a TiO_2-based SnO_2-Sb/polytetrafluoroethylene resin - PbO_2 electrode: reaction kinetics and mass transfer impact. Appl. Catal., B. 203, 515-525.
190. Xu, Q., Zhao T.S. 2013. Determination of the mass-transport properties of vanadium ions through the porous electrodes of vanadium redox flow batteries. Phys. Chem. Chem. Phys. 15, 10841-10848.
191. Xu, Y., Yang, J., Ou, M., Wang, Y., Jia, J. 2007. Study of *Microcystis aeruginosa* inhibition by electrochemical method. Biochem. Eng. J. 36, 215-220.

192. Zhang, G.S, Zhang, Y.C., Nadagouda, M., Han, C.S., O'Shea, K., El-Sheikh, S. M., Ismail, A. A., Dionysiou, D.D. 2014. Visible light-sensitized S, N and C co-doped polymorphic TiO_2 for photocatalytic destruction of microcystin-LR. Appl. Catal., B. 144, 614-621.
193. Zhou, S.Q., Shao, Y.S., Gao, N.Y., Deng, Y., Qiao, J.L., Ou. H., Deng, J. 2013. Effects of different algaecides on the photosynthetic capacity, cell integrity and microcystin-LR release of *Microcystis aeruginosa*. Sci. Total Environ. 463–464, 111–119.
194. Zhou, S.Q., Shao, Y.S., Gao, N.Y., Deng, Y., Li, L., Deng, J., Tan, C.Q. 2014. Characterization of algal organic matters of *Microcystis aeruginosa*: biodegradability, DBP formation and membrane fouling potential. Water Res. 52, 199-207.
195. Zhu, W., Zhou, X., Chen, H., Gao, L., Xiao, M., Li, M. 2016. High nutrient concentration and temperature alleviated formation of large colonies of *Microcystis*: Evidence from field investigations and laboratory experiments. Water Res. 101, 167-175.
196. Shao, L. and Hewitt, M.C., 2010. The kinetic isotope effect in the search for deuterated drugs. *Drug news & perspectives*, *23*(6), pp.398-404.
197. Sanderson, K., 2009. Big interest in heavy drugs.
198. Blake, M.I., Crespi, H.L. and Katz, J.J., 1975. Studies with deuterated drugs. *Journal of Pharmaceutical Sciences*, *64*(3), pp.367-391.
199. Westheimer, F.H., 1961. The magnitude of the primary kinetic isotope effect for compounds of hydrogen and deuterium. *Chemical Reviews*, *61*(3), pp.265-273.
200. Liu, Y.P., Lynch, G.C., Truong, T.N., Lu, D.H., Truhlar, D.G. and Garrett, B.C., 1993. Molecular modeling of the kinetic isotope effect for the [1, 5]-sigmatropic rearrangement of cis-1, 3-pentadiene. *Journal of the American Chemical Society*, *115*(6), pp.2408-2415.
201. Simmons, E.M. and Hartwig, J.F., 2012. On the Interpretation of Deuterium Kinetic Isotope Effects in C-H Bond Functionalizations by Transition-Metal Complexes. *Angewandte Chemie International Edition*, *51*(13), pp.3066-3072.